AN ABSTRACT OF THE THESIS OF

Corinne Patricia James for the degree of Doctor of Philosophy in Chemistry presented on March 11, 1987.

Title: Simple Models for the Structure and Dynamics of Polyatomic Fluids

Abstract approved: Redacted for privacy
Glenn T. Evans

Three areas of liquid state theory are considered.

First, Monte Carlo computer simulation of a two-dimensional hard disk fluid with an imbedded ellipse was undertaken to determine how a non-spherical molecule affects intermolecular ordering. The elliptical molecule (with axial ratios of 2, 5 and 10) altered the isotropic distribution of the disks only in the region very close to itself. Furthermore, the disk particles tended to arrange themselves along the least-curved portion of the ellipse. The results compared favorably with the scaled particle theory predictions of She and Evans (J. Chem. Phys. 85, 1513 (1986).).

Second, the self-diffusion coefficient, velocity autocorrelation function and distribution of collision times for a two-dimensional non-overlapping Lorentz gas were calculated using molecular dynamics simulation. Self-diffusion coefficients were found to agree at all densities with kinetic theory predictions (A. Weijland and J. M. J.

van Leeuwen, Physica 38, 35 (1968).) if the radial distribution function was taken into account. The density dependence of the decay of the velocity autocorrelation function was qualitiatively different than that predicted by kinetic theory.

Third, dynamics of small alkanes (composed of 4 to 15 methylene units) was investigated using the Rouse-Zimm model, the rotational isomeric state model and Brownian dynamics computer simulation in an effort to understand the chain length dependence of the rate of ring-closure reactions. It was found that the chain length dependence arose primarily from the equilibrium distribution of chain conformations rather than from differences in flexiblity of chains of differing lengths.

Simple Models for the Structure and Dynamics of Polyatomic Fluids

by

Corinne Patricia James

A THESIS

submitted to

Oregon State University

in partial fulfillment of
the requirements for the
degree of

Doctor of Philosophy

Completed March 11, 1987

Commencement June 1987

APPROVED:

Redacted for privacy

Professor of Chemistry in charge of major

Redacted for privacy

Head of department of Chemistry

Redacted for privacy

Dean of Graduate School

Date thesis is presented March 11, 1987

Typed by Corinne James for Corinne Patricia James

ACKNOWLEDGEMENTS

I would like to thank my major professor, Glenn T. Evans, for his guidance and patience in all aspects of this work. I also thank my husband, Bruce, for his unfailing support and patience.

I thank the National Science Foundation and the Petroleum Reasearch Fund for their support of this research.

TABLE OF CONTENTS

LIST OF FIGURES

LIST OF TABLES

SIMPLE MODELS FOR THE STRUCURE AND DYNAMICS OF POLYATOMIC FLUIDS

CHAPTER 1
INTRODUCTION

There exists no well-developed molecular theory which is able to predict the macroscopic properties of liquids and dense gases, primarily because of the difficulty of analyzing the collisions between molecules which characterize the liquid state. Such theories do exist for crystalline solids and for dilute gases since the intermolecular interactions in these materials can be simplified. In dilute gases, molecules are far apart and experience few collisions. The collisions which do take place are separated by relatively long periods of free translation. Because of this, dilute gas theory is based on the action of independent molecules. In crystalline solids, the individual molecules do not translate and the intermolecular interaction is dominated by long-range positional and orientational order. Interactions in solids are therefore effectively treated as a collective or an average phenomenon. The behavior of a molecule in a liquid or dense gas is governed by its not-quite-random interaction with other molecules. It is not practical to describe the complicated behavior of molecular liquids analytically or to simulate a real liquid on a macroscopic time scale, so the theory of liquids must rest upon the use of models. This thesis is a report of the investigation of three problems using models for the liquid state.

The modelling of molecular behavior can involve the consideration of a collection of molecules, each of which is simplified or the consideration of a single, fairly realistic molecule and the simplification of the surrounding molecules into an effective medium. Each of these types of models is used in work that is reported here.

The first problem that is considered is the change in equilibrium structure that is produced in a fluid of isotropic molecules by the introduction of a low concentration of anisotropic molecules. The packing in an isotropic fluid will, in the absence of external forces, by spherically symmetrical. At densities below the fluid-solid transition, the packing appears as a lack of spatial order. The presence of even a single anisotropic molecule will disrupt the normal packing of the fluid and introduce, at least in its immediate vicinity, orientational order. The extent of the order and its dependence on the density of isotropic molecules for a model system should provide some indication of the extent of orientational order in real solutions.

The model used to investigate this question represents a drastic simplification of a true liquid, but retains the features necessary to understand structural changes. A Monte Carlo computer simulation of a two-dimensional fluid of hard disks is used to model the fluid of isotropic molecules and the anisotropic molecule is taken to be a hard ellipse. The approximations of this model are the use of a two-dimensional, rather than a physically realistic three-dimensional system; the use of a Monte Carlo computer simulation to represent an equilibrium ensemble; the round or elliptical shape to represent molecules which may be irregular in shape; and the substitution of a

hard potential for a true intermolecular potential. The usefulness of each of these approximations will be considered.

The hard intermolecular potential is one for which the interaction energy is zero unless two molecules are in contact. For two molecules in contact, the interaction energy is infinite. This use of this potential ignores altogether the attractive part of a real intermolecular potential. This is a reasonable simplification to make for the problem considered here because the repulsive part of the potential is primarily reponsible for the structure of a fluid (1).

Molecules which can be represented by spheres in three dimensions include the rare gases, as well as more complicated molecules such as methane and some proteins. Linear molecules like nitrogen and carbon dioxide and even larger molecules such as butane are roughly elliptical in shape. The use of smooth convex bodies as models for the investigation of the structural changes occurring in an medium of isotropic molecules into which an anisotropic molecule has been introduced is sensible, because the model molecules have the necessary charcteristic of interest (either isotropy or anisotropy) and yet the analytic and numerical work is considerably simpler than it would be for more realistic molecular representations.

The Monte Carlo method (2) of computer simulation was chosen to mimic the equilibrium behavior of the fluid. An equilibrium average of a molecular property is determined by calculating its value for a large number of configurations of a collection of particles. The use of the Monte Carlo method for systems with hard potential forces is particlarly simple because any non-overlapping arrangement of particles

constitutes an equilbrium configuration and all of the non-overlapping configurations have equal weight. The concern in this work was with equilibrium averages of easily-calculated structural parameters such as the angle of each of the disk particles with respect to the semi-major axis of the ellipse and the average number of disk particles surrounding the ellipse at a given distance. The Monte carlo method provided a reasonable vehicle for the calculation of these quantities.

The use of a two-dimensional fluid in place of a three dimensional liquid appears to be unrealistic, however, many of the properties of three dimensional liquids are reproduced by a two-dimensional representation and a two-dimensional liquid is also useful for testing the predictions of theories which are valid for systems of general dimensionality. For the particular problem of the disruption of the hard disk fluid structure by an elliptical particle, the computer simulation of the two-dimensional system was used to examine the extent of the disruption and to compare to analytic scaled particle theory (SPT) predictions of the structure. A knowledge of the extent and nature of the disruption of the isotropic packing in two-dimensions can be extended to give at least a qualitative view of the same phenomenon in three dimensions. Furthermore, agreement or disagreement with the SPT predictions in two dimensions can provide an idea of the credibilty of the theory in three dimensions.

The second problem which was considered was molecular transport in liquids, specifically self-diffusion. The self-diffusion coefficient for liquids has been shown via kinetic theory to contain a non-analytic dependence of the density of the fluid at low densities. That is, the

density dependence becomes undefined as the density goes to zero. In addition, computer simulations of liquids have shown the initial velocity of a molecule to relax in an unexpected way. The expected decay of a molecule's velocity is by way of random collisions with other molecules in the fluid; this expectation leads to a prediction of exponential relaxation of the velocity. The exponential relaxation would leave a molecule with virtually no memory of its initial velocity after 10-20 mean collision times. In simulations, correlations between a molecule's initial velocity and its velocity at times even longer than 20 collision times have been demonstrated. Because the self-diffusion constant is the integral of the velocity correlation function, the anomolous velocity decay and the non-analytic density dependence are believed to be related.

The model which was used to investigate this problem is the two-dimensional Lorentz gas. The Lorentz gas (LG) is a collection of stationary scatterers traversed by non-interacting light particles. The model was originally developed by Lorentz for the description of conduction electrons in metals (3). It has proven to be a popular theoretical model because it exhibits a non-analytic density dependence of the diffusion constant and a non-exponential velocity relaxation, yet represents a considerable simplification of a molecular liquid.

For this work, the scatterers were taken to be non-overlapping, i.e., there exists a hard potential force between them which governs their arrangement. The overlapping LG has been studied as well (see references in ch. 4), but it was felt that the non-overlapping LG was a better model for a molecular liquid.

The interaction between the scatterers and the light particle is by way of the hard potential described previously, and the light particle is considered to be so light that it is massless. The two facts allow one to use simple elastic collision dynamics to describe the passage of a light particle through the arrangement of scatterers. The light particles do not interact with one another so that the behavior of only one particle need be considered and the behavior of an ensemble obtained by averaging over the equilibrium velocity distribution.

This model includes the approximations of three dimensions by two, and of an intermolecular potential by a hard potential which were used in the previous Monte Carlo study. The dynamics of the Lorentz model, that of a single massless, volumeless particle moving through an array of stationary scatterers was not intended to represent the dynamics of a molecular fluid. Rather, this model was used because it gives rise to properties analogous to those of fluids and because there was a greater chance of understanding the origin of these properties in the simpler Lorentz model than there is for a molecular liquid.

The simulation method chosen for the Lorentz model was the method of equilibrium molecular dynamics. In an equilibrium molecular dynamics simulation, the molecules are provided with initial positions and velocities from an appropriate equilibrium distribution function. The system is then allowed to evolve in time by the solution of the equations of motion for each particle. For the LG, only one particle has velocity, and because of the nature of the collisions with the stationary scatterers, the magnitude of the velocity is constant. This means that the velocity of the moving particle can be chosen to be

convenient computationally, and actual consideration of the velocity distribution need not be included. The equilbibrium distribution of the hard stationary scatterers is just the number of scatterers divided by the available volume. Their configuration can be obtained as any non-overlapping arrangement. The equations of motion for classical elastic collisions between a point particle and a stationary disk are also simple. The equilibrium molecular dynamics method is thus easily implemented in the case of the LG.

The third problem which was considered concerned the distance between the two ends of linear alkane chains. This distance will depend upon the equilibrium distribution of chain conformations and upon the flexibility and the rate of change between equilibrium conformations. Experiments have been performed which have determined the rate of electron exchange and flouresence quenching between chain ends. Whether this rate is determined by equilibrium considerations or by dynamical considerations cannot be ascertained from the experimental data and it was hoped that a theoretical study could provide some insight. The alkane chains were investigated using both analytic and computer techniques.

The analytic study utilized the Rouse-Zimm model (4); this model treats the alkane as a chain of beads connected by Hooke's Law springs. The motion of the molecule is represented by the normal modes of the collection of springs. The Rouse-Zimm mode has been successful in treating orientational motion in alkane chains (5) and should be useful in the understanding of chain motion required here.

Two different types of computer simulation were used. One, the rotational isomeric state model of Flory (6), was directed at an

analysis of the equilibrium distribution of chain conformations. In the model, molecules are considered to have constant bond lengths, bond angles and a three-fold symmetric torsional potential. All allowed conformations are constructed and weighed evenly in the calculation of an equilibrium average.

The model which was chosen to mimic the time-dependent properties of alkane chains represents a single, reasonably realistic molecule under the action of an effective field. This is the Brownian dynamics model. In the Brownian dynamics model, the solvent provides a frictional drag on each of the atoms and random 'kicks' at random points on the molecule. A bead and stick model is used for the alkane itself. The molecule is subject to a torsional potential forces and to constraints on bond length and bond angle.

Because the interest in the chain end problem was on single molecule behavior, realistic, three-dimensional models such as the Rouse-Zimm, the rotational isomeric state and the Brownian dynamics models were approproate and accessible.

Chapter 2 is a discussion of some of the fundamentals of statistical mechanics which will be used throughout the rest of this work. Each of Chapters 3-5 is a report of work directed towards one of the problems discussed above. The structure of a dilute solution of an anisotropic molecule in a solvent of isotropic molecules is considered in Chapter 3. The molecular dynamics of the Lorentz gas is in Chapter 4 and the study of the chain end separation of alkanes is given in Chapter 5.

REFERENCES FOR CHAPTER 1

1. J. A. Barker and D. Hensderson, Rev. Mod. Phys. 48, 587 (1976).

2. N. Metropolis, A. W. Rosenbluth, M. N. Rosenbluth, A. H. Teller, and E. Teller, J. Chem. Phys. 21, 1087 (1953).

3. H. A. Lorentz, Proc. Amst. Acad. 7, 438, 585 (1905).

4. P. E. Rouse, J. Chem. Phys. 21, 1272 (1953); B. H. Zimm, ibid 24, 269 (1954).

5. G. T. Evans, J. Chem. Phys. 74, 4621 (1981).

6. P. J. Flory, 'Statistcal Mechanics of Chain Molecules', Interscience, New York (1969).

7. M. Fixman, J. Chem. Phys. 69, 1527 (1978).

CHAPTER 2
BASIC THEORY

A. Introduction - Phase space distribution functions

The statistical mechanics of liquid state behavior utilizes the concepts of phase space and distribution functions. Because the idea of phase space is central to the computational details discussed in later chapters, a review of the general concept of phase space distribution functions, their connection with equilibrium and non-equilibrium properties and their time evolution is provided.

The theoretical development will use the classical mechanical canonical ensemble(1). In the canonical ensemble, the number of particles N, the system volume V and the temperature are held constant. An N-molecule, single-component system in three dimensional space has 3N degrees of freedom which describe the positions $\mathbf{r}_i$ of the N molecules and 3N degrees of freedom which describe the momenta of the particles $\mathbf{p}_i$. The possible states of the system may be described by the specification of the positions and momenta of each of the molecules. The phase space for the system is defined as the N-dimensional space in which each point $(\mathbf{r}_1,\ldots,\mathbf{r}_N,\mathbf{p}_1,\ldots,\mathbf{p}_N)$ represents one of the possible states of the system. For polyatomic molecules, rotational or vibrational degrees of freedom are included and, accordingly, the number of dimensions of phase space is increased to accomodate the increase in the number of possible system states.

The distribution of points in phase space will be controlled by the convective free flow of molecules and by the forces which act upon the

molecules in the system, i.e., the intermolecular potential and any external forces which may be present. A distribution function(1) may be defined which describes the probability of finding the system at any particular point in phase space, that is, with molecule 1 at $\mathbf{r}_1$ with momentum $\mathbf{p}_1$, molecule 2 at $\mathbf{r}_2$ with momentum $\mathbf{p}_2,\ldots,$ molecule N at $\mathbf{r}_N$ with momentum $\mathbf{p}_N$ at time t:

$$P^{(N)}(\mathbf{r}^N,\mathbf{p}^N,t)d\mathbf{r}^N d\mathbf{p}^N \qquad (1)$$

where $(\mathbf{r}^N,\mathbf{p}^N)$ represents the phase space point $(\mathbf{r}_1,\ldots,\mathbf{r}_N,\mathbf{p}_1,\ldots,\mathbf{p}_N)$ and $d\mathbf{r}^N d\mathbf{p}^N$ is the differential volume element $d\mathbf{r}_1\ldots d\mathbf{r}_N d\mathbf{p}_1,\ldots d\mathbf{p}_N$. This function is known as the N^{th} order probability density function. The function $P^{(N)}(\mathbf{r}^N,\mathbf{p}^N,t)d\mathbf{r}^N d\mathbf{p}^N$ tracks the positions and momenta of all the particles in the system and requires more information than can be easily obtained. Lower order distribution functions which describe the probability of finding a subset of the N molecules in a given state may be obtained by integration of the full probability density function over the positions and momenta of some of the particles. Lower-order or reduced distribution functions are useful in the determination of system parameters which can be calculated in terms of the positions and momenta of a few of the N particles or as a sum over the coordinates of a few particles. The probability of finding molecule 1 at $\mathbf{r}_1$ about $d\mathbf{r}_1,\ldots,$ molecule n at $\mathbf{r}_n$ about $d\mathbf{r}_n$ at time t regardless of the configuration of the n+1 through N^{th} molecules will be

$$P^{(n)}(\mathbf{r}^n,\mathbf{p}^n,t) = \int\ldots\int d\mathbf{r}^{N-n}d\mathbf{p}^{N-n}P^{(N)}(\mathbf{r}^N,\mathbf{p}^N,t). \qquad (2)$$

$P^{(n)}(\mathbf{r}^n,\mathbf{p}^n,t)$ is the n particle reduced distribution

function.

The more general case of the probability of the system being found with any molecule in dr_1 about r_1,..., and any molecule in dr_N about r_N may be treated by multiplying the specific probablility above by the number of ways the n molecules can be selected from the total N molecules

$$f^{(n)}(r^n,p^n,t) = \frac{N!}{(N-n)!} P^{(n)}(r^n,p^n,t) \tag{3}$$

$f^{(n)}(r^n,p^n,t)$ is the n particle generic reduced distribution function. When n is equal to one, the function $f^{(1)}(r^1,p^1,t)$ is known as the singlet distribution function. Likewise, $f^{(2)}(r^2,p^2,t)$ is the pair distribution function. The distribution functions may be written as a function of the velocity, rather than the momentum, indicated by $f^{(n)}(r^n,v^n,t)$.

The time-dependent phase space distribution function for an N-particle system will obey the Liouville equation

$$\frac{\partial}{\partial t} P^{(N)} + \{P^{(N)},H\} = 0 \tag{4}$$

where H is the Hamiltonian for the system. The expression within the Poisson brackets may be written explicitly as

$$\frac{\partial P^{(N)}}{\partial t} + \sum_j \frac{\partial P^{(N)}}{\partial r_j}\left(-\frac{\partial H}{\partial p_j}\right) + \sum_j \frac{\partial P^{(N)}}{\partial p_j}\left(-\frac{\partial H}{\partial r_j}\right) = 0 \tag{5}$$

where the sum over j is to be performed over the 3N cartesian coordinates of the positions and of the momenta of the molecules. The evaluation of the derivatives of the Hamiltonian gives

$$\frac{\partial P^{(N)}}{\partial t} + \sum_j \frac{p_j}{m_j}\cdot\nabla_{r_j} P^{(N)} + \sum_j F_j\cdot\nabla_{p_j} P^{(N)} = 0. \tag{6}$$

where F_j is the total force acting on the j^{th} particle, ∇_{r_j} is the gradient with respect to the position of particle j, ∇_{p_j} is the gradient with respect to the momentum of particle j, and the sums are over the N molecules in the system.

This equation can be expressed more succintly as

$$i\frac{\partial P^{(N)}}{\partial t} = \hat{L}P^{(N)} \tag{7}$$

with

$$\hat{L} = - i \sum_j \left(\frac{p_j}{m_j} \cdot \nabla_{r_j} + F_j \cdot \nabla_{p_j} \right) \tag{8}$$

The Liouville equation has the formal solution

$$P^{(N)}(r^N, p^N, t) = e^{-i\hat{L}t} P^{(N)}(r^N, p^N, 0) \tag{9}$$

which may be used to describe the evolution in time of the phase space distribution function.

The distribution functions, particularly the singlet and pair distribution functions, play a key role in the analysis of the equilibrium behavior of liquids and in the kinetic theory treatment of non-equilibrium phenomena and will be used throughout this work. The equilibrium pair distribution function is proportional to the radial distribution function which is important in the Monte Carlo study described in Chapter 3. A discussion of the radial distribution function will be followed by an analysis of the use of the non-equilibrium distribution functions in the Boltzmann-Enskog equation and in the treatment of macroscopic liquid properties via the time correlation function formalism. These techniques will be utilized in the interpretation of the molecular dynamics results of Chapter 4.

B. Equilibrium distribution functions

For a system of molecules at equilibrium, the phase space distribution function will be independent of the time and can be written $P^{(N)}(r^N,p^N)$. The interest in this work will be in the positional distribution of the particles at equilibrium and not in the distribution of momentum; consequently the discussion of equilibrium distribution functions will focus on the positional distribution. The configuration distribution function $P^{(N)}(r^N)$ indicates the probability of finding the molecules at specific positions independent of the momentum distribution and is defined by the integration of $P^{(N)}(r^N,p^N)$ over the momenta of the N particles,

$$P^{(N)}(r^N) = \int dp^N \; P^{(N)}(r^N,p^N). \tag{10}$$

The form of the distribution function may be determined from its definition as the probability of finding the system in a given state and from the principles of equilibrium statistical mechanics. If U, the intermolecular potential energy function is $U = U(r^N)$, a function of the positions of the N particles, the method of the most probable distribution gives the probability of finding the system in a given state in the form

$$P^{(N)}(r_N) = e^{(-\beta U)}/Z_N \tag{11}$$

where Z_N is the configuration integral $\int dr^N \; P^{(N)}(r_N)$. Lagrange's method of undetermined multipliers and comparison with macroscopic thermodynamics are used to find that the constant β appearing in the distribution function is equal to $1/k_BT$, where k_B is Boltzmann's constant and T, the absolute temperature. When this

function is integrated over the coordinates of the n+1 through N^{th} particles $dr^{N-n}dp^{N-n}$, a lower order distribution $P^{(n)}(r^n,t)$ analogous to $P^{(n)}(r^n,p^n,t)$ in eqn. (2) is obtained. As with $P^{(n)}(r^n,p^n,t)$, the function is multiplied by a factor of N!/(N-n)! to give a generic configuration distribution function

$$\rho^{(n)}(r^n) = \frac{N!}{(N-n)!}P^{(n)}(r^n). \tag{12}$$

When n is equal to one, the distribution function $\rho^{(1)}(r_1)$, is the probability that a molecule will be found in dr_1. In a gas or a liquid, a molecule is as likely to occupy one point as it is to occupy any other, so $\rho(r_1)$ is independent of r_1 and

$$\frac{1}{V}\int\rho^{(1)}(r_1)dr_1 = \rho^{(1)} = \frac{N}{V} = \rho. \tag{13}$$

The above expression agrees with the conclusion that if N particles are arranged randomly in a volume V the probability that a particle will be found with its center in any volume element dr will be equal to the number of particles divided by the available volume.

An n-particle correlation function, $g^{(n)}(r^n)$, is defined from $\rho^{(n)}(r^n)$ by

$$g^{(n)}(r^n) = \rho^{(n)}(r^n)/\rho^n. \tag{14}$$

The value of $g^{(n)}$ will be one when there are no correlations in the fluid, as in a dilute gas system; deviations from one reflect correlations between the particles when they are present. An example is the correlation in position of two particles introduced by the excluded volume of a third particle which would cause a deviation from one in $g^{(2)}(r^2)$. Substitution from eqn. (3) gives

$$g^{(n)}(r^n) = \frac{V_n N!}{N^n (N-1)!} \frac{\int \ldots \int e^{-\beta U} dr_{N-n}}{Z_N}$$

$$= V^n (1 + O(N^{-1})) \frac{\int \ldots \int e^{-\beta U} dr^{N-n}}{Z_N} \qquad (15)$$

When n is equal to 2, the function is referred to as the pair distribution function and when this function is averaged over all angular degrees of freedom, it becomes the radial distribution function(rdf). The rdf will be indicated by the abbreviated notation g(r).

The importance of the radial distribution function is due, in part, to the practice of defining the system energy U_N as the sum of pairwise interactions;

$$U_N = \sum_{ij} U(r_{ij}). \qquad (16)$$

where r_{ij} is $|r_i - r_j|$, the distance between particles i and j and $U(r_{ij})$ is a function of this distance only. If U_N is defined in this way, the averages of some equilibrium property A(r) of a three-dimensional fluid may be determined by

$$< A > = \int_V 4\pi r^2 dr \; g(r) \; A(r). \qquad (17)$$

The assumption of pairwise additive potentials has proven to be valid under many conditions and represents a considerable simplification of the three-body problem which would be encountered in a higher-order approximation. For the rigid systems examined in this work, the forces are exactly pairwise additive and a knowledge of g(r) or the angle-dependent g(r) will lead to information about all the equilibrium properties of interest.

C. Non-Equilibrium Distribution Functions - The Boltzmann-Enskog Equation

The knowledge of the distribution function at some arbitrary time τ can be used to obtain the average of a dynamical variable A(t) at time τ via

$$\langle A(\tau) \rangle = \int\ldots\int dr^N dp^N\ f^{(N)}(r^N,p^N,\tau)\ A(r^N,p^N,\tau). \tag{18}$$

The full time-dependent distribution function $f^{(N)}(r^N,p^n,t)$ requires detailed knowledge of all particles in the system and their evolution in time. The reduced distribution functions described in part A. are of more practical value. The Bogoliubov, Born, Green, Kirkwood and Yvon (BBGKY) hierarchy which relates a reduced distribution function $f^{(n)}(r^n,p^n,t)$ to the next highest-order distribution function $f^{(n+1)}(r^{n+1},p^{n+1},t)$ can be obtained from the Liouville equation(1). The first step in the derivation of the BBGKY hierarchy is to write the force F_j as the sum of the forces of the other particles acting upon particle j, namely, $\Sigma_i F_{ij}$. No external forces will be considered. The next step is to multiply the Liouville equation by N!/(N-n)! and to integrate over the position and momentum variables $dr^{N-n}dp^{N-n}$:

$$\frac{\partial f^{(n)}}{\partial t} + \sum_{j=1}^{n} \frac{p_j}{m_j}\cdot\nabla_{r_j} f^{(n)} + \frac{N!}{(N-n)!} \sum_{i,j=1}^{N} \int\ldots\int dr^{N-n}dp^{N-n}\ F_{ij}\cdot\nabla_{p_j} f^{(N)} = 0. \tag{19}$$

Members of the sum in the second term on the left were eliminated because $f^{(N)}$ vanishes when $p_i = \pm\infty$. The last term on the left hand side is the sum of two parts

$$\sum_{i,j=1}^{n} F_{ij}\cdot\nabla_{p_j} f^{(n)} + \frac{N!}{(N-n)!} \sum_{i=1}^{n} \sum_{i=n+1}^{N} \int\ldots\int F_{ij}\cdot\nabla_{p_j} f^{(n)}\ dr^{N-n}dp^{N-n} \tag{20}$$

and the second part of the above is just

$$\sum_{i=1}^{n} \iint \mathbf{F}_{jn+1} \cdot \nabla_{\mathbf{p}_j} f^{(n+1)} \, d\mathbf{r}^{n+1} d\mathbf{p}^{n+1} \tag{21}$$

The use of this term in eqn. (19) above gives an exact equation for $f^{(n)}$ in terms of an intergral over $f^{(n+1)}$,

$$\frac{\partial f^{(n)}}{\partial t} + \sum_{j=1}^{n} \frac{\mathbf{p}_j}{m_j} \cdot \nabla_{\mathbf{r}_j} f^{(n)} + \sum_{i,j=1}^{n} \mathbf{F}_{ij} \cdot \nabla_{\mathbf{p}_j} f^{(n)} + \sum_{i=1}^{n} \iint \mathbf{F}_{jn+1} \cdot \nabla_{\mathbf{p}_j} f^{(n+1)} \, d\mathbf{r}^{n+1} d\mathbf{p}^{n+1} = 0. \tag{22}$$

This is the BBGKY hierarchy.

The BBGKY hierarchy can be used to generate an approximate equation, the Boltzmann-Enskog equation for the time evolution of the pair distribution function $f^{(2)}(\mathbf{r}^2, \mathbf{p}^2, t)$(2). The singlet distribution function $f^{(1)}(\mathbf{r}_1, \mathbf{p}_1, t)$ for some particle 1, the singlet distribution function $f^{(1)}(\mathbf{r}_2, \mathbf{p}_2, t)$ for some particle 2, and the pair distribution function for particles 1 and 2 $f^{(2)}(\mathbf{r}_1, \mathbf{r}_2, \mathbf{p}_1, \mathbf{p}_2, t)$ will be indicated by the abbreviated notation $f^{(1)}(1,t)$, $f^{(1)}(2,t)$ and $f^{(2)}(1,2,t)$, respectively.

The lowest member of the BBGKY hierarchy relates $f^{(1)}(1,t)$ to $f^{(2)}(1,2,t)$ by

$$\partial_t f^{(1)}(1,t) + i\hat{L}_1 f^{(1)}(1,t) = -\iint d\mathbf{r}_2 d\mathbf{p}_2 \, \mathbf{F}_{12} \cdot \nabla_{\mathbf{p}_1} f^{(2)}(1,2,t) \tag{23}$$

where $\hat{L}_1$ is the one particle Liouville operator $\mathbf{v} \cdot \nabla_{\mathbf{r}}$; the next member of the hierarchy is

$$\partial_t f^{(2)}(1,2,t) + i\hat{L}_2 f^{(2)}(1,2,t) = -\iint d\mathbf{r}_3 d\mathbf{p}_3 \, \{\mathbf{F}_{13} \cdot \nabla_{\mathbf{p}_1} + \mathbf{F}_{23} \cdot \nabla_{\mathbf{p}_2}\} \, f^{(3)}(1,2,3,t) \tag{24}$$

where $\hat{L}_2$ is the two particle Liouville operator $\mathbf{v}_1 \cdot \nabla_{\mathbf{r}_1} + \mathbf{v}_1 \cdot \nabla_{\mathbf{r}_1} + \mathbf{F}_{12} \cdot \nabla_{\mathbf{p}_1} + \mathbf{F}_{21} \cdot \nabla_{\mathbf{p}_2}$. This equation

can be solved for $\mathbf{F}_{12}\cdot\nabla_{\mathbf{p}_1} f^{(2)}(1,2,t)$

$$\mathbf{F}_{12}\cdot\nabla_{\mathbf{p}_1} f^{(2)}(1,2,t) = -(\partial_t + \mathbf{v}_1\cdot\nabla_{\mathbf{r}_1} + \mathbf{v}_1\cdot\nabla_{\mathbf{r}_1} + \mathbf{F}_{21}\cdot\nabla_{\mathbf{p}_2}) f^{(2)}(1,2,t) - \iint d\mathbf{r}_3 d\mathbf{p}_3 \{\mathbf{F}_{13}\cdot\nabla_{\mathbf{p}_1} + \mathbf{F}_{23}\cdot\nabla_{\mathbf{p}_2}\} f^{(3)}(1,2,3,t) \quad (25)$$

Both sides of this equation are now integrated over the position and momentum coordinates of particle 2; the left hand side of eqn. (25) becomes

$$\iint d\mathbf{r}_2 d\mathbf{p}_2 \; \mathbf{F}_{12}\cdot\nabla_{\mathbf{p}_1} f^{(2)}(1,2,t). \quad (26)$$

The BBGKY hierarchy given by eqn. (22) and eqns. (23)-(26) are general equations which can be applied to any system, the development of the Boltzmann-Enskog equation which follows will be specialized to a system of hard convex particles with axial symmetry. For such particles, all interparticle forces will be delta functions, $\delta(\mathbf{R})$, where $\mathbf{R}$ represents the minimum distance between the surfaces of two particles; the delta function will be equal to zero unless the two particles are in contact.

Because $\mathbf{F}_{12}$ is a delta function on the contact surface of the particle, the integral over $\mathbf{r}_2$ can be converted to an integral over the infinitesimal volume just inside and just outside the convex body. The origin of the coordinate system is first changed such that $\mathbf{r}_2$ is replaced by $\mathbf{r}_{21}$ where $\mathbf{r}_{21}$ is $|\mathbf{r}_2-\mathbf{r}_1|$. The set of coordinates $\mathbf{k}$ and ι will now be introduced to represent the surface-to-surface distance between arbitrary convex particles. The surface normal or apse vector $\mathbf{k}$ is the unit vector perpendicular to the surface of the particle at a given point; for a convex body, each point on the surface is associated with a unique vector $\mathbf{k}$. The scalar distance along the apse vector will be indicated by ι. The

surface-to-surface distance between two particles, 1 and 2, can be represented by $\mathbf{k}\iota$ (Figure 2.1), where $\mathbf{k}$ is the surface normal to particle 1 in the direction of the point on the surface of particle 2 which is closest to particle 1 and ι is the minimum distance between the surfaces of the bodies. Since $\mathbf{k}$ is unique to a point on the surface of the particle, the specification of $\mathbf{k}\iota$ provides an unambiguous description of the the location of particle 2 with respect to particle 1 and $\int d\mathbf{r}_{21}$ can be replaced by an appropriate integral over $\mathbf{k}$ and ι. The Jacobian of the transformation is indicated by J,

$$d\mathbf{r}_{21} = \left\| \frac{d\mathbf{r}_{21}}{d\mathbf{k}d\iota} \right\| d\mathbf{k}d\iota = Jd\mathbf{k}d\iota. \tag{27}$$

The implementation of the volume integral in eqn (26) gives

$$\int d\mathbf{r}_2 \; \mathbf{F}_{12}\cdots \; = \int\int_{\iota=0-}^{\iota=0+} Jd\mathbf{k}d\iota \; \mathbf{F}_{12}\cdots. \tag{28}$$

The first term on the right hand side of eqn. (25), viz., $\partial_t f^{(2)}(1,2,t)$ will vanish upon integration because the distribution function will be effectively constant in time over the infinitesimal volume element. The last term on the right hand side involves contact between particles 1 and 3 and particles 2 and 3; contributions to the integral from such contact will disappear as the volume of integration becomes infinitely close to the surface of particle 1. The term

$$-\int\int d\mathbf{p}_2 Jd\mathbf{k}d\iota d\mathbf{p}_2 \; \mathbf{F}_{21}\cdot\nabla_{\mathbf{p}_2} f^{(2)}(1,2,t) \tag{29}$$

will vanish because of the momentum boundary conditions.

The integrated form of the second member of the BBGKY hierarchy is now

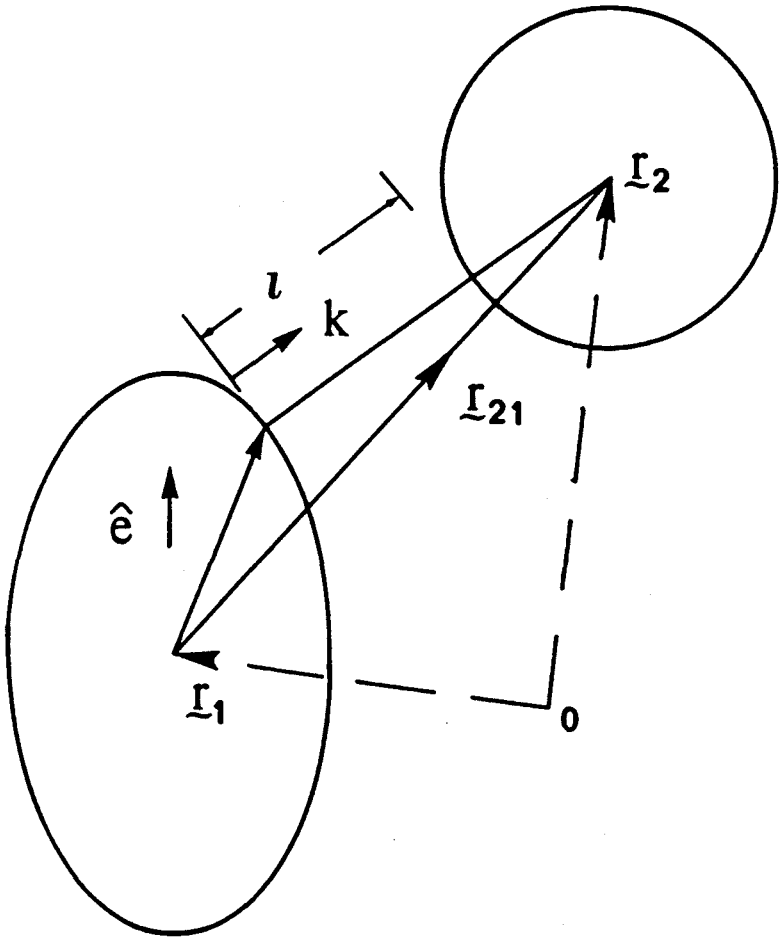

Figure 2.1 Definition of the surface-to-surface coordinate system.

$$-\int\int dp_2 Jdkd\imath\ F_{12}\cdot\nabla_{p_1} f^{(2)}(1,2,t)$$

$$= \int\int dp_2 Jdkd\imath\{v_1\cdot\nabla_{r_1} + v_1\cdot\nabla_{r_1}\}f^{(2)}(1,2,t). \qquad (30)$$

If the above result is substituted into eqn. (23) for the lowest member of the BBGKY hierarchy, then

$$(\partial_t + i\hat{L}_1)f^{(2)}(1,2,t) = \int\int dp_2 Jdkd\imath\{v_1\cdot\nabla_{r_1}+v_1\cdot\nabla_{r_1}\}f^{(2)}(1,2,t). \qquad (31)$$

The operator in the integral on the right hand side $\{v_1\cdot\nabla_{r_1} + v_1\cdot\nabla_{r_1}\}$ is equivalent to the streaming operator ∂/∂_t for a two particle system. The positions of particles 1 and 2 may be described in terms of center of mass ($\mathbf{R} = (\mathbf{r}_1 + \mathbf{r}_2)/2$) and relative ($\mathbf{r}_{21} = \mathbf{r}_2 - \mathbf{r}_1$) coordinates and the relative coordinate $\mathbf{r}_{21}$ may be expressed in terms of the apse vector $\mathbf{k}$ and the surface-to-surface distance $\imath$ previously described. The chain rule gives

$$\begin{aligned}\partial_t(\mathbf{r}_1,\mathbf{r}_2) &= \dot{\mathbf{r}}_1\cdot\nabla_{r_1} + \dot{\mathbf{r}}_2\cdot\nabla_{r_2}\\ &= \mathbf{v}_1\cdot\nabla_{r_1} + \mathbf{v}_1\cdot\nabla_{r_1}\\ &= \partial_t(\mathbf{R},\mathbf{k},\imath)\\ &= \dot{\mathbf{R}}\cdot\nabla_{\mathbf{R}} + \dot{\mathbf{k}}\cdot\nabla_{\mathbf{k}} + \dot{\imath}\cdot\partial_{\imath}. \qquad (32)\end{aligned}$$

where the derivative of a variable with respect to time has been indicated by placing a dot over the variable. The center of mass variable $\mathbf{R}$ makes no contributions to the integrals given above and will be neglected.

The equation for the time evolution of $f^{(1)}(1,t)$ is

$$(\partial_t + i\hat{L})f^{(1)}(1,t) = \int\int dp_2 Jdkd\imath\ (\dot{\imath}\partial_{\imath} + \dot{\mathbf{k}}\cdot\nabla_{\mathbf{k}})f^{(2)}(1,2,t). \qquad (33)$$

Integration over the $\imath$ coordinate gives

$$(\partial_t + i\hat{L})f^{(1)}(1,t) = \int\int dp_2 Jdk\{\dot{\imath}f^{(2)}(1,2,t)|_{0-}^{0+} + \dot{k}\cdot\nabla_k f^{(2)}(1,2,t)\}. \quad (34)$$

Because the systems of interest are isotropic, the divergence theorem can be used to eliminate the second term on the right hand side. At the lower limit 0-, the first term on the right hand side of eqn. (34) will vanish since the distribution function $f^{(2)}(1,2,t)$ is zero for overlapping particles.

What is left is a reduced form of the BBGKY hierarchy

$$(\partial_t + i\hat{L})f^{(1)}(1,t) = \int\int dp_2 Jdk\dot{\imath}\, f^{(2)+}(1,2,t) \quad (35)$$

where $f^{(2)+}(1,2,t)$ indicates that the pair distribution function is to be evaluated just off the surface of the particle of interest. A vector $\imath$ can be defined and examined to provide an alternate expression for the time derivative of $\imath$. If $\imath$ is defined in the direction of $\mathbf{k}$, then $\imath = k\imath$. The time derivative $\partial_t \imath$ is the change in the vector separating the surfaces of the particles; for two particles in relative motion the change will be $\mathbf{g}$, the relative velocity

$$\mathbf{g} = \mathbf{v}_2 - \mathbf{v}_1 + (\boldsymbol{\omega}_2 \times \mathbf{a}_2 - \boldsymbol{\omega}_1 \times \mathbf{a}_1) = \partial_t \imath. \quad (36)$$

with ω_i the angular velocity of particle i and, a_i the lever arm from the center of particle i to the point of contact. If both sides of this equation are multiplied by $\mathbf{k}$, $\partial_t \imath$ is

$$\partial_t \imath = \mathbf{k}\cdot\partial_t \imath = \mathbf{k}\cdot\mathbf{g}. \quad (37)$$

It will be seen that $\mathbf{k}\cdot\mathbf{g}$ is a useful quantity; it measures the velocity of the particle surfaces relative to each other. Immediately before a collision, the surfaces will be moving towards each other and

$\mathbf{k}\cdot\mathbf{g}$ will be less than zero; after collision when the particles are traveling away from each other, $\mathbf{k}\cdot\mathbf{g}$ will be greater than zero.

The BBGKY hierarchy is now written as

$$(\partial_t + i\hat{L})f^{(1)}(1,t) = \int\int dp_2 Jdk\ (\mathbf{k}\cdot\mathbf{g})\ f^{(2)+}(1,2,t). \tag{38}$$

This is an exact equation for the relationship between the singlet and the pair distributions for hard convex bodies in dilute gas systems; at this point approximations are introduced to treat the dynamics of collisions between particles.

The assumption of molecular chaos is made; it is assumed that in the past (before collison, t=0) the particles are uncorrelated, but that in the future (after collision, $t=\tau$) the particles will be correlated. This assumption breaks the time reversal symmetry of the system. If the particles are uncorrelated in the past, then the pair distribution function $f^{(2)}(1,2,0)$ can written as the product of two single particle distribution functions

$$f^{(2)}(1,2,0) = \chi(r_s,0)f^{(1)}(1,0)f^{(1)}(2,0). \tag{39}$$

The function $\chi(r_s,0)$ represents the spatial distribution function of the rigid bodies for t=0; r_s indicates the function at the surface of the particle. This function was introduced into the traditional Boltzmann analysis by Enskog; for an equilibrium fluid of spherical molecules $\chi(r_s,t)$ will be the radial distribution function.

It is further assumed that the time dependence of the reduced distribution functions $f^{(2)}(1,2,\tau)$ and $f^{(1)}(1,0)$ can be written in terms of the one particle Liouville operator $\hat{L}_1$ and the two particle Liouville operator $\hat{L}_2$, respectively. The complete

time evolution of these distribution functions is determined by the full Liouville operator which may be expressed as $\hat{L} = \hat{L}_1 + \hat{L}_2 + \hat{L}_3 + \ldots$ where $\hat{L}_1$ is the one particle Liouville operator, $\hat{L}_2$ is the two particle Liouville operator, $\hat{L}_3$ is the three particle Liouville operator... The assumption of the reduced form for the Liouville operator neglects the influence of events involving three or more particles and serves to limit the validity of the Boltzmann-Enskog equation to the dilute gas regime.

The time evolution can be written as

$$f^{(2)}(1,2,\tau) = e^{-i\hat{L}_2\tau} f^{(2)}(1,2,0)$$
$$= e^{-i\hat{L}_2\tau} \chi(r_s,0) f^{(1)}(1,0) f^{(1)}(2,0). \qquad (40)$$

If all the distribution functions can be expressed as functions of the same time τ, the equations relating them will involve only the time τ and will be much easier to solve. The time evolution of the single particle distribution function is

$$f^{(1)}(1,\tau) = e^{-i\hat{L}_1\tau} f^{(1)}(1,0) \qquad (41)$$

and correspondingly

$$f^{(1)}(1,0) = e^{+i\hat{L}_1\tau} f^{(1)}(1,\tau). \qquad (42)$$

Upon substitution for the zero-time singlet distribution function, eqn. (40) above becomes

$$f^{(2)}(1,2,\tau) = e^{-i\hat{L}_2\tau} e^{+i\hat{L}_1\tau} e^{+i\hat{L}_1\tau} \chi(r_s,\tau) f^{(1)}(1,\tau) f^{(1)}(1,\tau). \qquad (43)$$

An operator $\hat{S}^{(2)}$ is defined such that

$$\hat{S}^{(2)} = e^{-i\hat{L}_2\tau} e^{+i\hat{L}_1\tau} e^{+i\hat{L}_1\tau}. \qquad (44)$$

This operator is equal to one for times before the collision. The effect of applying this operator for a time τ following a collision is to convert post-collisional momenta to pre-collisional momenta.

Explicitly, the particles with momentum determined by the post-collisional distribution function $f^{(1)}(1,\tau)$ are acted upon such that they are translated back in time traveling a distance $-\mathbf{v}_i\tau$ (rotations are neglected in this simple example) and then are allowed to evolve forward in time with momentum from the pre-collisional distribution (Figure 2.2). The net result is

$$f^{(2)}(1,2,\tau) = \chi(\mathbf{r}_s,\tau)f^{(1)*}(1,\tau)f^{(1)*}(1,\tau) \tag{45}$$

where the asterisk represents the pre-collisional distribution function.

This form for the pair distribution function following collision can be substituted into the BBGKY hierarchy to give

$$\begin{aligned}(\partial_t + i\hat{L})f^{(1)}(1,t) &= \int\int d\mathbf{p}_2 J d\mathbf{k}\ (\mathbf{k}\cdot\mathbf{g})S^{(2)}f^{(2)}(1,2,\tau) \\ &= \int\int_{\mathbf{k}\cdot\mathbf{g}<0} d\mathbf{p}_2 J d\mathbf{k}\ (\mathbf{k}\cdot\mathbf{g})\chi(\mathbf{r}_s,\tau)f^{(1)}(1,\tau)f^{(1)}(2,\tau) \\ &+ \int\int_{\mathbf{k}\cdot\mathbf{g}>0} d\mathbf{p}_2 J d\mathbf{k}\ (\mathbf{k}\cdot\mathbf{g})\chi(\mathbf{r}_s,\tau)f^{(1)*}(1,\tau)f^{(1)*}(2,\tau).\end{aligned} \tag{46}$$

If $\mathbf{k}$ is changed to $-\mathbf{k}$ in the second integral and the last two integrals are combined, the result is the familiar form of the Boltzmann-Enskog(B-E) equation:

$$\begin{aligned}(\partial_t + i\hat{L})f^{(1)}(1,t) &= \int\int_{\mathbf{k}\cdot\mathbf{g}<0} d\mathbf{p}_2 J d\mathbf{k}\ (\mathbf{k}\cdot\mathbf{g})\chi(\mathbf{r}_s,\tau) \\ &\{f^{(1)}(1,\tau)f^{(1)}(2,\tau) - f^{(1)*}(1,\tau)f^{(1)*}(2,\tau)\}.\end{aligned} \tag{47}$$

This equation differs from the Boltzmann equation in that the finite size of the molecules is taken into account.

In addition to the assumption of molecular chaos mentioned earlier, this derivation rests upon two other important assumptions. One is that only binary collisions will be important. The action of a third particle has been ruled out by the choice of the Liouville operator

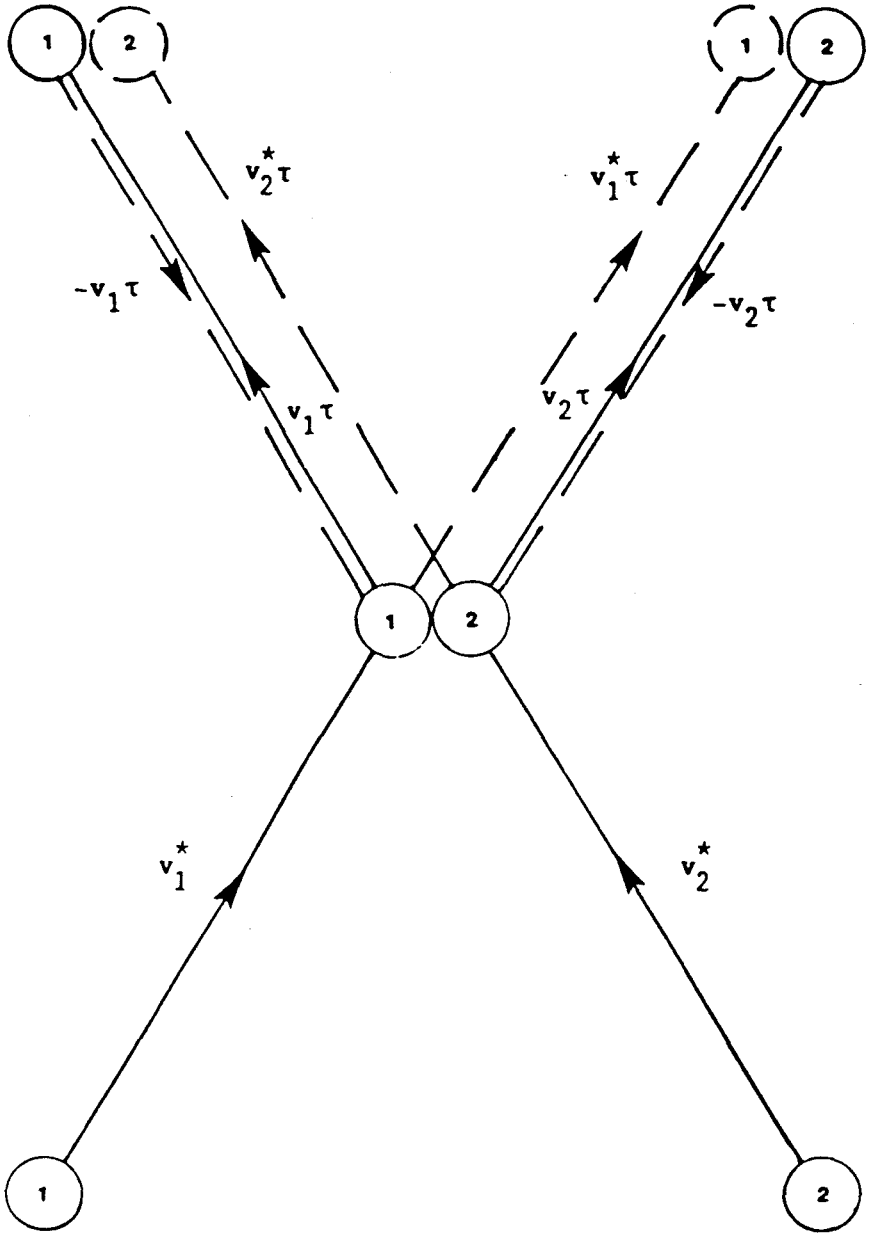

Figure 2.2 The action of the operator $\hat{S}_0$ at a time τ following a collision. The solid line indicates the trajectories of particle 1 and 2 before and for time τ after collision. The broken lines represent the trajectories which result from the application of $\hat{S}_0$.

L_2 for the pair distribution function as a function of two particle dynamics.. The use of $L_1 = \mathbf{v}\cdot\nabla_r$ for the singlet Liouville operator includes the assumption that interparticle interactions do not contribute to the time evolution of a specific particle. Both of these assumptions serve to restrict the validity of the Boltzmann-Enskog equation to low densities. Treatment of the behavior of more dense gases requires the inclusion of terms involving contributions from $\hat{L}_3$, $\hat{L}_4$, etc. which represent the dynamics of three-particle and higher order interactions. The inclusion of thses terms is the basis of ring-expansion techniques.

D. Time Correlation Functions

An important link between macroscopic experiment and microscopic theory is the time correlation function formalism. Time correlation functions may be used to represent transport coefficients such as the diffusion coefficient, the viscosity and the thermal conductivity, as well as spectral line shapes and other experimental observables. The relationship between the time correlation functions and macroscopic behavior which can be used to treat the general use of the formalism has been provided by Onsager(4) in his response-relaxation analysis. The interest here is in the specific case of the diffusion of a tagged particle in a fluid medium. This particular phenomenon can be easily related to the correlation function formalism without recourse to the Onsager methods(5); accordingly the discussion will be restricted to self-diffusion.

A time correlation function measures the relation of some property

A(t) at some time t_0 to some property B(t) at a later time τ. It is written as an average over an equilibrium distribution function

$$\langle A(t_0)B(\tau)\rangle = \int\int dr^N dp^N f_{eq}^N A(t_0) e^{+i\hat{L}(\tau-t_0)} B(t_0). \tag{48}$$

If the time t_0 is taken to be t=0, the notation for the correlation function can be abbreviated as $\langle A\, B(\tau)\rangle$ and the Liouville operator becomes $e^{-i\hat{L}\tau}$; this convention will be used throughout this work.

The self-diffusion coefficient, that is, the coefficient which describes the motion of a single tagged particle, can be obtained using Fick's law of diffusion

$$\partial_t P^{(1)}(r_1, v_1, t) = D^2 \nabla_r P^{(1)}(r_1, v_1, t) \tag{49}$$

where $P^{(1)}(r_1, v_1, t)$ is the specific probability distribution function for the tagged particle. The self-diffusion coefficient is D and it is assumed that D does not depend on the position of the particle. The solution to this equation is

$$P^{(1)}(r_1, v_1, t) = \frac{P^{(1)}(r_1, v_1, 0)}{2(\pi Dt)^{3/2}} e^{-(r(t)-r(0))^2/4Dt} \tag{50}$$

If an average of the change in position squared $(r(t)-r(0))^2 = \Delta r(t)^2$ is performed using $P^{(1)}(r_1, v_1, t)$, the result is

$$\langle \Delta r(t)^2 \rangle = 2dDt \tag{51}$$

where d is the dimensionality of the system.

Fick's law is a macroscopic law and the time t must be considered to be much larger than the microscopic time scale associated with the Liouville equation. The self-diffusion coefficient D can be determined by differentiating the above equation and taking the long-time limit

$$D = \lim_{t\to\infty} \frac{1}{2dt} \langle (\mathbf{r}_1(t)-\mathbf{r}_1(0))^2 \rangle$$

$$= \lim_{t\to\infty} \frac{1}{2d} \langle \mathbf{v}_1\cdot(\mathbf{r}_1(t)-\mathbf{r}_1(0))\rangle$$

$$= \lim_{t\to\infty} \frac{1}{2d}\int_0^t d\tau \langle \mathbf{v}(t)_1\cdot\mathbf{v}(\tau)_1 \rangle$$

$$= \frac{1}{d}\int_0^\infty d\tau \langle \mathbf{v}_1\cdot\mathbf{v}_1(\tau) \rangle \qquad (52)$$

The correlation function given above is the velocity auto-correlation function. The integral of a self-correlation function over all time gives rise to a relaxation time or correlation time for the correlation function variable. If the variable relaxes exponentially in time, with a relaxation time of τ_e, the time dependence is given by e^{-t/τ_e}. The self-diffusion coefficient is seen to be directly related to the velocity relaxation time.

For non-spherical molecules, an angular velocity ω_1 will be present along with the linear velocity. A rotational diffusion constant D_R analogous to the self-diffusion constant can be defined as

$$D_R = \frac{1}{d}\int_0^\infty d\tau \langle \omega_1(0)\cdot\omega_1(t) \rangle. \qquad (53)$$

The correlation times used in the diffusion coefficient definitions can be calculated using the B-E equation and a moment expansion of the distribution function. The specific case of the velocity relaxation time will be considered.

The time-dependent distribution function $f^{(1)}(1,t)$ is expanded about the singlet equilibrium distribution function $f_{eq}(1)$

$$f^{(1)(*)}(1,t) = f_{eq}(1)\ \{\ 1 + \frac{d\ \mathbf{v}_1^{(*)}\cdot\mathbf{v}(t)}{\langle \mathbf{v}_1\cdot\mathbf{v}_1 \rangle}\ \}. \qquad (54)$$

where $\upsilon(t)$ represents $\int d\mathbf{r}_1 d\mathbf{v}_1\ \mathbf{v}_1 f^{(1)}(1,t)$; the parenthetical asterisks indicate the form of the expansion of the pre-collisional singlet distribution function and d remains the dimensionality of the system. The function $f^{(1)}(2,t)$ is approximated by the equilibrium singlet distribution function $f_{eq}(2)$ and $\chi(\mathbf{r}_s,\tau)$ becomes the equilibrium configuration distribution function at the surface of the particle $g(\mathbf{r}_s)$. The B-E equation, as given by eqn. (47), is multiplied by $\mathbf{v}_1$ and integrated over the velocity of particle 1 to give

$$\begin{aligned}\int\int d\mathbf{v}_1 d\mathbf{r}_1\ (\partial_t + i\hat{L}_1) f^{(1)}(1,t)\mathbf{v}_1 &= \int\int\int\int_{\mathbf{k}\cdot\mathbf{g}<0} d\mathbf{v}_1 d\mathbf{r}_1 d\mathbf{v}_2 J d\mathbf{k} \\ &(\mathbf{k}\cdot\mathbf{g}) g(\mathbf{r}_s) f^{(1)}(1,\tau) f^{(1)}(2,\tau)\mathbf{v}_1 \\ &+ \int\int\int\int_{\mathbf{k}\cdot\mathbf{g}>0} d\mathbf{v}_1 d\mathbf{r}_1 d\mathbf{v}_2 J d\mathbf{k} (\mathbf{k}\cdot\mathbf{g}) g(\mathbf{r}_s) f^{(1)*}(1,\tau) f^{(1)*}(2,\tau)\mathbf{v}_1 .\end{aligned} \tag{55}$$

Note that in this equation $f^{(1)}(1,t)$ is written as a function of velocity rather than momentum; the B-E equation is equally valid in this form. The integral on the left hand side results in

$$\begin{aligned}\partial_t \upsilon(t) + \nabla_{\mathbf{r}_1} \cdot \int\int d\mathbf{v}_1 d\mathbf{r}_1\ \mathbf{v}_1 \cdot \mathbf{v}_1 f^{(1)}(1,t) &= \int\int\int\int_{\mathbf{k}\cdot\mathbf{g}<0} d\mathbf{v}_1 d\mathbf{r}_1 d\mathbf{v}_2 \\ J d\mathbf{k}\ (\mathbf{k}\cdot\mathbf{g}) g(\mathbf{r}_s) f^{(1)}(1,\tau) f^{(1)}(2,\tau)\mathbf{v}_1 \\ + \int\int\int\int_{\mathbf{k}\cdot\mathbf{g}>0} d\mathbf{v}_1 d\mathbf{r}_1 d\mathbf{v}_2 J d\mathbf{k}\ (\mathbf{k}\cdot\mathbf{g}) g(\mathbf{r}_s) f^{(1)*}(1,\tau) f^{(1)*}(2,\tau)\mathbf{v}_1 .\end{aligned} \tag{56}$$

The second term on the left hand side will vanish under the $\mathbf{r}_1$ integration. The moment expansion for $f^{(1)}(1,t)$ can be substituted into the above equation

$$\begin{aligned}\partial_t \upsilon(t) = &\int\int\int\int_{\mathbf{k}\cdot\mathbf{g}<0} d\mathbf{v}_1 d\mathbf{r}_1 d\mathbf{v}_2 J d\mathbf{k}\ (\mathbf{k}\cdot\mathbf{g}) g(\mathbf{r}_s) f_{eq}(1) f_{eq}(2) \\ &\mathbf{v}_1 \{\ 1 + \frac{d\ \mathbf{v}_1 \cdot \upsilon(t)}{\langle \mathbf{v}_1 \cdot \mathbf{v}_1 \rangle}\ \} + \int\int\int\int_{\mathbf{k}\cdot\mathbf{g}>0} d\mathbf{v}_1 d\mathbf{r}_1 d\mathbf{v}_2 J d\mathbf{k} \\ &(\mathbf{k}\cdot\mathbf{g}) g(\mathbf{r}_s) f_{eq}(1) f_{eq}(2)\mathbf{v}_1 \{\ 1 + \frac{d\ \mathbf{v}_1^* \cdot \upsilon(t)}{\langle \mathbf{v}_1 \cdot \mathbf{v}_1 \rangle}\ \}.\end{aligned} \tag{57}$$

If $\mathbf{k}\cdot\mathbf{g}$ is replaced by $-\mathbf{k}\cdot\mathbf{g}$ in the first integral, the result is equivalent to integration of the pre-collisonal velocities over $\mathbf{k}\cdot\mathbf{g}>0$. The two integrals can be combined to give

$$\partial_t \upsilon(t) = \iiint_{\mathbf{k}\cdot\mathbf{g}<0} dv_1 dv_2 J d\mathbf{k}\ (\mathbf{k}\cdot\mathbf{g}) g(r_s) f_{eq}(1) f_{eq}(2) \frac{d\ \upsilon(t)}{\langle \mathbf{v}_1\cdot\mathbf{v}_1\rangle} \{\mathbf{v}_1^*\cdot\mathbf{v}_1^* - \mathbf{v}_1\cdot\mathbf{v}_1^*\}. \tag{58}$$

The quantity $\{\mathbf{v}_1^*\cdot\mathbf{v}_1^* - \mathbf{v}_1^*\cdot\mathbf{v}_1\}$ can be written as

$$\tfrac{1}{2}(\mathbf{v}_1^* + \mathbf{v}_2^* + \mathbf{v}_1^* - \mathbf{v}_2^*)\cdot(\mathbf{v}_1^* - \mathbf{v}_1), \tag{59}$$

The velocity of particle 2 has been added and subtracted; this produces no net change but will aid in the simpification of the integral in eqn. (58). The quantity within the first set of parentheses is the sum of the total linear momentum of the two particles and the relative velocity of the two particles in the absence of angular momentum. Note that the neglect of angular momentum will limit the application of further simplification to spherical particles. Upon integration, the total linear momentum will vanish because it is a collisional invariant. The relative velocity is $\mathbf{g}$ and the difference between the pre- and post-collisional velocities of particle 1 is $-2\mathbf{k}(\mathbf{k}\cdot\mathbf{g})$. The substitution of these relations into eqn. (58) yields

$$\partial_t \upsilon(t) = -\iiint_{\mathbf{k}\cdot\mathbf{g}<0} dv_1 dv_2 J d\mathbf{k}\ (\mathbf{k}\cdot\mathbf{g})^3\ g(r_s) f_{eq}(1) f_{eq}(2) \upsilon(t)/\langle v_1^2\rangle. \tag{60}$$

The B-E equation prescribes that the velocity decay exponentially with a relaxation time τ_v, that time can be determined from the above equation using

$$1/\tau_v = \iiint_{\mathbf{k}\cdot\mathbf{g}<0} dv_1 dv_2 J d\mathbf{k}\ (\mathbf{k}\cdot\mathbf{g})^3\ g(r_s) f_{eq}(1) f_{eq}(2)/\langle v_1^2\rangle. \tag{61}$$

This equation can be used to describe velocity relaxation and, hence, the self-diffusion coefficient in systems of hard spheres which can be

treated under the conditions applicable to the Boltzmann-Enskog equation. It will be used in Chapter 4 in an analysis of diffusion in a Lorentz gas.

In this chapter, a number of general relations have been obtained for the equilibrium and non-equilibrium behavior of systems made up of rigid convex bodies. These general expressions will be evaluated for the specific materials of interest as the need arises.

REFERENCES FOR CHAPTER 2

1. D. A. McQuarrie, 'Statistical Mechanics', Harper and Row, New York (1976).

2. D. K. Hoffman and C. F. Curtiss, Phys. Fluids 7, 1887 (1964).

3. T. Kihara, Adv. Chem. Phys. 5, 147 (1963).

4. L. Onsager, Phys. Rev. 37, 405 (1931); 38, 2265 (1931).

5. J. R. Dorfman and H. van Beijeren in 'Statistcal Mechanics, Part B: Time-Dependent Prcoesses', edited by B. J. Berne, Plenum Press, New York (1977).

CHAPTER 3
STRUCTURE OF THE ELLIPSE-DISK FLUID

A. Introduction

Liquid structure is often described in terms of the radial distribution function g(r) given by eqn (15) of chapter 2. For a liquid in which all the particles are spherical, the packing about an arbitrarily chosen particle is isotropic and an orientation-independent radial distribution represents the structure. The simplest system that could be expected to display an orientation-dependent distribution function would be one in which a single anistropic particle was surrounded by spherically symmetric particles. The presence of the anisotropic particle will cause a disturbance of the normal isotropic arrangement of the particles in the liquid. A Monte Carlo study on a two-dimensional liquid consisting of a single ellipse in a bath of disks was undertaken to investigate packing in anisotropic molecular liquids. For this system, information about the radial distribution function and the angle-dependent distribution of disks about the ellipse was combined to provide an indication of the disruption of the isotropic packing of the disk particles in the neighborhood of an anisotropic particle.

This chapter describes a Monte Carlo investigation of a two-dimensional fluid comprised of an ellipse in a bath of disks. An introduction, primarily a review of previous simulations of hard convex body fluids, is given, followed by a discussion of the Monte Carlo technique itself, scaled particle theory, the details of this simulation study and a discussion of the results of the study in

relation to scaled particle theory predictions.

The present Monte Carlo study is an investigation of the angular correlations of the positions of the disk particles in the vicinity of the ellipse expressed in terms of the surface-to-surface distance between the particles rather than the center-to-center distance. Angular correlations in fluids are often investigated via a spherical harmonic expansion about the distance between molecular centers (1). This method has proven useful because the harmonics may be used to calculate physical properties and can be easily determined in computer simulations. However, for anisotropic molecules the convergence of the spherical harmonic expansions is slow for small center-to-center distances. This is because the center-to-center distance between two nonspherical particles in surface contact will vary with the relative orientation of the particles and the rdf of a given relative orientation may be discontinuous for some values of the center-to-center distance. For example, for two ellipsoidal molecules of semimajor axis b and semiminor axis c in a head-to-head configuration, the rdf must have a value of zero when the center-to-center distance r is less than 2b, however, for such molecules in a side-to-side configuration, the rdf may be greater than zero when r is less than 2b but larger than 2a. In terms of the

distance between molecular surfaces, the rdf will be a smooth, continuous function even for particles in contact, regardless of the relative orientation of the particles; expansion of the rdf about the surface-to-surface distance should provide a convergent series.

B. Literature survey

Previous Monte Carlo simulations of fluids of hard convex bodies have focused on neat fluids of ellipses(2), of spherocylinders(3-8), or on equimolar mixtures of spherocylinders and spheres(9,10). When angular correlations have been determined by these studies, they have generally been couched in terms of a spherical harmonic expansion in the center-to-center distance and the relative orientation of two spherocylinders, in contrast to the relative coordinates to be used in the present study.

Vieillard-Baron (2) has studied a two-dimensional liquid of highly anisotropic ellipses. The axial ratio of these ellipses was 6. The study was directed toward properties related to the phase transitions of a nematic liquid crystal. Three density-dependent phases were observed, a high-density solid-like phase, a nematic phase which exhibits orientational order, but no translational order, and a liquid phase. The pressure and the free energy of the system were also calculated. To facilitate these calculations, Vieillard-Baron was able to derive a 'contact function' which is zero only when two ellipses are in contact.

Monte Carlo studies of three-dimensional systems of hard spherocylinders have been carried out by Few and Rigby (3),

Vieillard-Baron (7), Monson and Rigby (8,9) and Boublik, Nezbeda and Trnka (4,5,6). The initial studies of these fluids by Few and Rigby (3) were shown to be incorrect by Boublik, et al (4) and more recent studies (4-9) should be consulted for correct data.

Vieillard-Baron (7) determined the equation of state for spherocylinders with a total length-to-breadth ratio, γ, of 3 and compared his results to existing scaled particle theory. Agreement between the computations and the SPT predictions was good for low and moderate densities; SPT is less accurate at high densities and underestimates the density at which the nematic transition occurs. The study of the $\gamma = 3$ system at high densities and a study of spherocylinders with $\gamma = 6$ at a moderate density proved impractical because of the amount of computer time required for these systems to reach equilibrium.

Boublik, Nezbeda and Trnka (4) and Boublik and Nezbeda (5) studied systems of spherocylinders with $\gamma = 2$ and 3. They determined the compressibility factors, P/nk_BT (where P is the pressure, n is the number of molecules and k_BT is Boltzmann's constant times the absolute temperature) and radial distribution function for these systems. Computer-calculated compressibilities were found to be systematically smaller than values predicted by SPT, but in good agreement with the data of Vieillard-Baron (7). As expected, the rdf displays features similar to those observed in the rdf of fluids comprised of spheres as determined using the Percus-Yevick equation(11) with corrections due to Verlet and Weiss (12). The two rdf differ, however in the position and width of the minima and maxima, even when

the spherocylinder rdf is converted to units analogous to those used in the spherical case.

The angular correlations in systems of spherocylinders were studied by Nezbeda (6) and by Monson and Rigby (8). Nezbeda's simulations involved particles with γ equal to 1.4,1.6 and 2.0; Monson and Rigby investigated spherocylinders with γ equal to 2 and 3. The angular correlations were expressed in terms of a series of spherical harmonics in R, the center-to-center separation, and the relative orientation of two spherocylinders. Both groups observed poor convergence of the series at distances less than the length of the spherocylinder. This lack of convergence is due to the discontinuity of the rdf in terms of the center-to center distance.

The radial distribution function and the compressibility for equimolar mixtures of spheres and spherocylinders with $\gamma = 2$ have been obtained in Monte Carlo studies by Monson and Rigby (9). Two types of mixtures were studied, one in which the volume of the spheres was equal to the volume of the spherocylinders and one in which the diameter of the hard spheres was equal to the breadth of the spherocylinders. The results of the compressibility calculations were compared to existing SPT predictions; agreement with the work of Pavlicek, et al. (10) was found to be good. From a calculation of the excess volumes of the mixture the authors concluded that the excess free energy of such mixtures is dependent upon the relative volumes of the components rather than on shape differences. Three kinds of rdf, based upon center-to-center particle separations, were calculated: a sphere-sphere rdf, a spherocylinder-spherocylinder rdf and a sphere-spherocylinder

rdf. The sphere-sphere rdf was similar to the distribution function of a pure hard sphere fluid, but some portions of the mixture rdf were observed to be out of phase in comparison to a hard sphere rdf. The spherocylinder-spherocylinder rdf was expanded in a series of spherical harmonics. For the mixture in which the particles were of equal breadth, the terms in the expansion are nearly identical to those observed in pure spherocylinder fluids at the same density. In contrast, the expansion in spherical harmonics of the spherocylinder-spherocylinder rdf for the mixture in which the particles are of equal volume gives rise to leading term different than that observed in the other mixture and in the pure fluid. The authors attribute this difference to the disruption in packing caused by the greater breadth of the spheres in relation to the spherocylinders. The sphere-spherocylinder rdf was expressed as a series of Legendre polynomials. The resummation of this series is well-behaved for configurations in which the spherocylinder and sphere are located in a 'head-on' arrangement, but for configurations in which the sphere is located closest to the cylinder portion of the spherocylinder, the lack of convergence and other anomolous behavior displayed in spherical harmonic rdf expansions is observed.

The angular distribution of disk particles in the simple dilute system studied here will be examined in terms of the surface-to-surface distance ι, described in Chapter 2. The Monte Carlo method of computer simulation will be used to determine the orientation of disks in contact with the ellipse particle with respect to the semi-major axis of the ellipse , along with the rdf in terms of ι, the

surface-to-surface distance.

C. The Monte Carlo Method

The basis of the Monte Carlo method is the use of random variables to solve mathematical problems. The method can be illustrated by the integration of an irregular function f(x). The integral I is defined by

$$I = \int_0^{\chi} f(x)dx$$

The function f(x) can be scaled such that the integration can be performed over the interval from 0 to 1

$$f'(x) = f(x)/f_{max}(x)$$

where χ is the maximum value of x and $f_{max}(x)$ is the maximum value of f(x). The new integral

$$I' = \int_0^1 f'(x)dx'$$

can be solved by a series of trials using random numbers supplied by a pseudorandom number generator. For each trial two random numbers between 0 and 1.0, q_1 and q_2, are chosen. The function is evaluated at $x = q_1$. The trial is counted as a success or a failure based on the value of q_2:

$f(q_1) < q_2$ failure

$f(q_1) \geq q_2$ success.

The value of the integral is then simply

$$I' = \frac{\text{number of successes}}{\text{number of trials.}}$$

The Monte Carlo method is superior to other numerical methods of

integration for functions with discontinuous derivatives or for multidimensional integration.

Although the use of Monte Carlo principles in problem solving was documented in 1873 (13) and in 1901 (14), the first systematic use of the technique was in 1944 by von Neumann and Ulam (15) to investigate the random diffusion of neutrons through fissile material. The code word Monte Carlo was coined for this project. In 1948 Metropolis, Fermi and Ulam (16) obtained Monte Carlo estimates of eigenvalues of the Schrödenger equation. The widely-used Metropolis algorithm was developed in 1953 by Metropolis, Rosenbluth, Rosenbluth, Teller and Teller(16) and applied to a simulation of a two-dimensional liquid of hard disks. This same algorithm was used in this work in a simulation of a two-dimensional liquid consisting of a single hard ellipse in a bath of disks.

The Metropolis algorithm models the behavior of a system governed by classical mechanics and pairwise-additive potentials. The system used is a square containing N particles. Because a finite number of particles is used, some consideration must be given to the edges of the sample region. The effect of the edges can be minimized, even for a sample containing a fairly small number of molecules, if periodic boundary conditions are employed. Periodic boundary conditions dictate that the square be surrounded by an infinite number of identical images of itself. A particle which leaves the defined region enters into another identical region of space. This can be viewed as the particle leaving from one side of the square and reentering from the opposite side. If N particles are placed within the square, the energy of the

system can be calculated from the interparticle potential

$$E = \sum_{i=j}^{N} \sum_{j}^{N} U(r_{ij}).$$

where r_{ij} is the separation between particles i and j and $U(r_{ij})$ is the separation dependent potential. For a canonical ensemble, statistical mechanical averages of an equilibrium system property F are defined by

$$< F > = \frac{\int F \exp(-E/k_B T) dr^N dp^N}{\int \exp(-E/k_B T) dr^N dp^N}$$

where $k_B T$ is the Boltzmann constant times the absolute temperature and (r^N, p^N) are the position and momenta coordinates of the N particles. The momentum coordinates may be integrated out if the properties of interest are dependent only on position and not on velocity. The integral which is left may be solved by the Monte Carlo technique; the integration is performed over a large number of computer-generated configurations. The averaging may be effected in either of two ways: the N particles may be placed in positions at random and each configuration given a weight $\exp(-U_N/k_B T)$ or the configurations may be chosen with a probability $\exp(-U_N/k_B T)$ and weighed evenly in the average.

The latter method is chosen for the hard particle system studied here. An initial lattice configuration of particles is altered by the movement of each of the particles by some random number. For systems with only hard potentials, the energy change ΔE following each move will be either 0 (when no two particles overlap) or ∞, (when two particles overlap). Moves which result in an overlap are discarded;

when this process has been completed for all of the particles, the resulting configuration is used in determining the desired average. The systematic movement of all the particles is repeated until a large number of configurations (10^5-10^6 in this case) have been included in the average.

D. Monte Carlo simulations of ellipse-disk fluid

The Monte Carlo calculations were undertaken on the OSU Chemistry Department VAX and the Boeing Computer Services Cray 1S. A run at moderate density typically required about 1 hour of time on the Cray and about 60 hours on the VAX. Because of the central role that the system-supplied pseudorandom number generator plays in MC, the library random number generator on each of the machines was tested for uniformity and randomness. The tests performed were a χ^2 test for uniformity, a serial test to determine the period of the random number generator and a runs-up test for randomness (17). These are considered to be the minimum tests which should be performed on a random number generator (17). The results of these tests on the library random number function on both the Cray and VAX were satisfactory.

The MC simulations were carried out on systems containing one ellipse in a bath of 89 disks. The ellipse was described by its semimajor and semiminor axes b and c, respectively. The disks had a radius of a. Three different ellipse geometries were studied; these were defined by axial ratios of 2,5 and 10. In all cases, the ellipse was of the same area as the disk, i.e., $bc = a^2$. Solvent density is measured in terms of the packing fraction $\rho^* = \pi a^2 N/A$ where A is

the area available to the N particles. The packing fraction of the systems studied covered a range from 0.05 to 0.60. At the lowest density the properties of the system should compare to those of a dilute gas and at the highest, the behavior should correspond to that of a dense liquid.

The Metropolis algorithm (16) was used to control the selection of configurations for averaging. For each new configuration an attempt was made to move each disk by an amount determined by two random numbers, q_1 and q_2, uniformly distributed on [-1.,1.]. The original coordinates of the particle (x_0,y_0) become $(x_0 + \alpha q_1, y_0 + \alpha q_2)$ where the parameter α is chosen for expediency. If approximately one-half of the moves are rejected (17), the initial lattice state will reach an equilibrium configuration quickly; α is chosen so that the rejection rate approaches one-half as nearly as possible. One of the aims of MC averaging is to maximize the amount of phase space which is sampled by the chosen configurations; thus for each new configuration rotation of the ellipse by an angle $\pi\beta q_3$ was alternated with translation. The parameter β was arbitrary and was chosen the same way α was chosen; q_3 is a random number between -1.0 and 1.0. The determination of overlap between disk particles was based on the distance between the centers of the particles, but for the ellipse, overlap was determined by the calculation of the surface-to-suface distance.

The calculation of the surface-to-surface distance ι between two convex figures is an analytic function only when figures are disks, so the calculation of the distance between the ellipse and the disk

required a numerical solution. The method selected for the present study involved the iterative determination of the minimum distance between the surface of the ellipse and the center of the disk. When the point on the surface of the ellipse which is closest to the disk is known, the surface normal at that point is also known. One of the properties of interest in this calculation was the angle θ that this surface normal makes with the director axis of the ellipse (See Figure 3.1). That quantity is easily calculated using this algorithm. The equation derived by Vieillard-Baron(2) which analytically determines whether there is overlap between two ellipses was not used in this work because it does not provide any information about the distance between two bodies not in contact and the focus of this work is on the orientational packing and the full radial distribution function for the ellipse.

At each density and for each of the differing ellipse geometries the MC program was used to generate 5×10^5 of the configurations described above. Averages were calcualated based on the last 4×10^5 configurations so as to minimize the effects of the initial lattice. Because of the smaller number of disk particles in the near vicinity of the ellipse particle, the averages for low density runs will provide results which are less accurate than those for high densities. For this reason runs at the lowest density used as many as 1×10^6 configurations.

The results of the simulations will be compared with predictions of Scaled Particle theory. Toward this end, a description of Scaled Particle Theory (SPT) and, in particular, the theory as it has been

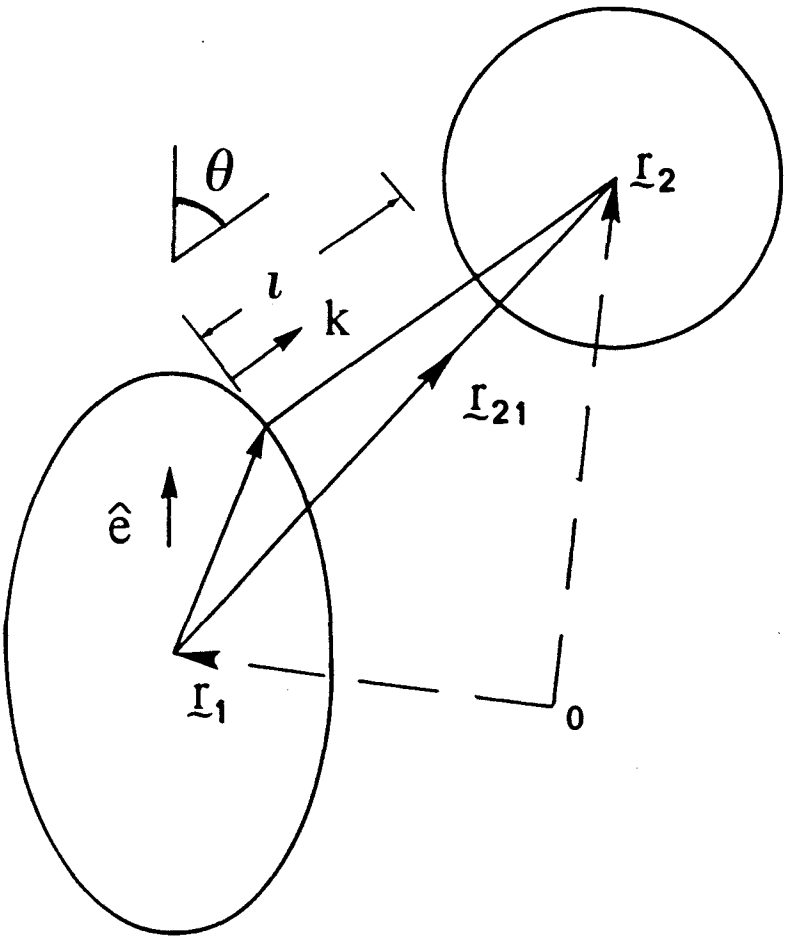

Figure 3.1 Definition of the angle θ.

developed for arbitrary convex bodies will be provided.

E. Scaled Particle Theory

Scaled particle theory was developed Reiss, Frisch and Lebowitz (18) in 1959 for the calculation of the equation of state for hard sphere fluids. It has since been applied to a number of materials, including two-dimensional rods and disks (19), liquid crystals (20) and general convex body systems (21,22,23). Most recently, SPT has been extended to the study of the orientation-dependent contact properties of convex bodies by She and Evans (23). The idea behind SPT is the addition of a virtual particle to a fluid using a coupling parameter related to the strength of the interaction between the virtual particle and the other particles in the system. The work required to include such a particle can be calculated and, from the work, a function G(r) which is related to the rdf can be determined.

A solution of N particles of diameter d, subject only to hard forces is considered. A virtual particle is added to the system; the total potential U, after addition of the virtual particle, will be the sum

$$U = U_{N+1} = \sum_{\substack{2 \\ i<j}}^{N} U(r_{ij}) + \sum_{2}^{N} U(r_{1j}, \xi)$$

where the first term represents the interaction potential of the intial N particle system and the second term is the potential due to the virtual particle. $U(r_{ij})$ is the separation-dependent potential and will be a Heaviside function on the contact surface for hard bodies. The potential for the scaled particle is defined such that

$$U(r_{ij},\xi) = \xi U(r_{ij}).$$

The coupling parameter ξ is also known as a scaling parameter and is the source of the term scaled in the name scaled particle theory. For the hard systems considered here, the use of the scaled interaction potential is equivalent to introducing an virtual particle with a radius λ dictated by, but not equal to, the scaling parameter.

The volume available to the virtual particle can be determined by considering the volume from which is excluded by the N particles of the system. An excluded volume surface of radius $d + \lambda$ can be drawn about the center of each of the system particles. The space which is not within any of the excluded volume surfaces is the free volume V_0 which the new particle might occupy. The probabilty of finding a cavity in this free volume which is large enough for the virtual particle will be given by

$$P_0(\lambda) = V_0/V$$

where V is the total volume of the system. From fluctuation theory, it is known that the probability of finding a void of appropriate volume is $P_0(\lambda) = \exp(-W(\lambda)/k_BT)$

where $W(\lambda)$ is the work required to introduce the virtual particle into the system. The two equations can be combined to give an expression for the reversible work necessary to add the virtual particle of radius λ to the fluid.

$$W(\lambda) = -k_BT \ln(V_0/V).$$

The work may be related to a function $G(\lambda)$ where $G(\lambda)$ is a measure of the number of particles on the excluded volume surface of the virtual particle. The quantity $\rho G(\lambda)$, where ρ is the number density of

particles in the N particle fluid, is the concentration of particles on the excluded volume surface. The probability that a molecule will be found within the spherical shell of differential volume $4\pi\lambda^2 d\lambda$ enclosing the excluded volume of the virtual particle is then $4\pi\lambda^2 \rho G(\lambda) d\lambda$ and the probability that the differential volume element will not contain a molecule is $1 - 4\pi\lambda^2 \rho G(\lambda) d\lambda$. The probability that both the excluded volume of the virtual particle itself and the differential volume element surrounding it will be empty is

$$P_0(\lambda + d\lambda) = P_0(\lambda)(1 - 4\pi\lambda^2 \rho G(\lambda) d\lambda) = P_0 + (\partial P_0/\partial\lambda) d\lambda$$

which is equivalent to

$$\frac{\partial \ln P_0}{\partial \lambda} = - 4\pi\lambda^2 \rho g(\lambda).$$

This leads to an integral equation for $P_0(\lambda)$:

$$P_0(\lambda) = \exp\left(-\int_0^\lambda 4\pi\Xi^2 \rho G(\Xi) d\Xi \right)$$

where the probability is normalized by the condition that $P_0(0)$ be equal to one.

It should be noted that $G(\lambda)$ is closely related to the radial distribution function $g(r)$ and, in fact, when λ is equal to d, the radius of the fluid particles, $G(d)$ will be equal to $g(d)$, the radial distribution function at contact. Constraints on $G(\lambda)$ and on its derivatives are used to obtain the value of $G(\lambda)$ and, hence, $g(\lambda)$. Among the constraints on $G(\lambda)$ are those introduced by the macroscopic pressure when $\lambda = \infty$ and those imposed by the excluded volume for $\lambda < d$. Approximate contact radial distributions have been obtained in this fashion for spherical particles.

Modifications to traditional SPT described above have been made

to accomodate general hard convex bodies (HCB). Angle-averaged distribution functions for HCB have been obtained (21,22) by the replacement of the spherical volume used in the determination of the cavity size by an appropriate convex body volume along with similar adjustments to the surface area and radius of curvature. She and Evans (23) have provided a version of SPT which can be used to obtain orientation-dependent properties of a single convex body in a fluid of spheres. The predictions of this theory will be compared to the MC calculations discussed in this chapter.

The modifications that She and Evans made to existing SPT had as a central point the concept of differential bulging. The work required to introduce an arbitrary scaled convex body into a system of N spherical particles is determined. An infintesimal bulge is then created at a specific locale on the surface of the particle and the additional work required to create the bulge calculated. Constraints on g(r) at the location of the bulge, found from the consideration of the required work and from geometric arguments, provide a method for the determination of the orientation-dependent contact position distribution function of the spherical particles. This theory has been applied to the calculation of properties of the dilute ellipse-disk fluid (24) which is the subject of the Monte Carlo investigation reported here. The simulation and SPT results will be discussed in the next section.

F. Results and discussion

Monte Carlo computer simulations were performed on systems containing a single ellipse in a bath of spheres. Three different ellipse geometries were considered; the axial ratio of the ellipse, that is, the ratio of the semi-major ellipse axis to the semi-minor ellipse axis was either 2, 5, or 10. The density was varied from the dilute gas range (packing fraction = 0.05) to the liquid range (packing fraction = 0.60). For each system, the full rdf out to three disk particle diameters was calculated and an average of the orientation of disk particles in contact with the ellipse was determined. The specific orientational variable considered was the cosine of the angle that the vector normal to the surface at the point of contact makes with the semi-major or director axis of the ellipse, referred to as cos θ. Averages of this variable and its even moments $\cos^{2m}$ were calculated for m = 1 to 10. These $g(\iota)$ and cos θ results were combined in a polynomial expansion about the even moments of cos θ to give an expression for the angle dependent distribution of disk particles $g(\iota,\mathbf{k})$.

The angle-averaged rdf determined for the ellipse particle was found to be quite similar to the rdf for a liquid of disks at the same density. Examination of Figures 3.2-3.4 demonstrates that at low densities the pure disk rdf is superimposable upon the ellipse-disk rdf except in the vicinity of the ellipse itself. Differences in the two distribution functions are apparent only when the surface-to-surface distance is less than 0.3 of a disk diameter and then only for the most

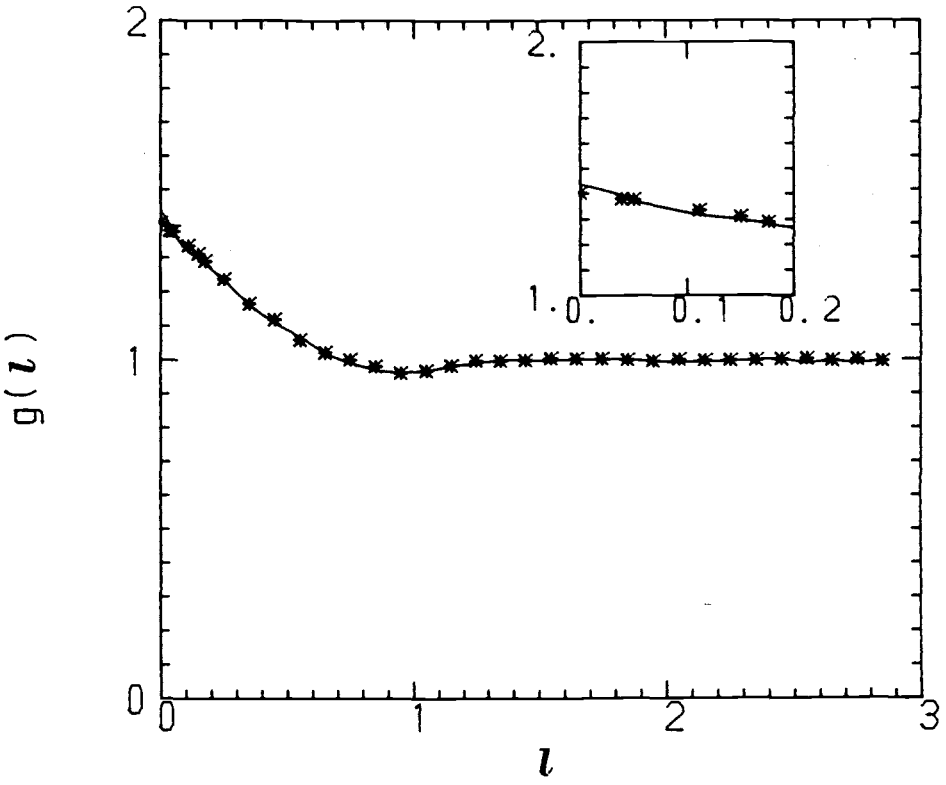

Figure 3.2 The radial distribution function g(ι) as a function of the surface-to-surface distance ι at a packing fraction ρ^* of 0.20 as calculated by MC simulation. The asterisks represent the rdf for a single ellipse of axial ratio 2 in a bath of disks of like area. The line is the rdf for an analogous pure disk fluid. The inset is a blow-up of the rdf in the region closest to the particle surface.

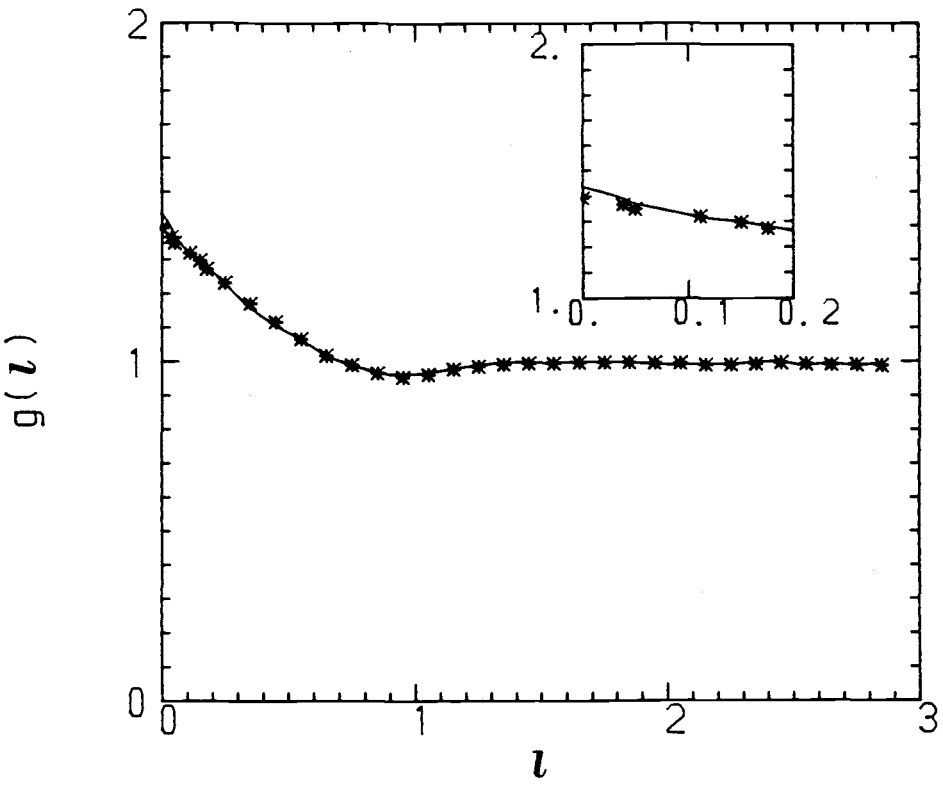

Figure 3.3 The same as figure 3.2, but the axial ratio of the ellipse is 5.

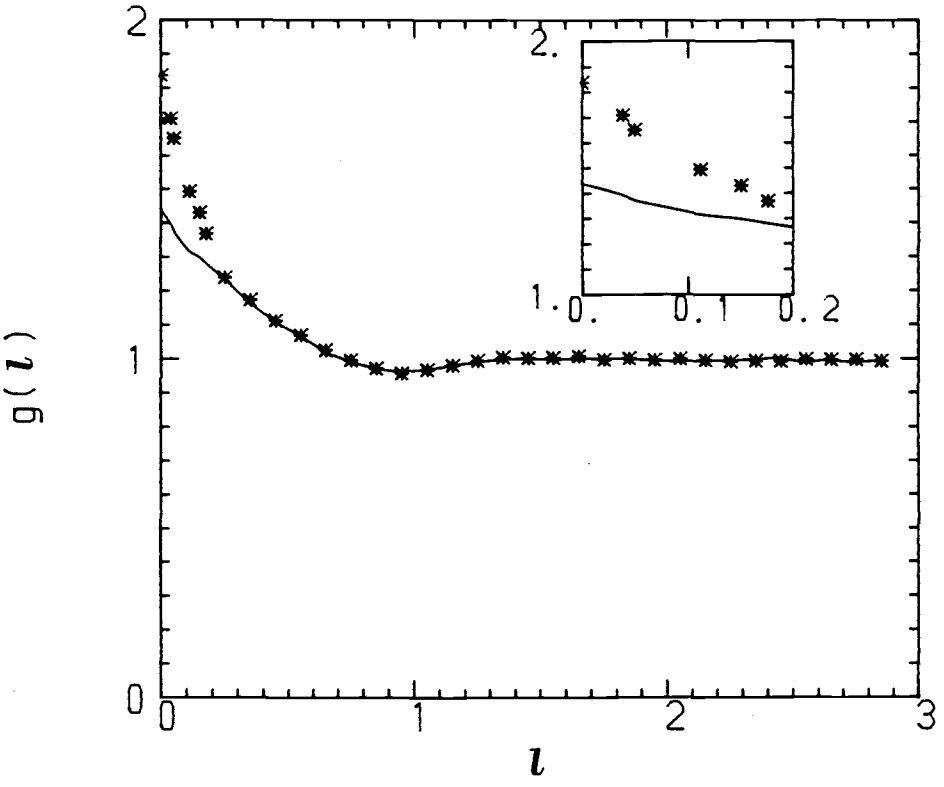

Figure 3.4 The same as figure 3.2, but the axial ratio of the ellipse is 10.

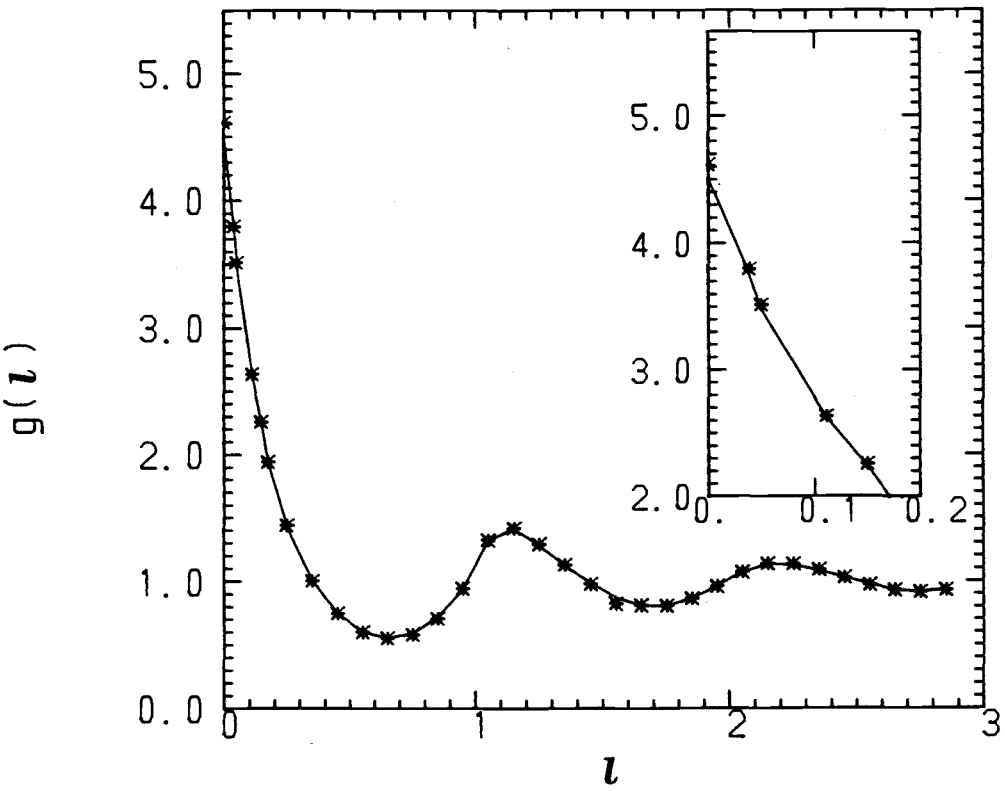

Figure 3.5 The radial distribution function g(ι) as a function of the surface-to-surface distance ι at a packing fraction ρ^* of 0.60 as calculated by MC simulation. The asterisks represent the rdf for a single ellipse of axial ratio 2 in a bath of disks of like area. The line is the rdf for an analogous pure disk fluid. The inset is a blow-up of the rdf in the region closest to the particle surface.

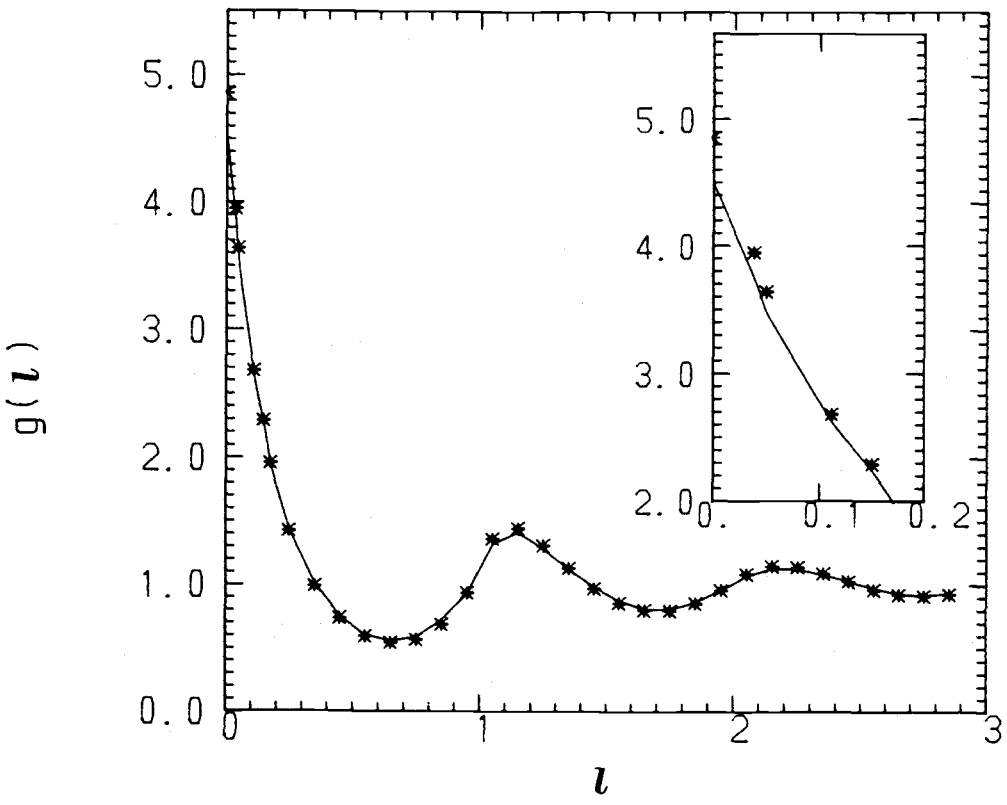

Figure 3.6 The same as figure 3.5, but the axial ratio of the ellipse is 5.

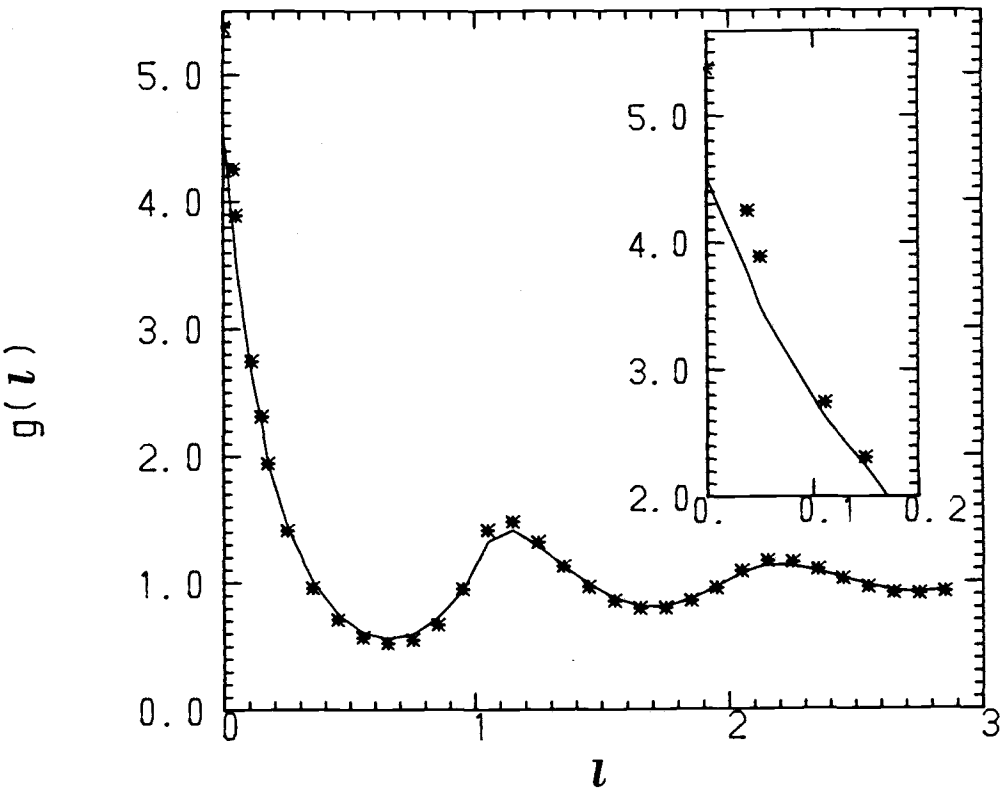

Figure 3.7 The same as figure 3.5, but the axial ratio of the ellipse is 10.

anisotropic of the ellipses. At the highest density considered (packing fraction = 0.6, Figures 3.5-3.7), the differences between the two distribution functions, although slight, are visible at surface-to-surface distances greater than a disk diameter and, as expected, increase in magnitude as the axial ratio of the ellipse increases. The contact value of the distribution function would be expected to be greater for an ellipse than it would for a disk of equal volume because of the greater amount of surface area available on the ellipse. The discrepancy between the pure disk rdf and the ellipse-disk rdf at low densities is due to this effect alone and hence localized to the regions very close to the ellipse. At higher densities, it is clear that the packing of the disks is affected well away from the ellipse. The maxima and minima of the rdf for the ellipse-disk are more pronounced than those of the disk rdf, perhaps indicating a more solid-like configuration and what might be considered the earliest stages of orientational order.

The values obtained for the contact value of $g(\iota)$, $g(0)$, are given in Table 3.1. The agreement between the SPT results and the MC results is good at low densities and for the least anisotropic of the ellipses. Values for $g(\iota)$ for ι not on the surface of the ellipse were obtained by counting the number of disk molecules whose centers were within a distance $\iota \pm \delta\iota$ where ι for ι ranges from 0.05 to 2.95 disk diameters in intervals of 0.1 disk diameters and $\delta = 0.05$ disk diameters and then using appropriate numerical differentiation formulas. The contact values $g(0)$ were determined by fitting the first three $g(\iota)$ values to an exponential $ae^{-c\iota}$ where a and c are arbitrary

Table 3.1. g(0) SPT and MC Results

axial ratio	packing fraction	g(0) SPT	g(0) MC
1	0.05	1.083	1.066
1	0.20	1.422	1.439
1	0.35	1.995	1.989
1	0.50	3.091	3.071
1	0.60	4.510	4.581
2	0.05	1.086	1.081
2	0.20	1.435	1.404
2	0.35	2.010	1.972
2	0.50	3.066	3.097
2	0.60	4.354	4.613
5	0.05	1.107	1.044
5	0.20	1.551	1.392
5	0.35	2.319	2.005
5	0.50	3.814	3.178
5	0.60	5.767	4.852
10	0.05	1.139	1.349
10	0.20	1.735	1.837
10	0.35	2.806	2.639
10	0.50	4.998	4.157
10	0.60	8.001	5.371

constants determined by the curve fitting procedure.

It should be noted that the MC number given here is five percent greater than the value determined by Chae, Rae and Rae (CRR) (25) for the identical system. The SPT predictions are in better agreement with the CRR number than with the present value; this should be considered a reflection of the inaccuracy in the determination of the value of g(0). As the density of the liquids increases, the agreement between the SPT predictions and the MC results would be expected to deteriorate

and this is borne out by the data. Agreement is fair, however, for most of the densities studied. The SPT predictions seem to consistently overestimate the MC values at high densities and the difference between the SPT and MC values is largest for the most anisotropic of the ellipses.

The orientational properties of the fluid are expressed as the averages of the cos of the angle between the director axis of the ellipse and the surface normal at the point of contact between an ellipse and a disk. The averages of the moments of cos θ given in Figures 3.8 - 3.10 are

$$T_{2m} = \langle \cos^{2m}(\theta) \rangle / \langle \cos^{2m}(\theta) \rangle_{x=0}$$

where x is the packing fraction and the denominator represents the average value of the moment at zero denstiy. From strictly geometrical considerations, these zero-density orientational averages for an ellipse would be expected to be lower than they would be for a disk. This can be illustrated using the surface normals to a convex body which lie in the first quadrant and recognizing that the average values of $\cos^{2m}\theta$ and its moments will be the same for all quadrants. In the first quadrant are surface normals for which θ will be between 0 and π/2. For a disk particle, the angle θ will be evenly distributed about π/4, but for an ellipse, a greater portion of the surface normals will correspond to θ greater than π/4 than to θ less than π/4. Surface normals with θ greater than π/4 lie on the 'flat' portion of the ellipse. The average value of $\cos^{2m}$ will be accordingly reduced in comparison to the same average over a disk surface; this reduction is reflected in the Jacobian J used to effect the transformation from

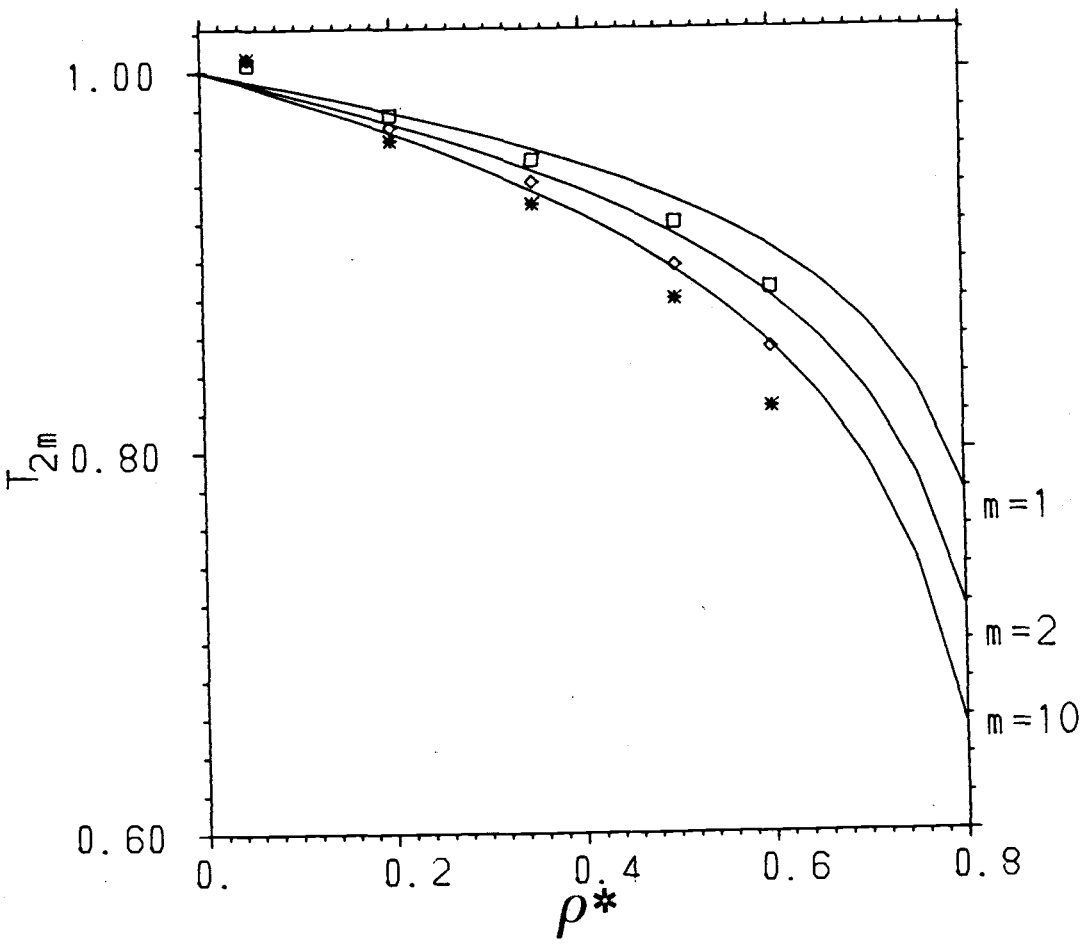

Figure 3.8 The moments $T_{2m} = \langle\cos^{2m}(\theta)\rangle / \langle\cos^{2m}(\theta)\rangle_{\rho^*=0}$ as a function of the packing fraction ρ^* for an ellipse with an axial ratio of 2. The lines are the values as calculated using SPT; m for each line is indicated at the right. The MC results are given by the squares (m=1), diamonds (m=2) and asterisks (m=10).

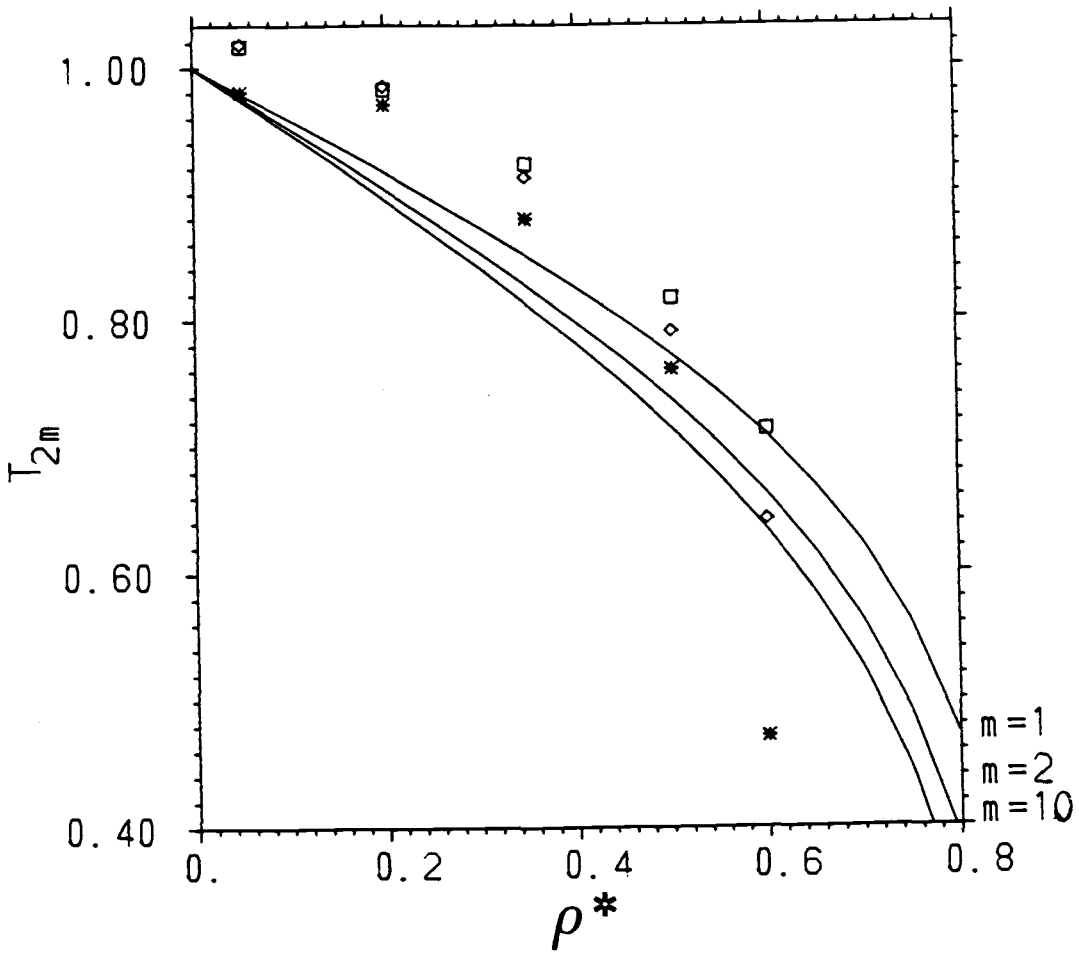

Figure 3.9 The same as figure 3.8, but the ellipse has an axial ratio of 5.

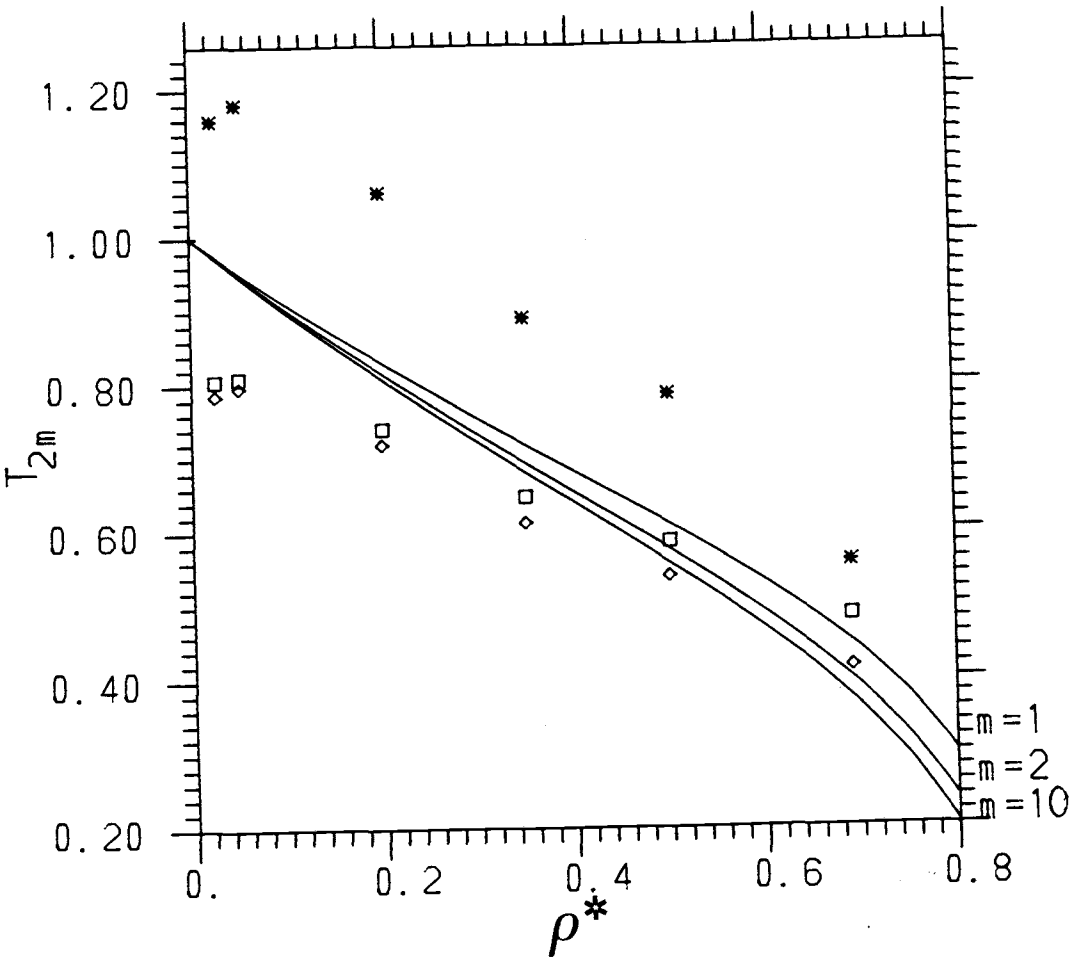

Figure 3.10 The same as figure 3.8, but the ellipse has an axial ratio of 10.

center-to-center coordinates to the coordinates **k**, the surface normal, and ι, the surface-to-surface separation. The expression for the Jacobian is given in eqn. (26) of chapter 2. All averages reported here are given relative to the exact zero-density values. The latter can be computed directly and without approximation from purely geometric arguments. The variations of T_{2m} from unity will then be a measure of multi-particle correlations rather than a function of the geometric factor J.

The moments of cos θ from the MC simulations are plotted along with the SPT result in Figures 3.8 - 3.10. For all of the ellipse-disk systems studied, the values of T_{2m} decrease as the density of the system increases. This trend indicates that at the higher densities, the disks which come into contact with the ellipse are likely to be aligned along the regions of the ellipse surface with the least curvature. The effect is amplified for the more anisotropic ellipses. The SPT predictions are in agreement qualitatively for all of the ellipses and quantitatively for the ellipses with axial ratios of two and five.

The information about the angular correlations in the fluid may be combined with the contact radial distribution function g(0) to give an orientation-dependent g(0). This can be accomplished through an orthogonal function expansion of the radial distribution function. The expansion in terms of a set of polynomials, $e_i(\theta)$ can be written

$$g(\theta,0) = g_{iso}(0)\{ 1 + \Sigma\, e_i(\theta)w_i(x) \}$$

where $g_{iso}(0)$ is the isotropic contact rdf given by Table 3.1 and $w_i(x)$ are the density dependent expansion coefficients. The

Table 3.2

Coefficients of the polynomials e^1 and e^2

Axial Ratio	packing fraction	$w_1(x)$	$w_2(x)$
2	0.05	0.0419	0.0052
2	0.20	-0.0244	0.0072
2	0.35	-0.0502	0.0139
2	0.50	-0.0859	0.0155
2	0.60	-0.1231	0.0238
5	0.05	0.0124	0.0052
5	0.20	-0.0132	0.0178
5	0.35	-0.0575	0.0260
5	0.50	-0.1360	0.0570
5	0.60	-0.2134	0.0206
10	0.05	-0.1162	-0.0036
10	0.20	-0.1519	0.0688
10	0.35	-0.2063	0.0798
10	0.50	-0.2428	0.0854
10	0.60	-0.2519	0.0831

coefficients $w_i(x)$ were found to be small, only $w_1(x)$ differed significantly from 0.0. The coefficients $w_1(x)$ and $w_2(x)$ are given in Table 3.2. The first of the orthonormal polynomials

$$e_1(\theta) = \{ \cos^2\theta - \langle\cos^2\theta\rangle_0 \}/\{ \langle\cos^4\theta\rangle_0 - \langle\cos^4\theta\rangle_0^2 \} \qquad (1)$$

was used to calculate the values of $T_{2m}(x)$ given in Table 3.3. The good agreement between the MC results and the polynomial results indicates that the contact rdf can be approximated by a small set of orthogonal functions expressed in terms of the surface-to-surface distance and orientational polynomials orthogonal with respect to the Jacobian, J. Expressed in this way, the rdf is nearly isotropic even for highly elongated molecules, in contrast to the rdf in terms of the

Table 3.3. Values of $T_{2m}(x)$ from Monte Carlo (MC) calculations and those from Eqn. (1) with one orientational polynomial(Poly) .

		m = 1		m = 2		m = 10	
Axial Ratio	packing fraction	MC	Poly	MC	Poly	MC	Poly
2	0.05	1.004	1.007	1.007	1.005	1.007	1.007
2	0.20	0.977	0.977	0.971	0.970	0.964	0.960
2	0.35	0.953	0.953	0.942	0.937	0.930	0.917
2	0.50	0.920	0.920	0.898	0.893	0.880	0.858
2	0.60	0.885	0.885	0.854	0.846	0.823	0.796
5	0.05	1.017	1.017	1.019	1.021	0.981	1.026
5	0.20	0.982	0.982	0.985	0.977	0.970	0.971
5	0.35	0.923	0.923	0.912	0.901	0.880	0.878
5	0.50	0.817	0.817	0.791	0.767	0.761	0.710
5	0.60	0.713	0.713	0.642	0.634	0.472	0.546
10	0.05	0.803	0.803	0.785	0.761	1.165	0.708
10	0.20	0.739	0.739	0.721	0.682	1.056	0.621
10	0.35	0.643	0.643	0.614	0.572	0.879	0.485
10	0.50	0.584	0.584	0.539	0.499	0.788	0.398
10	0.60	0.583	0.583	0.538	0.493	0.770	0.389

center-to-center distance. This is consistent with the results of studies of the spherical harmonic expansion of the rdf for non-spherical molecules using a Gaussian overlap model for the intermolecular potential and the distance between equipotential surfaces(26,27) or the distance between the repulsive cores(27) of the molecules as expansion variables which resulted in convergent expansions series.

In additon to the systems listed, a single fluid of moderate density (packing fraction = 0.50) containing an ellipse of axial ratio 2 with an area one-half the area of the disks was simulated. The contact rdf for this system was smaller than the contact rdf of the corresponding pure disk fluid, reflecting the smaller surface area of the ellipse relative to the disk. The full radial distribution function reverted to that of the pure disk fluid within a few tenths of a disk diameter (Figure 3.11). The angular correlations for this system were similar to those observed for the analogous system in which the ellipse was of the same area as the disks.

The MC simulations of a dilute ellipse-disk fluid in two dimensions have provided insight into the orientational and structural properties of isotropic fluids perturbed by the presence of a single anisotropic particle. The ellipse particle significantly disrupted the normal isotropic packing of the disk particles only in the region close to the ellipse particle itself. An analysis of the packing in the region of the ellipse indicates that the disk particles tend to arrange themselves along the least-curved portions of the ellipse surface. The radial distribution function was obtained in terms of ι, the surface

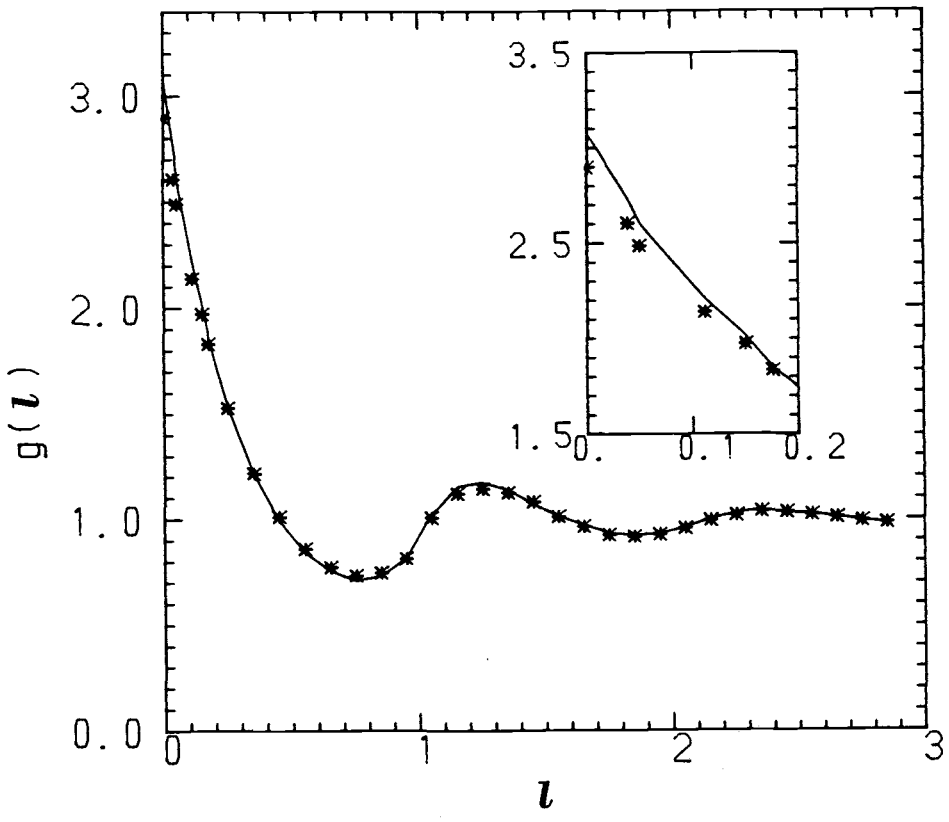

Figure 3.11 The radial distribution function g(ι) as a function of the surface-to-surface distance ι at a packing fraction ρ^* of 0.50 as calculated by MC simulation. The asterisks represent the rdf for a single ellipse of axial ratio 2 in a bath of disks; the ellipse has an area equal to one-half the area of a disk. The inset is a blow-up of the rdf in the region closest to the particle surface.

separation of the particles, and an orthogonal polynomial expansion of the contact rdf employed; demonstrating the utility of the surface-to-surface coordinate system in the analysis of convex particle fluids. The MC results compared favorably with the SPT predictions for the system and with previous simulations of convex body fluids (2-10).

REFERENCES FOR CHAPTER 3

1. C. G. Gray and K. E. Gubbins, 'Theory of Molecular Fluids, Volume 1. Fundamentals', Oxford University Press, New York (1984).

2. J. Viellard-Baron, J. Chem. Phys. 56, 4729 (1972).

3. G. A. Few and M. Rigby, Chem. Phys. Lett. 20, 433 (1973).

4. T. Boublik, I. Nezbeda, and O. Trinka, Czech. J. Phys. B26, 1081 (1976).

5. I. Nezbeda and T. Boublik, Czech. J. Phys. B28, 353 (1978).

6. I. Nezbeda, Czech. J. Phys. B30, 601 (1980).

7. J. Viellard-Baron, Molecular Physics 28, 809 (1974).

8. P. A. Monson and M. Rigby, Chem. Phys. Lett. 58, 122 (1978).

9. P. A. Monson and M. Rigby, Molecular Physics 39, 977 (1980).

10. J. Pavlicek, I. Nezbeda and T. Boublik, Czech. J. Phys. 29B, 1061 (1979).

11. J. K. Percus in 'Equilibrium Theory of Classical Fluids', edited by H. L. Frisch and J. L. Lebowitz, Benjamin, New York, II-33 (1964); J. K. Percus and G. J. Yevick, Phys. Rev. 110, 1 (1958).

12. L. Verlet and J. J. Weiss, Phys. Rev. 5, 939 (1972).

13. A. Hall, Messeng Math 2, 113 (1873).

14. Lord Kelvin, Phil Mag 2, 1 (1901).

15. A. Blair, N. Metropolis, J. von Neumann, A. Taub and M. Tsingou, 'A Study of The Numerical Solution to Two-dimensional Hydrodymanical Problem', Contract W-7405-Eng-36 Los Alamos Scientific Lab., NM (1957).

16. N. Metropolis, A. W. Rosenbluth, M. N. Rosenbluth, A. H. Teller, and E. Teller, J. Chem. Phys. 21, 1087 (1953).

17. D. Knuth, 'The Art of Computer Programming, Volume 2, Seminumerical Algorithms', Wesley (1961); A. M. Law and W. D. Kelton, 'Simulation Modeling and Analysis', McGraw-Hill, New York (1982); R. Y. Rubenstein, 'Simulation and the Monte Carlo Method', Wiley, New York (1981).

18. H. Reiss, H. L. Frisch and J. L. Lebowitz, J. Chem. Phys. 31, 369 (1969).

19. E. Helfand, H. L. Frisch and J. L. Lebowitz, J. Chem. Phys. 34, 1036 (1961).

20. G. Lasher, Sci. Res. 4, 22 (1969); M. A. Cotter and D. E. Martire, J. Chem. Phys. 52, 1902,1909 (1970).

21. A. B. Ritchie, Jr., J. Chem. Phys. 46, 608 (1967); E. Meeron and A. J. F. Siegert, J. Chem. Phys. 48, 3139 (1968); R. M. Gibbons, Mol. Phys. 17, 81 (1969).

22. T. Boublik, Mol. Phys. 27, 1415 (1974); ibid 29, 412 (1975); ibid. 51, 1429 (1984).

23. R. S. C. She and G. T. Evans, J. Chem. Phys. 85, 1513 (1986).

24. R. S. C. She, C. James, and G. T. Evans, J. Chem. Phys. 85, 1513 (1986).

25. D. G. Chae, F. H. Ree and T. Ree, J. Chem. Phys. 50, 1581 (1969).

26. V. N. Kabadi and W. A. Steele, Ber. Bunsenges. Phys. Chem. 89, 9 (1985).

27. V. N. Kabadi, Ber. Bunsenges. Phys. Chem. 90, 332 (1986).

CHAPTER 4
THE NON-OVERLAPPING LORENTZ GAS

A. Introduction

The Lorentz Gas (LG) provides an interesting problem from a purely theoretical standpoint as well as serving as a model for diffusive phenomena such as neutron transport in dense materials(1) and the motion of electrons in impure metals(2). The model was initially formulated by Lorentz(3) as a description of the diffusion of conduction electrons in metals. The LG follows the classical motion of a volumeless light particle through a matrix of randomly-placed stationary scatterers. The ratio of the mass of the light particle to that of the heavy particle is considered to be small enough to be effectively zero. This system is an attractive candidate for numerical modelling and analytic study because of its simplicity, yet it acts as an effective test for analytic theories of the more complex liquid state(4-7). The work reported here involves the computer simulation of a two-dimensional LG with non-overlapping scatterers; this corresponds to the motion of a point particle through a 2-d hard disk fluid which has been frozen in time. The work will be compared to previous simulation of the overlapping LG(8-10), previous simulations of the non-overlapping LG at low densities (11,12) and to existing analytic work, much of which has been done for the overlapping LG(13-23).

There are three aspects of the Lorentz gas which are of interest from a theoretical point of view. One of these is the percolation problem in the overlapping Lorentz model. As the density of scatterers is increased, the likelihood of the the light particle being trapped by

a configuration of the overlapping scatterers is also increased. A density is eventually reached where the probability of the particle being trapped is great enough that the self-diffusion coefficient vanishes. This density is known as the percolation threshold. For the non-overlapping Lorentz gas, which is the focus of this work, there is no percolation threshold and no further mention will be made of percolation.

The other two problems of interest for the Lorentz gas arise in the theory of both the non-overlapping and overlapping versions of the LG, in models of molecular liquids and in some simple stochastic models. In the early 1960's, based on the work of Bogoliubov(23) and Zwanzig(25), it was believed that transport coefficients of dense gases could be expressed as power series in density. However, Dorfman and Cohen(25) demonstrated that there existed a logarithmic divergence in the density dependence of the transport coefficients, i.e., $D \sim (\rho + \rho\ln(\rho))^{-1}$. Other calculations on dense gases confirmed the divergences (26). Weijland and van Leeuwen(13) undertook an investigation of the density dependence of the diffusion coefficient in a Lorentz model in an effort to elucidate the origin of the anomalous density dependence. A logarithmic divergence similar to that seen in dense gas theory was observed. This topic will be discussed fully in the next section.

The second problem is to provide an explanation for the non-exponential decay of the velocity autocorrelation function C(t), where

$$C(t) = \langle v \cdot v(t) \rangle / \langle v^2 \rangle$$

and **v** is the velocity of the light particle. The velocity autocorrelation function (VAF) is related to the self-diffusion coefficient by

$$D = \frac{1}{d}\int_0^\infty d\tau \, < \mathbf{v}_1 \cdot \mathbf{v}_1(\tau) > \qquad (1)$$

Equation (1) is identical to eqn. (52) of Chapter 2 and relates the macroscopic diffusion constant in Fick's law to the microscopic time scale considered here. In the Lorentz gas, the relaxation of the the velocity is controlled by the collisions of the light particle with the stationary scatterers; because the scatterers are randomly placed, at low density all collisions are expected to be completely uncorrelated with previous collisions and simple kinetic theory predicts that the velocity relaxes via a single exponential function. Simulations of the LG indicate that even at very low densities the velocity autocorrelation function in two dimensions decays with a negative long time tail which goes as $1/t^2$. Figure 4.1 shows a velocity autocorrelation function for a two-dimensional non-overlapping Lorentz gas at a packing fraction of 0.1; plotted alongside is the exponential decay predicted by kinetic theory.

A positive tail is observed in the velocity autocorrelation function of hard disk liquids at low densities, for high density, a negative tail is observed(26,27). The origin of the positive tail is thought to be hydrodynamic or vortex modes in the liquid; theoretical predictions based on this assumption are in reasonable agreement with computer simulation of hard-disk fluids(28). The tail observed in the liquid simulations was the impetus for the initial kinetic theory investigation of the LG VAF by Ernst and Weijland(14). The origin of

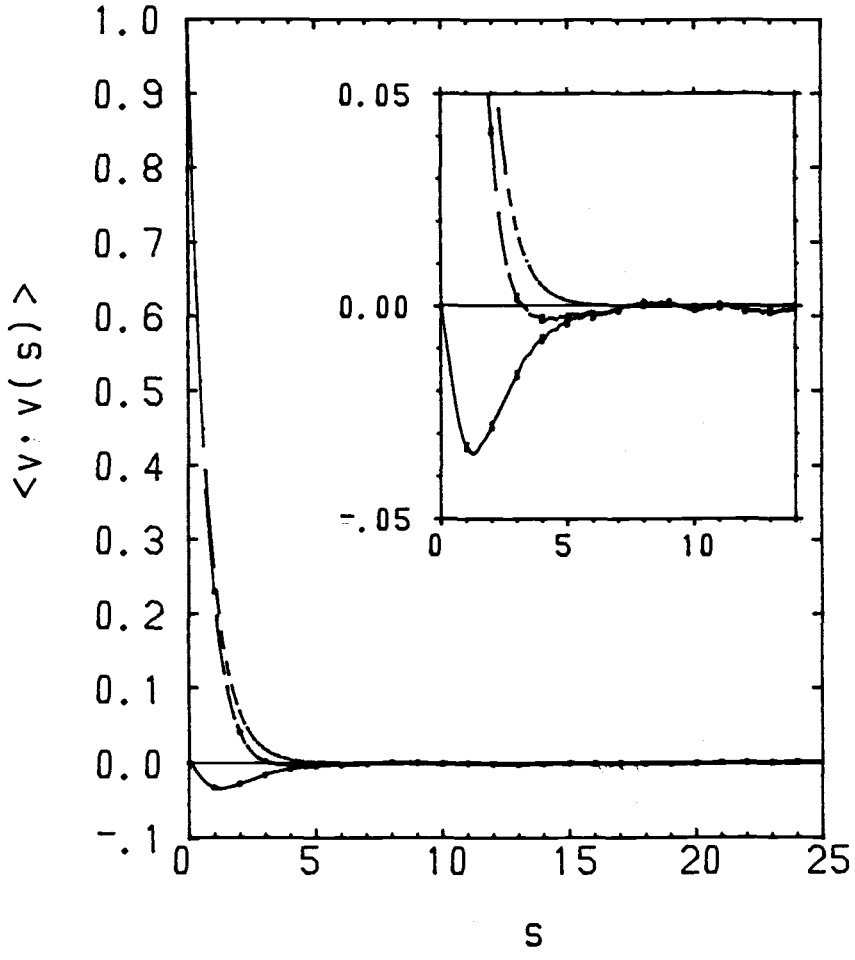

Figure 4.1 The velocity autocorrelation function for the non-overlapping Lorentz gas at a packing fraction $N\pi\sigma^2/V = 0.1$. The time, s, is given in units of the Enskog mean free time, $\pi\sigma/(\rho^*\langle v\rangle g(r_s))$. The lower, solid line is the difference $\langle v\cdot v(s)\rangle - \exp(-4s/3)$, the broken line is $\langle v\cdot v(s)\rangle$ and the uppermost, dotted line is the Enskog prediction $\exp(-4s/3)$. Error bars are one standard deviation above and one standard deviation below the simulation values.

the long time tail is related to the source of the logarithmic density dependence of the self-diffusion coefficient. The long-time tail in the LG has generated a large volume of theoretical work, primarily devoted to the overlapping Lorentz gas (14-21).

The focus of this work is the diffusion constant in the non-overlapping LG; only the work of van Leeuwen and Weijland(13) has centered on this problem. In the next section, the calculation of the diffusion constant in the non-overlapping LG using Boltzmann-Enskog kintic theory and the methods of van Leeuwen and Weijland(13) will be discussed. In Section C the theoretical work on the long-time tail (14-22) will be discussed briefly. In Section D, the results of the simulation of the non-overlapping Lorentz gas will be presented and compared to existing theory.

B. Kinetic Theory for the Diffusion Constant

1. Boltzmann-Enskog Kinetic Theory

The Boltzmann-Enskog equation will be used to first analyze the velocity relaxation and self-diffusion coefficient for the non-overlapping Lorentz gas. Equation (61) of Chapter 2 gives an expression for the inverse of the velocity relaxation time

$$1/\tau_v = -\tfrac{1}{2}\int\int\int_{\kappa\cdot g<0} d\mathbf{v}_1 d\mathbf{v}_2 J d\kappa\ (\kappa\cdot g)^3\ g(r_s) f_{eq}(1) f_{eq}(2)/\langle v_1^2\rangle. \qquad (2)$$

In eqn. (2), $\mathbf{v}_i$ is the velocity of particle i, κ is the surface normal between the surfaces of particles 1 and 2, J is the Jacobian for the transformation between center-to center coordinates and surface-to-surface coordinates given by eqn. (27) in Chapter 2, $\mathbf{g}$ is the relative velocity of particles 1 and 2, $g(r_s)$ is the

equilibrium pair distribution function in terms of the surface-to-surface distance r_s, $f_{eq}(i)$ is the singlet equilibrium distribution function for particle i, i. e., $f^{(1)}(\mathbf{r}_i,\mathbf{v}_i,0)$, and $\langle v_1^2 \rangle$ is the average square velocity of particle 1. The variable κ, rather than the $\mathbf{k}$ used in chapter 2, is used to represent the surface normal vector to prevent confusion with the Fourier space variables $\mathbf{k}$ which will be introduced shortly.

Equation (2) can be simplified for the Lorentz gas considered here by taking into account the disk shape and the fixed position of the scatterers and the constant speed of the moving particle. Throughout this chapter, the moving particle will be indicated by particle 1, the static disks will be particles 2 through N. The positions of all particles will be indicated, as they were in chapter 2, by the set $\mathbf{r}^N = (\mathbf{r}_2,\mathbf{r}_3,\ldots,\mathbf{r}_N)$. Because the scattering particles have no velocity, the distribution function $f_{eq}(2)$ will be $\rho\delta(0)$ and the integral $\int d\mathbf{v}_2\ f_{eq}(2)$ will be equal to ρ. Notation can be simplified if it is recognized that this will be true for any integration over $d\mathbf{v}_i$ for i not equal to one and dropping all references to the particle velocities for particles 2 through N. The unsubscripted variable $\mathbf{v}$ can then be used to indicate the velocity of particle 1. For an interaction between a point particle and a disk, J will be σ, the radius of the scattering particle. The surface normal κ will always point in the direction of $\mathbf{r}_{12}$ with $\mathbf{r}_{12}$ the vector between the light particle and the center of the stationary disk. Because there is no rotation in this system and the scatterers do not move, the relative velocity g will be equal to the velocity of

particle 1. Equation (2) becomes

$$1/\tau_v = -\sigma\rho \iint_{K\cdot v<0} dv dK\ (K\cdot v)^3\ g(r_s) f_{eq}(1)/\langle v^2\rangle. \qquad (3)$$

The LG consists of a single particle colliding elastically with N stationary scatterers, following each collision, the moving particle's initial velocity will change in direction, but not in magnitude. Because the velocity of the moving particle is of constant magnitude, but can point in any direction, the singlet equilibrium distribution function will a be delta function for the magnitude of the velocity divided by 2π;

$$f_{eq}(v) = \delta(v - \langle v\rangle)/2\pi \qquad (4)$$

where $v_1 = |v_1|$. The use of the delta function is equivalent to taking an ensemble average over a microcanonical ensemble. The integral in eqn. (3) can be carried out to give

$$1/\tau_v = 8\rho\sigma\langle v\rangle g(r_s)/3$$

in which ρ is the density, N/V, of scattering particles.

The collision frequency τ_c, where τ_c is the mean free time or the average time between successive collisions, for the Lorentz gas can be determined from a similar integral;

$$1/\tau_c = -\iiint_{K\cdot g<0} dv_1 dv_2 J dK\ (K\cdot g)\ g(r_s) f_{eq}(1) f_{eq}(2).$$

to be

$$1/\tau_c = 2\rho\sigma\langle v\rangle g(r_s). \qquad (5)$$

This leads to the observation that the velocity relaxation time τ_v will be equal to 4/3 times the mean free time, that is, $4\tau_c/3$. All of the results given above apply to the overlapping Lorentz gas if $g(r_s)$ is taken to be 1 and to the non-overlapping Lorentz gas if a hard-disk fluid value is used for $g(r_s)$. The time t can be scaled by

the mean free time to provide a convenient reduced time unit; time given in these units will be indicated by $s = t/\tau_c$.

The diffusion coefficient predicted by Boltzmann-Enskog kinetic theory can be determined using eqn. (52) of chapter 2

$$D = \frac{1}{d}\int_0^\infty dt \; \langle \mathbf{v}\cdot\mathbf{v}(t) \rangle \tag{6}$$

and the relaxation times calculated above. The time correlation function is predicted to be

$$\langle \mathbf{v}\cdot\mathbf{v}(t) \rangle = \langle v^2 \rangle e^{-(4/3)s}; \tag{7}$$

then the self-diffusion coefficient can be written

$$D_E = .375 \langle v \rangle^2 \tau_c = 3\langle v \rangle/(16\rho\sigma g(r_s)). \tag{8}$$

The subscript E indicates that this result is the prediction of Enskog kinetic theory. The effect of increasing the density of the scatterers enters τ_c through the radial distribution function and as an explicit factor of the density; both of these serve to lower the diffusion constant as the density increases. The assumptions of molecular chaos and the inclusion of only bimolecular collision events limit the validity of eqn. (8) to the dilute gas regime. In fact, in computer simulations of even very dilute ($\pi n\sigma^2 = 0.01$) arrangments of scatterers, the VAF is exponential only at very short times.

2. Higher-order Kinetic Theory

The divergent density dependence of the self-diffusion coefficient arises when an attempt is made to include the effects of three-body and higher correlations into the theory. For a two-dimensional Lorentz gas

the three-particle events give rise to the divergence and in three dimensions the three-body term is well-behaved, but the inclusion of four-body effects leads to divergence. The present development of the density expansion will, for the most part, follow Zwanzig's derivation of the density expansion for molecular liquids(24), but will take into account simplifications which can be made for the Lorentz gas. Only the portions of the derivation which are necessary for the consideration of the two-dimensional hard disk LG will be discussed.

The expression for the diffusion constant given by eqn. (6) can be written explicitly as

$$D = \tfrac{1}{2}\int dt \iint d\mathbf{r}^N d\mathbf{v}\, f_{eq}^{(N)}(\mathbf{r}^N,\mathbf{v})\mathbf{v}\cdot e^{i\hat{L}t}\mathbf{v}. \qquad (9)$$

Note that for the LG the distribution function is listed as a function of the positions of all the particles (both static and moving) and of the velocity of the moving particle. The distribution function can be separated into two parts, the configuration distribution function for all the particles and the velocity distribution for particle 1,

$$f_{eq}^{(N)}(\mathbf{r}^N,\mathbf{v}) = P^{(N)}(\mathbf{r}^N) f_{eq}(\mathbf{v}) \qquad (10)$$

where $P^{(N)}(\mathbf{r}^N)$ is given by eqn. (11) of chapter 2 and $f_{eq}(\mathbf{v})$ is the delta function given in eqn. (4) above.

The long time limit of the integral of the correlation function can also be obtained using the Laplace transform and taking the limit of $z \to 0$,

$$D = \lim_{z\to 0} \tfrac{1}{2} \iint d\mathbf{r}^N d\mathbf{v} \int dt\, \exp(-zt)\, P^{(N)}(\mathbf{r}^N) f_{eq}(\mathbf{v})\, \mathbf{v}\cdot e^{i\hat{L}t}\mathbf{v}. \qquad (11)$$

Time integration gives rise to the resolvent operator G(z), defined by

$$G(z) = \int dt\ \exp(-zt)\exp(i\hat{L}t) = (z - i\hat{L})^{-1}. \qquad (12)$$

The equation for D becomes

$$D = \tfrac{1}{2} \lim_{z \to 0} \iint d\mathbf{r}^N d\mathbf{v}\ P^{(N)}(\mathbf{r}^N) f_{eq}(\mathbf{v})\ \mathbf{v} \cdot G(z)\mathbf{v}. \qquad (13)$$

The notation $\langle \ldots \rangle_r$ will be used to indicate a variable which has been averaged over the configuration distribution function $P^{(N)}(\mathbf{r}^N)$, but not over the velocity distribution of particle 1,

$$\langle \ldots \rangle_r = \int d\mathbf{r}^N\ P^{(N)}(\mathbf{r}^N) \ \ldots$$

Since the velocity of particle 1 is independent of position, the diffusion constant can be written as

$$D = \tfrac{1}{2} \lim_{z \to 0} \int d\mathbf{v}\ f_{eq}(\mathbf{v})\ \mathbf{v} \cdot \langle G(z) \rangle_r \mathbf{v}. \qquad (14)$$

The focus of the problem is now the specification of the operator $\langle G(z) \rangle_r$ which includes the effects of all the particles in the system yet operates only on the velocity of the moving particle. Because it is a function of all the system particles, a well-behaved series expansion of G(z) in terms of the density of static particles would be expected to exist

$$\langle G(z) \rangle_r = \Gamma_1(z) + \rho\Gamma_2(z) + \rho^2\Gamma_3(z) + \ldots \qquad (15)$$

The first operator in the expansion, $\Gamma_1(z)$, is $1/z$ which diverges for $z \to 0$. The rest of the members of the series also diverge for small z rendering the expansion useless for the calculation of the diffusion coefficient.

The reciprocal of $\langle G(z) \rangle_r$,

$$B(z) = \langle G(z) \rangle_r^{-1},$$

will be used to obtain a new density expansion; this is accomplished by inverting the density expansion of $\langle G(z) \rangle_r$,

$$B(z) = B_1(z) + \rho B_2(z) + \rho^2 B_3(z) + \ldots \tag{16}$$

The inverse of the diffusion constant will be given by

$$D^{-1} = \int dv\, f_{eq}(v)\, v\cdot(B_1(z) + \rho B_2(z) + \rho^2 B_3(z) + \ldots)v.$$

The first three operators in this series are found to be

$$\begin{aligned} B_1(z) &= [\Gamma_1(z)]^{-1} = z \\ B_2(z) &= -z^2\Gamma_2(z) \\ B_3(z) &= -z^2\Gamma_3(z) + z^3[\Gamma_2(z)]^2. \end{aligned} \tag{17}$$

In two dimensions, the operator $B_3(z)$ leads to a term non-analytic in density, so only the first three terms in the $B(z)$ expansion need be considered. The evaluation of these terms is accomplished using the binary collision expansion of the resolvent operator $G(z)$.

The Liouville operator $\hat{L}$ given by eqn. (8) of chapter 2 can be separated into two parts, a free-streaming operator $\hat{L}_0$ and a collision operator $\hat{L}_1$,

$$\hat{L} = \hat{L}_0 + \hat{L}_1$$

The free-streaming operator for the LG will just be $v\cdot\partial/\partial r_1$. The collision part of the operator is formally defined by

$$\hat{L}_1 = \Sigma_\alpha \hat{L}_\alpha = \Sigma_j\, F_{1j}\cdot\partial/\partial p$$

where p is the momentum of particle 1. For a LG the definition given above is useful only in that it makes it possible to represent $\hat{L}_1$ as the sum of operators for the interaction between the moving particle and each of the stationary particles.

The free-streaming resolvent operator is $G_0 = (z - i\hat{L}_0)^{-1}$. The expansion of the full resolvent operator uses the binary collision operator T_α defined as the solution to the equation

$$T_\alpha = -i\hat{L}_\alpha + i\hat{L}_\alpha G_0 T_\alpha. \tag{18}$$

This operator is related to the Boltzmann collision operator via

$$\lim_{z\to 0}\lim_{v\to\infty} VT_{12}F(v^*) = -\int_{\kappa\cdot v<0} Jd\kappa\ (\kappa\cdot v)\ \ [F(v) - F(v^*)] \qquad (19)$$

where $F(v)$ is a function of the velocity v and the superscript asterisk indicates precollisional velocity. The rhs is a simplified form of eqn. (47) of chapter 2 applicable to LG collision dynamics. Note that the collision operator is the simple Boltzmann operator and does not contain the radial distribution function. To treat accurately the dynamics of the non-overlapping LG, the radial distribution function would have to be included at this point.

The binary collision expansion G is

$$G = G_0 - \Sigma_\alpha G_0 T_\alpha G_0 + \Sigma_\alpha \Sigma_{\beta\neq\alpha} G_0 T_\alpha G_0 T_\beta G_0 -$$
$$\Sigma_\alpha \Sigma_{\beta\neq\alpha} \Sigma_{\gamma\neq\beta} G_0 T_\alpha G_0 T_\beta G_0 T_\gamma G_0 + \ldots \qquad (20)$$

The exclusions $\gamma\neq\beta$, etc., exclude only the pair specified and no others. Note that all pairs include particle 1. This gives rise to terms such as

$$G_0 T_{12} G_0 T_{13} G_0 T_{12} G_0 .$$

A Fourier expansion in space can be used to simplify the terms $B_n(z)$. The set of orthonormal functions

$$V^{-N/2}\exp(i\mathbf{k}^N\cdot\mathbf{r}^N)$$

will be used; $\mathbf{k}^N$ represents the set of wave vectors $(k_1, k_2, \ldots, k_N)$. The matrix representation in k-space of an operator O will be

$$O(k|k') = V^{-N}\int dr^N \exp(-ik^N\cdot r^N) O \exp(ik'^N\cdot r^N) \qquad (21)$$

The representation of the averaged resolvent operator in k-space

requires the configuration distribution function and the unaveraged resolvent operator in k-space. The form of the configuration distribution function will be

$$P(\mathbf{k}^N) = \int d\mathbf{r}^N \exp(i\mathbf{k}^N \cdot \mathbf{r}^N) P(\mathbf{r}^N). \tag{22}$$

Because G(z) operates only on functions which are independent of position, $\mathbf{k}'$ can be set to 0 and only one matrix element $G(\mathbf{k}|0)$ of $G(\mathbf{k}|\mathbf{k}')$ will appear in the expression for the averaged resolvent operator,

$$\langle G(z) \rangle_r = \int d\mathbf{k}^N P(\mathbf{k}^N) G(\mathbf{k}|0).$$

The Fourier expansion of the streaming part of the resolvent operator is

$$G_0(\mathbf{k}|\mathbf{k}') = \gamma(\mathbf{k}) \delta(\mathbf{k}-\mathbf{k}')$$

with

$$\gamma(\mathbf{k}) = (z - i\mathbf{v}\cdot\mathbf{k}^N).$$

Equation (20) can be written

$$G(\mathbf{k}|0) = z^{-1}\delta(\mathbf{k}) - z^{-1}\Sigma_\alpha \gamma(\mathbf{k}) T_\alpha(\mathbf{k}|0) \tag{23}$$
$$+ z^{-1}\Sigma_\alpha \Sigma_{\beta\neq\alpha} \Sigma_{\mathbf{k}'} \gamma(\mathbf{k}) T_\alpha(\mathbf{k}|\mathbf{k}') \gamma(\mathbf{k}') T_\beta(\mathbf{k}'|0) - \ldots$$

The factor of z^{-1} in front of each term is the result of the rightmost G_0's which appear in eqn. (20).

This expression for the resolvent operator, equation (20) can now be written as

$$\langle G(z) \rangle_r = t_0 + t_1 + t_2 + \ldots \tag{24}$$

where each of the t_i represents the partially averaged form of the terms which appear in the series of eqn. (23). A heuristic approach will be used to obtain the correspondence between terms in the binary collision expansion eqn. (23) and the density expansion, eqn. (15).

Equations (16) and (17) can then be used to get the coefficients B_n of the inverse expansion and eventually a finite expression for D as a function of density. Equation (23) gives the resolvent operator as a sum of sums with the terms grouped as a function of the number of binary collisions which each one represents. The term t_0 corresponds to no binary collisions, t_1 to one binary collision, and so forth. Equation (15) is a power series in the density and it is reasonable to expect that the terms of the expansion of eqn. (23) which will contribute to each of the Γ_n of eqn. (15) will be determined by the number of scatterers involved, rather than the number of collisions. That is, Γ_1, which is density-independent, will be comprised of contibutions which result from the the free motion of the moving particle, Γ_2, which is linear in the density, will be the result of the interaction of the moving particle and one scatterer, Γ_3, which is quadratic in the density of scatterers, will arise from collision sequences involving two stationary disks and the moving particle, and so on. It is then necessary to regroup the terms of eqn. (24) according to the number of scatterers involved in the collision sequences.

The first term of the series Γ_1 will involve the free propagation of the moving particle and will correspond to t_0 in eqn. (24). The next term Γ_2 which involves the collision of particle 1 with one of the stationary scatterers can also be represented by a single term for eqn. (24), t_1. It is impossible for particle 1 to recollide with the original static disk without the intervention of a third particle so t_1 representing one binary collision will be the sole contribution to

Γ_1. There are a number of collision sequences which involve the moving particle and two of the scatterers. The simplest of these are included in t_2 of the t_i expansion of G(z) and involve the collision of the moving particle with one of the stationary scatterers followed by a collision with a different stationary scatterer. In addition to the two-scatterer collision events described by t_2, the just-described collision sequence can be followed by a recollision of the moving particle with the initial scatterer. This sequence is illustrated in Figure 4.2b. When the possiblity of recollision is considered, a large number of events can be conceived of which involve two static scatterers and are not included in t_2.

Figure 4.2 (6) illustrates four types of collision sequences which can occur in a Lorentz gas. Collision events may be reducible or irreducible; a reducible collision event is one for which there exists a point at which the trajectory can be cut to produce two sequences which will both involve fewer particles than the original collision sequence. An irreducible event is then a trajectory which when cut at any point will produce two sequences, at least one of which will involve the same number of particles as the original collision sequence. Additionally, collision sequences may be classified as non-ring, ring or repeated ring. A ring collision event involves the collision of the moving particle with an intial scattering particle, its further collision with different particles followed by recollision with the initial particle in the sequence. Repeated ring events include an intial ring sequence followed by additional ring sequences resulting in collision with the initial particle of the initial ring.

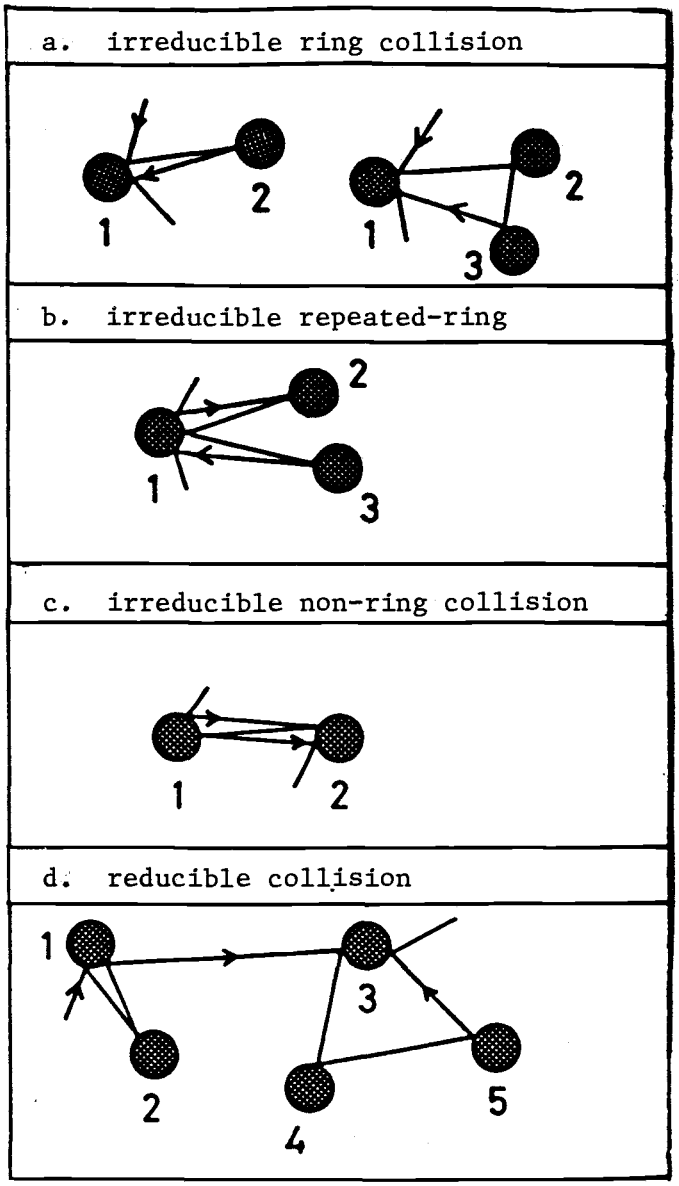

Figure 4.2 (ref 6) Classification of Collisions in the Lorentz Gas.

This system of classification is useful for describing the collision events which are considered in the following development.

The third term, Γ_3, of eqn. (15), the density expansion of the resolvent operator, will be composed of terms which correspond to collision events of the moving particle with two scatterers. This includes t_2 plus irreducible ring events between the moving particle and two of the static disks included in t_3. The latter are represented in $T_\alpha G_0$ language as

$$\Sigma_\alpha \Sigma_{\beta\neq\alpha} G_0 T_\alpha G_0 T_\beta G_0 T_\alpha G_0 . \tag{25}$$

The operator of eqn. (25) will be denoted by $t_{3,2}$ to distinguish it from other three collision sequences. There are other binary collision sequences which appear in t_4 and higher terms which involve particle 1 and two of the static scatterers; these are repeated ring events and reducible and irreducible non-ring events consisting of four or more collisions. The density dependence and divergence of Γ_3 and hence the diffusion constant will be dominated by the relatively more frequent events of t_2 and t_3 (24).

The parts of the resolvent operator expansion which are necessary for the calculation of the first three terms of the density expansion eqn. (15) will now be evaluated.

The first term, t_0, is simply $1/z$ and is independent of the density.

The second term t_1 will be

$$t_1 = z^{-1} \Sigma_k P(k) \Sigma_\alpha \gamma(k) T_\alpha(k|0)$$

There are N-1 equivalent pairs α which contain molecule 1, so the sum over α may be replaced by a multiplicative factor of N-1,

$$t_1 = z^{-1}\ (N-1)\ \Sigma_k P(k)\gamma(k)T_\alpha(k|0).$$

The binary collision operator will be diagonal in wave vectors not involved in the collision(24), that is,

$$T_{12}(k|k') = \delta(k_1 + k_2 - k_1' - k_2')\prod_{n=3}^{N}\delta(k_n - k_n'). \quad (26)$$

The wave vector dependence of T_{12} is then written explicitly as

$$T_{12}(k|0) = T_{12}(k_1,k_2|0) = T_{12}(k_1,-k_1|0).$$

This can be substituted into t_1 to give

$$t_1 = z^{-1}\ (N-1)\ \Sigma_{k_1} P(k_1,-k_1)(z-iv\cdot k_1)^{-1}T_{12}(k_1,-k_1|0).$$

At this point, the representation of configuration distribution function in terms of a cluster function will further simplify the equation for t_1. If the distribution function $P(R^N)$ is integrated over $dr_3 \ldots dr_N$, the result is a reduced distribution function $P^{(2)}(r^2) = (N-2)!\rho^2 g(r_{12})/N!$ where $g(r_{12})$ is the pair correlation function given by eqn. (14) of chapter 2. For a large system $P^{(2)}(r^2)$ can be written as

$$P^{(2)}(r^2) = (1/V^2)(1 + h_{12})$$

where h_{12} is a short-ranged cluster function which is dependent upon the separation between particles 1 and 2, $r_{12} = r_2 - r_1$.
The Fourier integral of this function will be

$$P(k_1,-k_1) = \delta(k_1) + V^{-1} \int dr_{12}\exp(ik_1\cdot r_{12})\ h_{12}. \quad (27)$$

The rightmost term of equation (27) will be indicated by the abbreviated notation $h(k_1)$.

The equation for t_1 separates into two parts

$$t_1 = z^{-2}V^{-1}(N-1)\ VT_{12}(0|0)$$
$$- z^{-1}V^{-1}(N-1)\ \Sigma_{k_1}\ v^{-1}\ h(k_1)(z - iv\cdot k_1)^{-1}VT_{12}(k_1,-k_1|0) \quad (28)$$

Further reduction of this term is not possible without

consideration of the variable which it is to operate upon and its relationship to the Γ_n and B_n expansions. The terms t_2 and t_3 will now be considered; in a later section the action of t_1, t_2 and t_3 on $\mathbf{v}$ and the consequent contributions to the diffusion coefficient will be evaluated.

The reduction of the term t_2 can be accomplished using the procedure that was applied to t_1. Two binary collision operators appear in t_2,

$$t_2 = z^{-1}\Sigma_{\mathbf{k}}\Sigma_{\mathbf{k}'}\Sigma_{\alpha}\Sigma_{\beta\neq\alpha}P(\mathbf{k})\int\gamma(\mathbf{k})T_{\alpha}(\mathbf{k}|\mathbf{k}')\gamma(\mathbf{k}')T_{\beta}(\mathbf{k}'|0) \qquad (29)$$

The sum over β can be replaced by a factor of (N-1) times the pair (12) and only $\mathbf{k}_1'$ and $\mathbf{k}_2'$ will appear from the set $\mathbf{k}'$. The pair α must also include molecule 1 and the sum may be eliminated by a factor of (N-2) times the pair (13). Equation (26) can be used to eliminate $\mathbf{k}_4,\mathbf{k}_5,\ldots\mathbf{k}_N$ to give

$$t_2 = (N-1)(N-2)z^{-1}\sum_{\mathbf{k}_1,\mathbf{k}_2,\mathbf{k}_3,\mathbf{k}_1',\mathbf{k}_2'}P(\mathbf{k}^3)\ \gamma(\mathbf{k}^3)T_{13}(\mathbf{k}_1,\mathbf{k}_2,\mathbf{k}_3|\mathbf{k}_1',\mathbf{k}_2',0)$$
$$\times\ \gamma(\mathbf{k}_1',\mathbf{k}_2')T_{12}(\mathbf{k}_1',\mathbf{k}_2'|0) \qquad (30)$$

where $\mathbf{k}^3$ represents the set $(\mathbf{k}_1,\mathbf{k}_2,\mathbf{k}_3)$. Conservation of wave vectors requires that

$$\mathbf{k}_1 + \mathbf{k}_2 + \mathbf{k}_3 = 0$$

and

$$\mathbf{k}_1' + \mathbf{k}_2' = 0.$$

Equation (26) sets $\mathbf{k}_2 = \mathbf{k}_2'$ following the action of T_{13}. This leaves only two of the original five $\mathbf{k}$ sums which appear in eqn. (30),

$$t_2 = (N-1)(N-2)z^{-1}\sum_{\mathbf{k}_1,\mathbf{k}_1'}P(\mathbf{k}^3)\ \gamma(\mathbf{k}^3)T_{13}(\mathbf{k}_1,-\mathbf{k}_1',\mathbf{k}_1'+\mathbf{k}_1|\mathbf{k}_1',-\mathbf{k}_1',0)$$
$$\times\ \gamma(\mathbf{k}_1',-\mathbf{k}_1')T_{12}(\mathbf{k}_1',-\mathbf{k}_1'|0). \qquad (31)$$

As in the reduction of t_1, the Fourier transform of the distribution function is now considered. The reduced distribution function which will appear in t_2 will be

$$P^{(3)}(\mathbf{r}_1,\mathbf{r}_2,\mathbf{r}_3) = \int\ldots\int d\mathbf{r}_4\ldots d\mathbf{r}_N\ P^{(N)}(\mathbf{r}^N).$$

This function is expanded as

$$P^{(3)}(\mathbf{r}_1,\mathbf{r}_2,\mathbf{r}_3) = (1/V^3)(1 + h_{12} + h_{23} + h_{13} + h_{123});$$

for the present purposes, it is sufficient to combine all of the cluster functions into one term indicated by $h_{(3)}(\mathbf{r}^3)$. The Fourier transform of the triplet distribution function can then be written as

$$P^{(3)}(\mathbf{k}_1,\mathbf{k}_2,\mathbf{k}_3) = \delta(\mathbf{k}_1)\delta(\mathbf{k}_2)\delta(\mathbf{k}_3) + h_{(3)}(\mathbf{k}^3)$$

and t_2 separates into two parts

$$t_2 = (N-1)(N-2)V^{-2}z^{-3}\ VT_{13}(0|0)\ VT_{12}(0|0)$$

$$+ (N-1)(N-2)z^{-1}\sum_{\mathbf{k}_1',\mathbf{k}_1} h_{(3)}(\mathbf{k}^3)\ \gamma(\mathbf{k}^3)T_{13}(\mathbf{k}_1,-\mathbf{k}_1',\mathbf{k}_1'+\mathbf{k}_1|\mathbf{k}_1',-\mathbf{k}_1',0)$$

$$\times\ \gamma(\mathbf{k}_1',-\mathbf{k}_1')T_{12}(\mathbf{k}_1',-\mathbf{k}_1'|0). \qquad (32)$$

The other contribution to the term quadratic in density in the expansion of the resolvent operator will be $t_{3,2}$ given by the partial average of the operator of eqn. (25). This is written in Fourier space as

$$t_{3,2} = -(N-1)(N-2)z^{-1}\sum_{\mathbf{k},\mathbf{k}',\mathbf{k}''}P(\mathbf{k})\ \gamma(\mathbf{k})T_{12}(\mathbf{k}|\mathbf{k}')$$

$$\gamma(\mathbf{k}')T_{13}(\mathbf{k}'|\mathbf{k}'')\gamma(\mathbf{k}'')T_{12}(\mathbf{k}''|\mathbf{k}').$$

This expression can be treated as was the expression for t_2 using the k-space representation of the distribution function to give

$$t_{3,2} = -(N-1)(N-2)z^{-1}\sum_{\mathbf{k},\mathbf{k}',\mathbf{k}''}P(\mathbf{k})\ \gamma(\mathbf{k})T_{12}(\mathbf{k}|\mathbf{k}')$$

$$\gamma(\mathbf{k}')T_{13}(\mathbf{k}'|\mathbf{k}'')\gamma(\mathbf{k}'')T_{12}(\mathbf{k}''|\mathbf{k}'). \qquad (33)$$

The distribution function necessary for the evaluation of eqn. (33) is the triplet distribution function. The cluster function expansion of the triplet distribution function can be substituted into eqn. (33) and the sum over the Fourier transform variable $\mathbf{k}_1$ converted to an integral to give

$$t_{3,2} = -(N-1)(N-2)V^{-2}z^{-2}(2\pi)^{-2}\int d^2\mathbf{k}_1\ T_{12}(0|\mathbf{k}_1,-\mathbf{k}_1)(z-i\mathbf{v}\cdot\mathbf{k}_1)^{-1}$$
$$\times T_{13}(\mathbf{k}_1,-\mathbf{k}_1,0|\mathbf{k}_1,-\mathbf{k}_1,0)(z-i\mathbf{v}\cdot\mathbf{k}_1)^{-1}T_{12}(\mathbf{k}_1,-\mathbf{k}_1|0)$$
$$-(N-1)(N-2)z^{-1}V^{-3}\sum_{\mathbf{k},\mathbf{k}',\mathbf{k}''}h_{(3)}(\mathbf{k}^3)\ \gamma(\mathbf{k})T_{12}(\mathbf{k}|\mathbf{k}')$$
$$\times \gamma(\mathbf{k}')T_{13}(\mathbf{k}'|\mathbf{k}'')\gamma(\mathbf{k}'')T_{12}(\mathbf{k}''|\mathbf{k}'). \qquad (34)$$

The form of the terms from the t_i expansion of the resolvent operator which will be needed for the determination of the first three terms in the expansion of the inverse resolvent operator as a function of density has been established and the next step is the explicit evaluation of the contributions to B(z) and finally D^{-1}.

The first term, $B_1(z)$, is independent of the density; eqn. (17) gives $B_1(z)$ equal to $[\Gamma_1(z)]^{-1}$ which is equal to z. This is confirmed by the binary collision analysis in which the only term independent of density is the free propagation term t_0 which gives z for $B_1(z)$.

The coefficient of the series linear in density $B_2(z)$ is equivalent to $-z^2\Gamma_2$ where $\Gamma_2(z)$ is the coefficient of the density expansion of $\langle G(z)\rangle_r$ also linear in density. This corresponds to terms in the binary collision expansion involving one stationary scatterer; only t_1 will contribute. Equation (28) gives the expression for t_1. There appears in the second term on the rhs of eqn. (28) an integral over the short-ranged cluster function; this function will serve to keep integrand finite as $z\to 0$. In front of the

integral is a factor of z^{-1}. Since eqn. (17) indicates that $\Gamma_2(z)$ is to be multiplied by z^2 to give $B_2(z)$, the second term of t_1 will not contribute to $B_2(z)$ in the limit $z\to 0$. $\Gamma_2(z)$ is then given by

$$\Gamma_2(z) = t_1/\rho = z^{-2}\ VT_{12}(0|0) \tag{35}$$

and, consequently, the correction to the inverse diffusion constant will be

$$\int dv\ f_{eq}(v)\ v\cdot B_2(0)v = -\lim_{z\to 0} \int dv\ f_{eq}(v) v\cdot z^2\Gamma_2(z)v$$

$$= \int dv\ f_{eq}(v)\ v\cdot \int_{K\cdot v<0} JdK\ (K\cdot v)\ (v-v^*).$$

$$= 16\sigma/(3\langle v\rangle).$$

The third term in the series arises from the action of of t_2 and parts of t_3. Equation (32) gives an expression for t_2. The second term on the rhs will vanish for the same reasons given for the vanishing of the cluster function part of t_1. The first term on the rhs will be divergent as $z\to 0$ even when multiplied by z^2 because of the factor of z^{-3},

$$t_2/\rho^2 = z^{-3}\ VT_{13}(0|0)\ VT_{12}(0|0)$$

The coefficient $B_3(z)$ includes, however, a contribution $-z^3\Gamma_2(z)^2$ and

$$\Gamma_2(z)^2 = z^{-4}\ VT_{12}(0|0)VT_{13}(0|0).$$

This will exactly cancel the divergent t_2 and $B_3(z)$ will be given by $z^2 t_{3,2}/\rho^2$. As with the previous terms t_i, the portion of $t_{3,2}$ containing the cluster function will vanish in the limit $z\to 0$ leaving

$$B_3(z) = (2\pi)^{-2} \int d\mathbf{k}_1\ T_{12}(0|\mathbf{k}_1,-\mathbf{k}_1)(z-iv\cdot\mathbf{k}_1)^{-1} \tag{36}$$

$$\times\ T_{13}(\mathbf{k}_1,-\mathbf{k}_1,0|\mathbf{k}_1,-\mathbf{k}_1,0)(z-iv\cdot\mathbf{k}_1)^{-1}T_{12}(\mathbf{k}_1,-\mathbf{k}_1|0)$$

Physically, eqn. (36) describes the collision of the moving particle with one of the stationary scatterers, followed by free propagation at its new velocity, collision with a different stationary scatterer and a concommitant change of velocity, and finally free propagation until recollision with the original scatterer. The contribution to the diffusion coefficient will be of the form

$$\int d\mathbf{v}\, f_{eq}(\mathbf{v})\, \mathbf{v}\cdot B_3(0)\mathbf{v}. \tag{37}$$

This equation was evaluated for the Lorentz gas by van Leeuwen and Weijland. The procedure is lengthy and will not be reproduced here, although the general method will be outlined.

The integral given by eqn. (36) and required for eqn. (37) is evaluated using the correspondence between the T_{12} operators and the Boltzmann collision operator given in eqn. (19). The Boltzmann collision operator is first interpreted in terms of real and virtual collisions. The operator acting upon any function of $\mathbf{v}$, $F(\mathbf{v})$ is

$$-\int_{K\cdot v<0} JdK\, (K\cdot v)\, (F(\mathbf{v})-F(\mathbf{v}^*)).$$

This is a difference of two events, one in which the velocity changes (indicated by $\mathbf{v}$ if $\mathbf{v}^*$ is precollisional velocity) due to collision with another particle and one in which the velocity does not change ($\mathbf{v}^*$). The first of these is referred to as a real collision and the latter as a virtual collision. The virtual collision is one in which the particle penetrates the scatterer and continues with its original velocity. To evaluate eqn. (37), one notes that while the first and last collisions may be either real or virtual and hence require the full B-E operator, the middle collision must be real in order to cause the change in velocity required to return the particle

to the original scatterer. This allows one to use only the portion of the B-E operator which describes a real collision. van Leeuwen and Weijland use the Fourier transform of the δ-function condition for collision on the positions of the moving particle and the scatterer and the explicit application of the Boltzmann operators to obtain the action of the collision operators on **v**. For a two-dimensional Lorentz gas the result is

$$\int d\mathbf{v}\, f_{eq}(\mathbf{v})\, \mathbf{v}\cdot B_3(0)\mathbf{v} = -(8/3)^2(\sigma^3 \ln z)/\langle v\rangle .$$

This quantity posseses a singularity at $z = 0$.

The inverse density expansion thus does not give the desired finite coefficients in the $z\to 0$ limit. The physical explanation for the divergence is that $t_{3,2}$ includes collision sequences in which scatterers 2 and 3 are very far apart. In the limit of $z\to 0$ (or $t\to\infty$), the distance between the scatterers diverges. Weijland and van Leeuwen (13) converted the singularity as a function of z to a function of the density using a renormalization technique which effectively damped the possible distance between successive collisions using the mean free path. Their method will be outlined below.

The first step in removing the divergence for $z\to 0$ is the summation of the ring diagrams. The ring sum, t_R, is defined in terms of the t_i operators as

$$t_R = \Sigma_i t^{(1)}_{i+1,i} \; ; \tag{38}$$

the expression $t^{(1)}_{i+1,i}$ refers to the operator in the series t_i given by eqn. (24) which contains i+1 collisions involving i scattering centers. This is just, as the name implies, the sum over irreducible

ring collision sequences. The superscript (1) indicates that only the first term of the cluster expansion of the distribution function is included; higher terms will vanish for the same reasons as were given for the elimination of the second terms of eqns. (28), (32) and (34). The contribution to the inverse diffusion coefficient from each of the ring events can be written as

$$c_{i+1,i} = \int d\mathbf{v}\, f_{eq}(\mathbf{v})\, \mathbf{v}\cdot\int d\mathbf{r}^N t^{(1)}_{i+1,i}\mathbf{v}$$
$$= \int d\mathbf{v}\, f_{eq}(\mathbf{v})\, \mathbf{v}\cdot\int d\mathbf{r}^N\, T_\alpha[G_0T]^{i-1}G_0T_\alpha \qquad (39)$$

where T without the subscript indicates $\int d\mathbf{r}_n\, T_n$. Equation (39) is written in r-space rather than k-space for notational simplicity. The use of r-space will be maintained for the remainder of the discussion. It can be seen from eqn. (20) that

$$\Sigma_i\, [G_0T]^{i-1}G_0 = G - G_0.$$

Following substitution from eqn. (20), the contribution of all the rings to the inverse diffusion constant becomes

$$c_R = \rho\int d\mathbf{v}\, f_{eq}(\mathbf{v})\, \mathbf{v}\cdot\int d\mathbf{r}^N\, t_R\, \mathbf{v}$$
$$= \rho\int d\mathbf{v}\, f_{eq}(\mathbf{v})\, \mathbf{v}\cdot\int d\mathbf{r}_2\, T_\alpha[G - G_0]T_\alpha\mathbf{v}. \qquad (40)$$

The traditional method of solution of a ring sum such as eqn. (40) is to use the following equation to obtain successively higher order approximations to G:

$$G = G_0 + \rho G_0TG. \qquad (41)$$

For the LG the result is the same as that obtained from eqn. (37), a singularity of the form ln(z). To eliminate the divergence, Weijland and van Leeuwen separated T into its real and virtual components,

$$G = G_0 + \rho G_0(T^r - T^v)G. \qquad (42)$$

and rearranged eqn. (42) to give

$$(G_0^{-1} + T^v)G = 1 + \rho T^r G. \tag{43}$$

The virtual portion of T serves only to multiply functions of the velocity by $2v\sigma$; it is T^r which accounts for the effects of a collision. Equation (43) can be written as

$$(z + 2\rho v\sigma - iL_0)G = 1 + \rho T^r G. \tag{44}$$

and this expression used to obtain succesively higher appoximations to G. The net effect of this procedure is to damp the free propagation which occurs between collisions.

The zeroth order approximation will be

$$G^{(0)} = (z + 2\rho v\sigma - L_0)^{-1}.$$

If this is inserted into eqn. (40) for the ring sum, the result is

$$c_R = \rho\int d\mathbf{v}\, f_{eq}(\mathbf{v})\, \mathbf{v}\cdot\int d\mathbf{r}_2\, T_\alpha[(z+2\rho v\sigma-iL_0)^{-1}-(z-iL_0)^{-1}]T_\alpha\mathbf{v}. \tag{40}$$

The first and last operators indicate the collision of particle 1 with the same scatterer, but the operator in the middle does not prescribe any change in the velocity between the two collisions. It is not possible for the particle to recollide with the same scatterer without an intervening change in velocity, so this integral will vanish and the next approximation to G must be considered.

The next approximation will be

$$G^{(1)} = [z + 2\rho v\sigma - iL_0]^{-1}\rho T^r[z + 2\rho v\sigma - iL_0]^{-1}.$$

If this is substituted into the ring sum, the result is an expression nearly identical to the r-space version of the contribution of $t_{3,2}$ to the inverse diffusion coefficient (eqns. (36) and (37)),

$$c_R = \rho^2\int d\mathbf{v}\, f_{eq}(\mathbf{v})\, \mathbf{v}\cdot\int d\mathbf{r}_2\, T_\alpha$$
$$\times [z + 2\rho v\sigma - iL_0]^{-1}\rho T^r[z + 2\rho v\sigma - iL_0]^{-1}T_\alpha\mathbf{v}. \tag{41}$$

Each appearance of z in $B_3(z)$ is replaced by $z + 2\rho v\sigma$. Weijland and

van Leeuwen calculate this contribution to the inverse diffusion coefficient by setting z equal to 0 and taking the lim $\rho \to 0$. The contribution of the ring sum to the inverse diffusion constant is

$$c_R = -(8/3)^2(\sigma\langle v\rangle)^{-1}\rho\sigma^2\ln(\rho\sigma^2).$$

It can be demonstrated that this is the principal contribution to the diffusion coefficient from the ring sum. Further contributions to the expansion have been calculated (8) and the most complete expression, in the form which is most useful for comparison with later results is

$$D/D_B = \{ 1 - (4/3)\rho\sigma^2\ln(\rho\sigma^2) - .8775\rho\sigma^2 + 4.519[\rho\sigma^2\ln(\rho\sigma^2)]^2 \}^{-1} \quad (42)$$

where D_B is the Boltzmann diffusion constant $3\langle v\rangle/(16\rho\sigma)$.

The absence of any factor of the rdf in the expression given here for the diffusion constant prescribes that this result makes no distinction between the overlapping and non-overlapping LG. The rdf was eliminated when the higher-order terms of the cluster expansion of the t_i's were taken to vanish. In fact, the careful analysis of van Leeuwen and Weijland indicates that some of the cluster expansion terms do contribute to the diffusion constant. They calculate only the contibutuion to t_2 of lowest-order in density and find that it is equal to $16\sigma^3 g^{(1)}(\sigma)/(3\langle v\rangle)$, where $g^{(1)}$ is the lowest order density correction to the rdf. This is also the lowest-order Enskog correction to the diffusion constant; use will be made of the relationship between this contribution and the Enskog correction to Boltzmann kinetic theory, but not of the actual value.

At low densities, eqn. (42) is in good agreement with the results of Bruin (8) and of Alder and Alley (9,10) for the overlapping LG but overestimates D/D_B at higher densities. Efforts to improve on

estimates of the diffusion constant for the specific case of the overlapping LG will be reviewed in the next paragraphs.

Masters and Keyes (19) used the repeated-ring approximation of kinetic theory and a self-consistent repeated ring theory to calculate the diffusion constant for the overlapping LG. Their results are the product of numerical analysis and are presented graphically in Figure 4.3a(19). For the repeated ring theory, agreement with the results of Alder and Alley (9,10) and of Bruin (8) is good at low densities, but poor for high densities. The self-consistent theory provides good agreement with the simulation results at low and high densities, but overestimates the diffusion constant at intermediate density.

Götze, Leutheusser and Yip used a self-consistent mode-coupling theory to determine the density dependence of the diffusion constant for two-dimensional (21) and three-dimensional (22) overlapping scatterers. They report that the leading non-analytic low-density correction to the reduced diffusion constant for the two-dimensional case is equal to the result of van Leeuwen and Weijland to within a factor of $8/3\pi$ (21). For the three-dimensional LG (23), the reduced diffusion constant is given in graphical form rather than as an analytic expression (Figure 4.3b); agreement with the computer simulation results of Bruin (8) is good, particularly at low densitites; the Alder and Alley simulation results are not included. Götze, Leutheusser and Yip (22) do not make a comparison with the results of van Leeuwen and Weijland, but it appears that they are quite similar and that the lowest order density correction is the same.

The next section will provide an overview of calculations of the

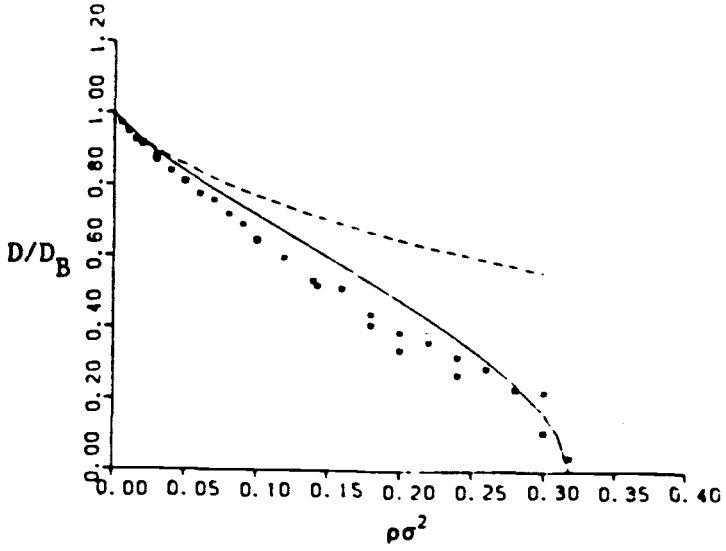

a. The density dependence of the diffusion constant for the 2-d non-overlapping Lorentz Gas as calculated by Masters and Keyes(19). The squares are the molecular dynamics results of Bruin(8) and of Alder and Alley(9,10). The dashed line is the repeated ring approximation result and the solid line is the self-consistent result. The diffusion constants are normalized by the Boltzmann value of the diffusion constant, $D_B = 3\langle v\rangle/(16\rho\sigma)$. (ref. 19)

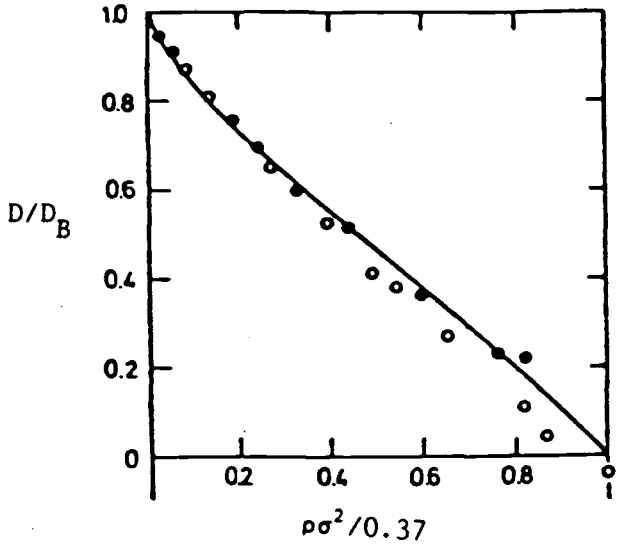

b.The density dependence of the diffusion constant for the 2-d non-overlapping Lorentz Gas as calculated by Götze, Leutheusser and Yip. The molecular dynamics results of Bruin(8) are given by the closed circles and the data of Alder and Alley (9,10) are given by the open circles. The solid line is the mode-coupling result. Normalization is the same as in a., The density is reduced by the percolation density $\rho\sigma^2 = 0.37$. (ref. 21)

Figure 4.3

long-time behavior of the VAF for the LG.

C. Calculation of the Long-time Tail

In contrast to the diffusion constant which has only been completely analyzed by van Leeuwen and Weijland in 1968, the long-time tail of the VAF for the non-overlapping LG has recently been calculated by Machta, Ernst, van Beijeren and Dorfman(18) (MEvBD). Several calculations for the overlapping LG have also appeared; a brief review of each of the methods and a summary of the results as they might apply to the non-overlapping LG will be provided.

The origin of the long-time tail can be explained on physical grounds using the following scheme(5): Consider the moving particle at $\tau=0$, traveling with an initial velocity in the positive x-direction; at time $\tau=\tau_0$, it collides with a scatterer at position 0. The point of collision will be chosen as the origin of the coordinate system, but the position of the center of the scatterer need not be specified. Because the scattering mechanism is isotropic, the post-collisional velocity of the light particle, averaged over the configuration of the scatterers, will be uncorrelated with the inital velocity and subsequent collisions should not act to 'recorrelate' the velocities. However, since the first collision occurred at the origin, there can be no scatterers in the volume V_0, indicated by the shaded area in Figure 4.4, and therefore if the particle returns to V_0, it will maintain its velocity for a longer than average length of time. For a two-dimensional LG, the long time probabilty density of the moving particle will be given by a Gaussian of the form of eqn. (50) of

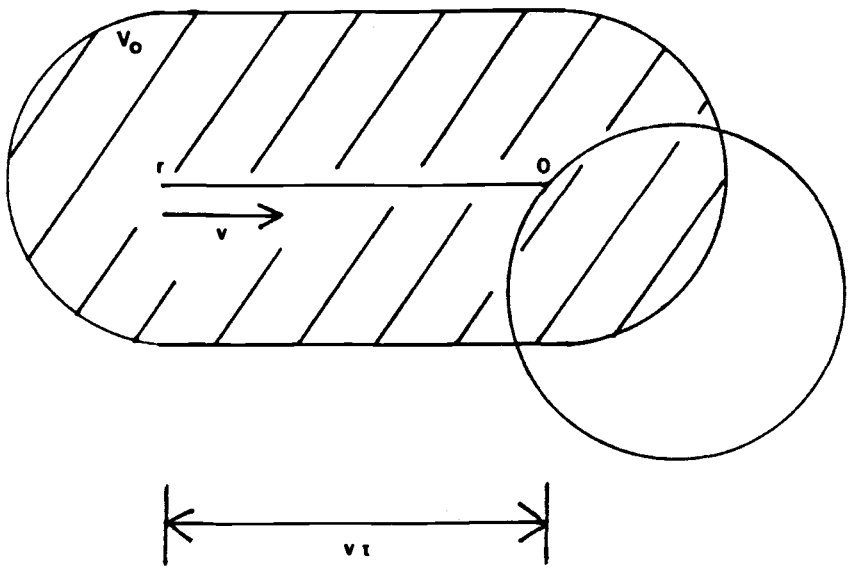

Figure 4.4 The origin of the long-time tail in the VAF of the Lorentz gas. The particle is initially (t=0) at r traveling with velocity v. Collision with a scatterer occurs at time τ and the origin of the coordinate system is taken to be the point of contact. The probability of the particle returning to the area V_0 from the right is greater than the probability of its returning from the left. (ref. 5)

$$P^{(1)}(\mathbf{r},t) = \frac{P^{(1)}(\mathbf{r},0)}{2(\pi Dt)} e^{-(\mathbf{r}(t)-\mathbf{r}(0))^2/4Dt} \qquad (43)$$

Because this distribution function is a Gaussian centered at the origin, the particle will have a greater chance of entering V_0 from the right rather than from the left. In that case, the velocity would be in the opposite direction of and negatively correlated with the inital velocity.

The long-time values of the VAF in simulations of the overlapping (8-10) and non-overlapping (12) LG and in the present work on the non-overlapping LG are found to be proportional to $-t^{-2}$. All of the theoretical predictions (14,19-22) are in agreement with this result and only the magnitude of the tail is in dispute.

The first attempt at calculating the long-time VAF was that of Ernst and Weijland (14). They applied the model of van Leeuwen and Weijland for the LG diffusion constant to a calculation of the long-time behavior of the VAF. The Laplace transform of the VAF can be written as the sum

$$\begin{aligned} \langle \mathbf{v}\cdot\mathbf{v}(z)\rangle &= \{\, z + \mathbf{v}\cdot[t_1 + t_R]\,\mathbf{v}\,\}^{-1} \qquad (44) \\ &= \{\, z + \mathbf{v}\cdot[t_1 + T_\alpha G(z,\mathbf{k}) T_\alpha]\,\mathbf{v}\,\}^{-1} \end{aligned}$$

where t_1 is defined by eqn. (28), $G(z,\mathbf{k})$ is $[z-i\mathbf{k}\cdot\mathbf{v}-t_1]^{-1}$ and T_α is defined by eqn. (18). The VAF at long times will be dominated by the leading singularity of eqn. (44) in the limit of small z. The leading term of the second term on the rhs can be determined using the hydrodynamic eigenvalues and modes of the Boltzmann-Enskog equation. The Fourier transform of the B-E equation may be written as an

eigenvalue equation,

$$(i\mathbf{k}\cdot\mathbf{v} + t_1)\psi_k(\mathbf{v}) = \omega_k\psi_k(\mathbf{v}). \tag{45}$$

Because number density is conserved, in the limit of $\mathbf{k}\to 0$ there exists an eigenfunction $\psi_0(\mathbf{v})$ with eigenvalue ω_k equal to zero. For small $\mathbf{k}$, the eigenvalue ω_k is small and negative and the eigenfunction is referred to as a hydrodynamic mode. In liquids, each of the variables which appear in the hydrodynamic equations associated with a transport coefficient: the number density, momentum, and energy, constitutes a hydrodynamic mode. For the Lorentz gas, the only hydrodynamic mode is diffusion which corresponds to changes in number density. The eigenvalue ω_k and eigenfunction $\psi_k(\mathbf{v})$ for small $\mathbf{k}$ can be determined from a perturbation expansion of eqn. (45) in powers of k. The eigenvalue is $-k^2D_B$ and the eigenfunction is $1 + i\mathbf{k}\cdot\mathbf{v}(2D_B)$ where D_B is the Boltzmann value of the diffusion coefficient $(2\mathbf{v}\cdot t_1\mathbf{v})^{-1} = 3\langle v\rangle/(16\rho\sigma)$. A projection operator, P_k, can be defined which projects a function $F(\mathbf{v})$ along the hydrodynamic mode $\psi_k(\mathbf{v})$,

$$\hat{P}_k F(\mathbf{v}) = \psi_k(\mathbf{v})\int d\mathbf{w}\psi_k^{*}(\mathbf{w})F(\mathbf{w})/\int d\mathbf{w}\psi_k^{2}(\mathbf{w}). \tag{46}$$

Then, in the limit of small $\mathbf{k}$, the operator $G(z,\mathbf{k})$ can written as

$$G(z,\mathbf{k}) = (z - \omega_k)^{-1}\hat{P} \simeq (z + k^2D_B)^{-1}\hat{P} \tag{47}$$

Equation (47) can be substituted into eqn. (44) for the Laplace transform of the correlation function and T_α replaced by t_1 to give

$$\langle\mathbf{v}\cdot\mathbf{v}(z)\rangle = \{\, z + (2D_B)^{-1} + (8\rho\pi^2)^{-1}\int d\mathbf{k}\, k^2/(z + k^2D_B)\,\}^{-1} \tag{48}$$

Ernst and Weyland then invert the Laplace transform using a power series expansion and evaluate the k integral to give the asymptotic expression, to lowest order in density as

$$\langle \mathbf{v}\cdot\mathbf{v}(t)\rangle_{EW} \sim -1/(\rho t^2). \tag{49}$$

for two dimensions and more generally

$$\langle \mathbf{v}\cdot\mathbf{v}(t)\rangle_{EW} = -(2\pi d D_B^2/\rho)(4\pi D_B t)^{-(\frac{1}{2}d+1)} \tag{50}$$

when d is the dimensionality of the system. As in the calculation of the diffusion constant of van Leeuwen and Weijland, the result could be applied equally to the overlapping or non-overlapping LG.

Keyes and Mercer (20) made a similar analysis of the VAF at long times using a more recent version of the higher order kinetic theory (29) than that used by Ernst and Weijland. The new version differs from the old version in that the first collision operator T_α which appears in the ring expression t_R in eqn. (44) is replaced by its complex conjugate $\bar{T}_\alpha$. This gives rise to additional terms in the memory function which produce a correction to the Ernst and Weijland results. The results are given explicitly for the three-dimensional case,

$$\langle \mathbf{v}\cdot\mathbf{v}(t)\rangle = (1 + 4\rho\sigma^3\pi/3)^2\langle \mathbf{v}\cdot\mathbf{v}(t)\rangle_{EW}. \qquad \text{3 dimensions} \tag{51}$$

Masters and Keyes (19) determined a repeated ring correction for a two-dimensional overlapping LG to be

$$\langle \mathbf{v}\cdot\mathbf{v}(t)\rangle = (1 + \rho\sigma^2\pi D_R/D_B)^2\langle \mathbf{v}\cdot\mathbf{v}(t)\rangle_{EW} \tag{52}$$

where D_R is the repeated ring diffusion constant obtained by Masters and Keyes and given by Figure 4.3a and D_B is the Boltzmann diffusion constant $D_B = 3\langle v\rangle/(16\rho\sigma)$.

Keyes and Masters (19) also analyzed the VAF for the two- and three-dimensional overlapping LG in the limit of high and low densities using a self-consistent repeated ring equation and the variational principle. At low densities, the calculated value is the same as that

obtained by van Leeuwen and Weijland. As the density approaches the percolation threshold, an additional tail is predicted to exist.

Götze, Leutheusser and Yip (21) calculated the correction to the Ernst and Weyland long-time tail for the two-dimensional LG as

$$\langle \mathbf{v}\cdot\mathbf{v}(t)\rangle = (D_B/D_{MC})(D_{MC}/D_B + \rho\sigma^2\pi)^2\langle \mathbf{v}\cdot\mathbf{v}(t)\rangle_{EW} \qquad (53)$$

with D_{MC} the mode-coupling value of the diffusion coefficient obtained by GLY and presented in Figure 4.3b.

The most recent attack on the problem of the long-time behavior of the VAF for the LG was by Machta, Ernst, van Beijeren and Dorfman in 1984 (18). They provided a mode-coupling theory for the motion of a single particle in a static random medium applicable to variety of models. MEvBD applied their work to the non-overlapping as well as the overlapping LG in two dimensions.

The basis of the theory is the definition of a fluctuating diffusion tensor $\mathbf{K}(\mathbf{r},X)$ and a spatially varying free volume fraction $\Psi(\mathbf{r},X)$ where X is the set containing the number of scatterers N-1 and their positions $(\mathbf{r}_2,\mathbf{r}_3,\ldots,\mathbf{r}_N)$. The current $\mathbf{J}(\mathbf{r},t)$ of the diffusing particles is given by

$$\mathbf{J}(\mathbf{r},t) = -\mathbf{K}(\mathbf{r},X)\cdot\nabla(c(\mathbf{r},t)/\Psi(\mathbf{r},X)) \qquad (54)$$

where $c(\mathbf{r},t)$ is the concentration of moving particles. For the Lorentz models, $\Psi(\mathbf{r},X)$ is set to unity when $\mathbf{r}$ is outside the stationary scatterers and vanishes otherwise. The integral of $\Psi(\mathbf{r},X)$ over the volume of the system, $\Psi_0(X)$, will then be equal to the free volume available to the moving particle for a given configuaration X.

Spatial correlations are considered to be short-ranged with a correlation length of L_0 and an average over cells in configuration

space with sides of length $L_c >> L_0$ is used to coarse grain space. This coarse-graining is applied to $K(r,X)$, $c(r,t)$, and $\Psi(r,X)$ in eqn. (54).

The Fourier transform of the correlation function for the fluctuation of the concentration from equilibrium is the intermediate scattering function,

$$F(k,t) = \langle \hat{c}_{-k}(0)\hat{c}_k(t)\rangle / \langle \hat{c}_{-k}(0)\hat{c}_k(0)\rangle. \qquad (55)$$

The average in eqn. (55) is performed first over the configuration X with a weight function W(X) which is defined for each specific model and then over a grand canonical ensemble containing a distribution $P_M(r^M,v^M)$ of moving particles in r and v for configuration X. The fluctuation $\hat{c}_k$ is $c_k - \langle c_k\rangle_X$, the difference between the value of c_k and the average value for a given configuration X. The average of eqn. (55) can be written as the symmetrical average over a single moving particle

$$F(k,t) = \langle \Sigma_i \, e^{ik\Delta x_i(t)}\rangle / \langle \hat{c}_{-k}(0)\hat{c}_k(0)\rangle \qquad (56)$$

with $\Delta x(t) = x(t) - x(0)$ where the x-axis is taken to be in the same direction as k. Equation (56) can be used to generate the moments $\langle[\Delta x(t)]^n\rangle$ and the first derivative of the first moment $\langle[\Delta x(t)]^2\rangle$ will be the time-dependent diffusion constant D(t),

$$D(t) = (d/dt)\tfrac{1}{2}\langle[\Delta x(t)]^2\rangle.$$

The time derivative of the diffusion constant will be the VAF $\langle v_x(0)v_x(t)\rangle$ in which v_x is the x component of the velocity of the moving particle. Using these formulas and mode-coupling theory, MEvBD arrive at a form for the long-time behavior of the VAF,

$$\langle v_x(0)v_x(t)\rangle \simeq -2\pi D_B{}^2 \Delta_K (4\pi D t)^{-2}$$

where Δ_K is the mean square fluctuation

$$\Delta_K = \langle \delta K_0(X) : \delta K_0(X) \rangle / [2V(D\Psi)^2] \tag{57}$$

and

$$\delta K_0^{\alpha\beta} = \int dr \, [K_{\alpha\beta}(r,X) - D\Psi\delta_{\alpha\beta}]. \tag{58}$$

The magnitude of the long-time tail can be determined once Δ_K is specified.

For the non-overlapping LG, the calculation of Δ_K would require an extensive kinetic theory analysis of the fluctuations in $\langle \hat{v} G_z \hat{v} \rangle$ where G_z is the resolvent operator. Rather than carry out such calculations, MEvBD approximate Δ_K based on the density and arrangement of scatterers. The fluctuation of a function δA_0 is split into two parts, one caused by fluctuations in the number of scatterers and the other, orthogonal to the the first, caused by the arrangement of scatterers,

$$\delta A_0 = (\partial \langle A_0 \rangle / \partial \langle N \rangle) \delta N + \delta_\perp A_0$$

where $\langle \delta N \delta_\perp K_0 \rangle = 0$. The mean square fluctuation will be

$$\langle (\delta A_0)^2 \rangle = (\partial \langle A_0 \rangle / \partial \langle N \rangle)^2 \langle (\delta N)^2 \rangle + \langle (\delta_\perp A_0)^2 \rangle. \tag{59}$$

The number fluctuation $\langle (\delta N)^2 \rangle$ can be written in terms of the compressibilty of a hard disk fluid at a temperature T,

$$\langle (\delta N)^2 \rangle = V S_0(\rho) = V \rho k_B T (\partial \rho / \partial p)_T \tag{60}$$

Equation (54) and the definition of the diffusion constant in terms of the time correlation function of v can be combined to give an expression for K_0

$$K_0 = \lim_{z \to 0} \Psi_0 \langle \hat{v} G_z \hat{v} \rangle_{X,1}$$

with $\langle \ldots \rangle_{X,1}$ indicating the average over a single configuration X. Now K_0 can replace A_0 in eqn. (59) to give

$$\Delta_K = \left(\frac{1}{D\Psi} \frac{dD\Psi}{d\rho} \right)^2 S_0(\rho) + \frac{1}{2V(d\Psi)^2} \langle \delta_\perp K_0 : \delta_\perp K_0 \rangle. \quad (61)$$

The above equation is exact for Δ_K, but the second term on the rhs has not been calculated. MEvBD approximate Δ_K by the first term on the right hand side of eqn. (61). This gives for the long time tail:

$$\langle v_x(0)v_x(t)\rangle \simeq -2\pi \frac{D_B^2}{\rho^2} S_0(\rho) \left(\frac{\rho}{D} \frac{dD}{d\rho} - \frac{\rho\pi\sigma^2}{1 - \rho\pi\sigma^2} \right)^2 (4\pi Dt)^{-2}. \quad (62)$$

The D which appears in eqn. (62) is the density-dependent diffusion constant as calculated by van Leeuwen and Weijland(13) and given by eqn. (42). The authors also provide an expression for the long-time tail of the overlapping LG, it is

$$\langle v_x(0)v_x(t)\rangle_{ov} \simeq -2\pi \frac{D_B^2}{\rho} (\rho) \left(\frac{\rho}{D} \frac{dD}{d\rho} - \rho\pi\sigma^2 \right)^2 (4\pi Dt)^{-2}. \quad (63)$$

All the above calculations of the magnitude of the long-time tail have been shown (18) to underestimate the tail as calculated by the computer simulation of a low-density non-overlapping LG by Lewis and Tjon (12) and low-density overlapping LG by Alder and Alley (9,10).

The long-time tail of the VAF has also been studied using the Burnett coefficient (9,10,19) which is defined by

$$B(t) = (d/dt)\{\langle [\Delta x(t)]^4 \rangle - 3\langle [\Delta x(t)]^2 \rangle^2\}/4!$$

where $\Delta x(t)$ is the displacement of a single particle from its initial positon $\Delta x(t=0)$. The calculation of the Burnett coefficient from theoretical grounds will not be given here.

The long-time limit of the VAF has been also been studied near the percolation threshold (15), in periodic lattices (16) and disordered hopping models which mimic the behavior of the LG(17).

In the next section, the method of simulation of the non-overlapping LG will be discussed and the results of the simulation compared to the theoretical predictions of Sections B and C.

D. Molecular Dynamics Simulation of the Non-overlapping Lorentz Gas

The simulation of the non-overlapping LG was performed by following a point particle placed at random in a configuration of hard disks. An initial velocity was altered by the classical elastic collision of the particle with the stationary scatterers. The particle was followed through a configuration for a specified number of mean collision times and a large number of configurations (600-2000) were used to ensure that the results were representative of a true average over random configurations. As the particle moved through the disks, the program calculated the velocity autocorrelation function, the mean-square displacement of the moving particle and the distribution of collision times.

The description of the simulation will refer to the density of scatterers in terms of the packing fraction, $\rho^* = N\pi\sigma^2/V$. All times are scaled by the Enskog mean free time given in eqn. (5) and written as a function of the packing fraction as

$$\tau_c = \pi\sigma/(2\rho^*\langle v\rangle g(r_s)).$$

Times are given as $s = t/\tau_c$ in units of τ_c.

The configurations through which the particle moved consisted of a number of scatterers N with radius σ placed in a square of side length L and volume V. Periodic boundary conditions were used when the particle reached the edge of the box. For packing fractions of 0.2 and

above, 500 scatterers were used. At low density, 2000 particles were used to reduce the possible effects of the periodic boundary conditions and to reduce the chance of the particle traveling completely across the system without encountering another particle. The positions of the scatterers were determined in one of two ways, depending on the density of the system. For high densities, $\rho^* > 0.5$, a traditional MC algorithm was used (30). An initial regular lattice was allowed to evolve for a large number of MC cycles to obtain a random configuration. Further configuations were obtained by altering the random configuration by a smaller number of MC cycles. The MC method proved to be time-consuming and, at the high densities for which it was used, to constitute a significant portion of the simulation time. For low and intermediate densities, configurations were obtained by direct generation. Scatterers were placed randomly in the system one at a time and checked for overlap with previously placed scatterers. If there was overlap, a new random position was tried, if not, the particle was left in position and an attempt made to add another particle. This process was repeated until the required number of particles had been included in the system. The method of random placement was originally to have been used only for the very lowest densities, but its utility at higher densities was examined because of the time required by the MC algorithm. It was found to be an effective method for generating random configurations for packing fraction up to 0.5. Above $\rho^* = 0.5$, there was a sharp increase in the amount of time required by the method of random placement.

In each configuration, the path of the moving particle was followed

for $1300\tau_c$ for densities of $\rho^* \leq 0.5$ or $650\tau_c$ for higher densities. Although a single trajectory was run for each configuration, a number of correlation functions were obtained. The average VAF from single trajectory was an average of 2500 correlation functions given by

$$\langle v(0)\cdot v(\zeta)\rangle = (2500)^{-1} \Sigma_i \, (v(s_i)\cdot v(s_i+\zeta))/v^2 \qquad (64)$$

where the sum over i goes from one to 2500. The starting times for the trajectories were separated by an interval $\Delta s_i = s_{i+1} - s_i$, Δs_i was taken to be $0.5\tau_c$. Correlation functions are calculated with ζ = zero to ζ_{max} at intervals of $0.1\tau_c$. The intervals Δs_i and $\Delta\zeta$ were chosen based on the work of Bruin (8) on the overlapping LG. The maximum time ζ_{max} was $50.0\tau_c$ for packing fractions ≤ 0.5 and $25.0\tau_c$ for higher packing fractions. The mean square displacement was averaged in the same manner as the VAF. The mean square displacement at time ζ averaged for a single configuration given by

$$\langle(\Delta r)^2\rangle = (2500)^{-1} \Sigma_i \, [r(s_i + \zeta) - r(s_i)]^2\sigma^2.$$

In addition to the VAF and the displacement, the functions required to obtain the standard deviations of the VAF and the displacement from trajectory to trajectory were calculated.

The distribution of collision times was also determined. The time elapsed between each set of successive collisions was used to calculate the proportion of collision sequences corresponding to time intervals ranging from 0 to $8.0\tau_c$ in intervals of $0.04\tau_c$. Standard deviations for the collision time distribution were calculated. Each trajectory provided ~1300 (650 for high densities) collision sequences which could be included in the collision time distribution.

The number of configurations (≡ number of trajectories) used to obtain the averages given in Table 4.1 varied with the packing fraction. For $\rho^* \leq 0.3$, 1000 configurations were used; for $0.3 < \rho^* \leq 0.5$, 2000 configurations were used and for the highest densities, $\rho^* > 0.5$, 600 configurations were used. The small number of configurations utilized for high densities is a reflection of the large amount of time required to generate the MC configurations as well as doubts about the ability of the MC method to provide configurations which differ significantly from one another at these densities. The highest density chosen, $\rho^* = 0.8$, is above the first-order fluid-solid phase transition observed in simulations of two-dimensional fluids(31).

The diffusion constant was calculated from the VAF and from the mean square displacement. The diffusion constant can be determined by the numerical integration of the VAF. The mean square displacement value of the diffusion constant is determined from the slope of a plot of mean square displacement versus time for long times. The two calculations are in good agreement with each other. The ratio of the diffusion constant to the Boltzmann diffusion constant (D/D_B) is given in table 4.1. Also given in table 4.1 is the ratio $(D/D_B)_{vLW}$, as calculated using eqn. (42)., and $(1/g(r_s))(D/D_B)_{vLW}$. Plotted in figure 4.5 are the VAF calculation of D/D_B and $(1/g(r_s))(D/D_B)_{vLW}$. The rdf at contact for the moving particle in a bath of disks is given by $g(r_s) = 1/(1-\rho^*)$ (32).

It can be seen from both the figure and the table that the simulation results are in excellent agreement with $(1/g(r_s))(D/D_B)_{vLW}$, even at the highest density studied. The

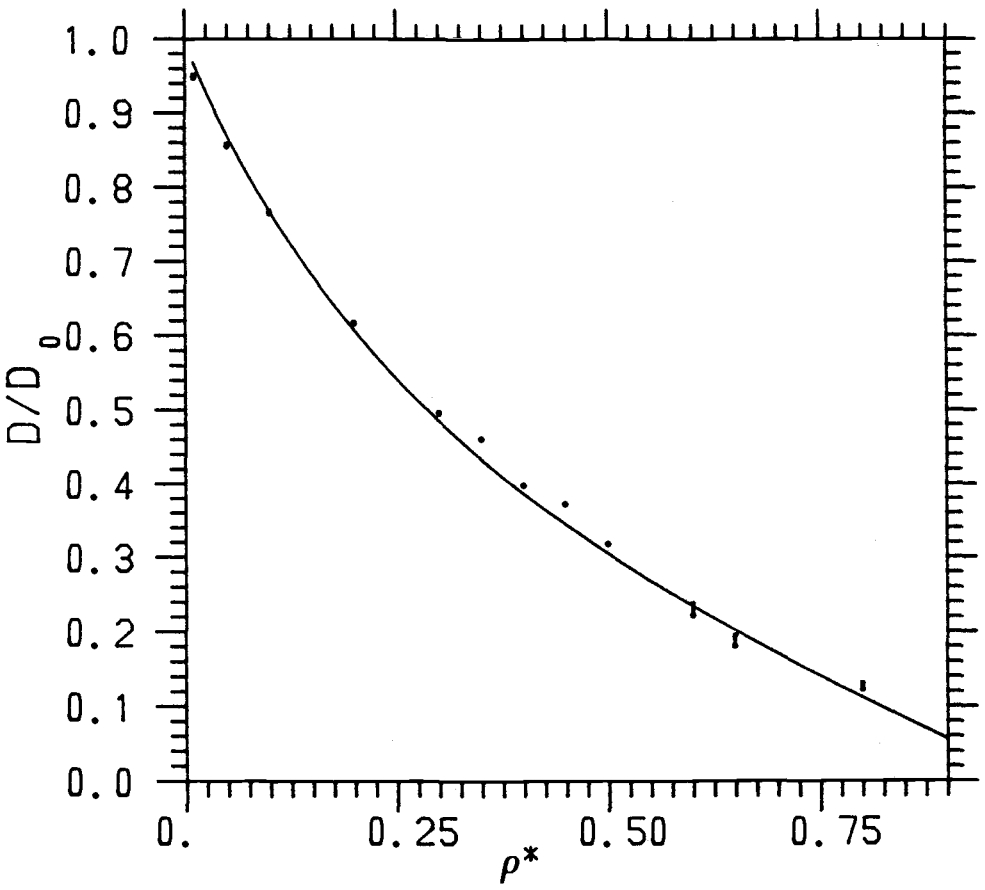

Figure 4.5 The reduced diffusion coefficient for the non-overlapping Lorentz gas plotted as a function of the packing fraction. The points are D/D_B as calculated by the simulation. The error bars are one standard deviation above and one standard deviation below the average value. The line is $[1/g(r_s)](D/D_B)_{vLW}$ (ref. 13).

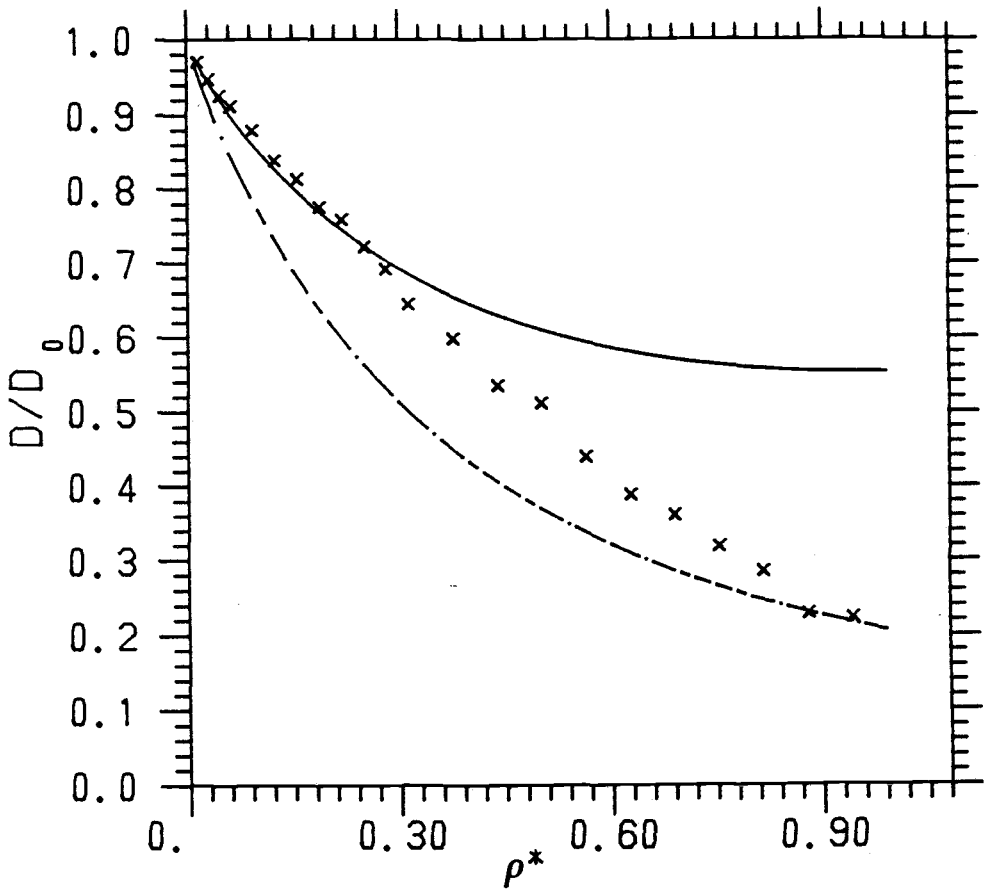

Figure 4.6 The reduced diffusion coefficient for the overlapping Lorentz gas plotted as a function of the packing fraction ρ^*. The crosses are D/D_B as calculated by Bruin's simulation (ref. 8). The solid line is $(D/D_B)_{vLW}$ (ref. 13). The broken line is $[1/g(r_s)](D/D_B)_{vLW}$.

Table 4.1

The diffusion constant for the non-overlapping LG

ρ^*[a]	$D/D_B(v)$[b]	$D/D_B(r)$[c]	$(D/D_B)_{vLW}$[d]	$(1/g(r_s))(D/D_B)_{vLW}$[e]
0.01	0.97(1)	0.95(1)	0.98	0.97
0.05	0.86(1)	0.88(1)	0.91	0.87
0.10	0.76(1)	0.78(1)	0.85	0.77
0.20	0.62(1)	0.63(2)	0.76	0.61
0.30	0.49(1)	0.50(1)	0.69	0.48
0.35	0.46(1)	0.47(1)	0.67	0.43
0.40	0.40(1)	0.40(1)	0.65	0.39
0.45	0.37(1)	0.38(1)	0.63	0.34
0.50	0.32(1)	0.33(1)	0.61	0.30
0.60	0.23(1)	0.23(1)	0.59	0.23
0.65	0.19(1)	0.19(1)	0.58	0.20
0.80	0.13(1)	0.14(1)	0.56	0.11

[a] ρ^* is the packing fraction $\pi N\sigma^2/V$ where N/V is the number density of scatterers and σ is the scatterer radius. [b]The value given is D/D_B as calculated by Simpson's rule integration of the velocity autocorrelation function; the number given in parentheses is the uncertainty in the last digit. D_B is the Boltzmann value of the diffusion constant $3\langle v\rangle\pi\sigma/8\rho^*$. [c]The value given is D/D_B as calculated from a least sqaures fit of $\langle(\Delta r)^2\rangle$ versus t. For densities $\rho^* \leq 0.5$, the fit was over 40 to 50 mean collision times. For densities $\rho^* > 0.5$ the fit was over 20 to 25 mean collision times from the origin. [d]The value given is D/D_B as determined by van Leeuwen and Weijland (ref. 13) and given by eqn. (42). [e]The value given is the van Leeuwen and Weijland result given in the previous column divided by the contact value of the radial distribution function $(1/(1-\rho^*))$.

$(1/g(r_s))(D/D_B)_{vLW}$, even at the highest density studied. The derivation of eqn. (42) did not make a distinction between the overlapping and non-overlapping LG's, so the result should be applicable to either. The agreement between $(D/D_B)_{vLW}$ and the overlapping LG diffusion constant results, shown in figure 4.6, is reasonable for low density , but $(D/D_B)_{vLW}$ overestimates the diffusion constant for the non-overlapping LG at all but the very lowest densities. One of the primary differences between the overlapping and non-overlapping LG's is the structure of the non-overlapping LG represented by the radial distribution function. There is no rigorous basis for the inclusion of the radial distribution function in the denominator of $(D/D_B)_{vLW}$, but the idea is supported by the fact that the Enskog diffusion coefficient which takes into account the structure of the fluid differs from the Boltzmann diffusion coefficient by a factor of $g(r_s)$. The diffusion coefficient $(D/D_B)_{vLW}$ was also divided by the radial distribution function of the overlapping LG, $\exp(-\rho^*)$ (18), and compared to the results of Bruin, but the agreement between theory and simulation was not significantly improved, as can be seen from figure 4.6.

The VAF's displayed the expected behavior for all densities except $\rho^* = 0.8$. For densities other than 0.8, the VAF displayed an initial rapid decay to nearly zero, followed by a more gradual decay to below zero and a gradual return to near zero. Plots of the VAF's are shown in figures 4.1 and 4.7-17. The VAF is plotted, along with the Enskog prediction for the VAF, $\langle v \cdot v(t) \rangle = \exp(-4s/3)$, and the difference between the the two. The error bars are one standard deviation above

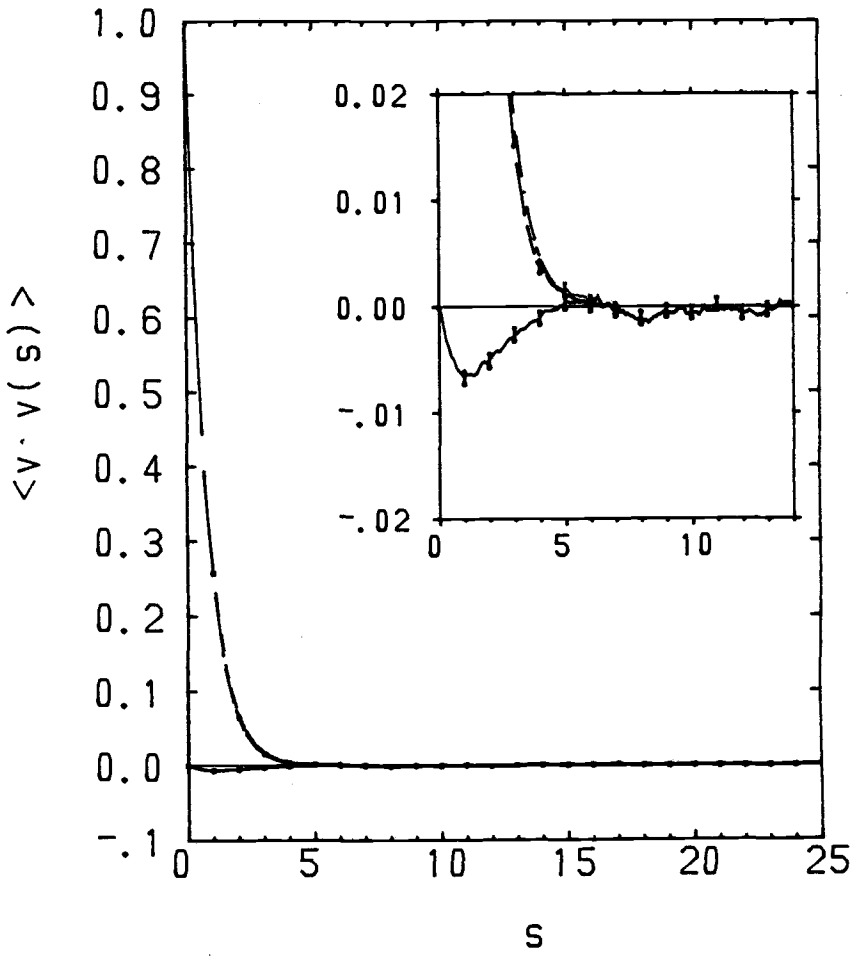

Figure 4.7 The velocity autocorrelation function for the non-overlapping Lorentz gas at a packing fraction $N\pi\sigma^2/V = 0.01$. The time, s, is given in units of the Enskog mean free time, $\pi\sigma/(\rho^*\langle v\rangle g(r_s))$. The lower, solid line is the difference $\langle \mathbf{v}\ \mathbf{v(s)}\rangle - \exp(-4s/3)$, the broken line is $\langle \mathbf{v}\ \mathbf{v}(s)\rangle$ and the uppermost, dotted line is the Enskog prediction $\exp(-4s/3)$. Error bars are one standard deviation above and one standard deviation below the simulation values.

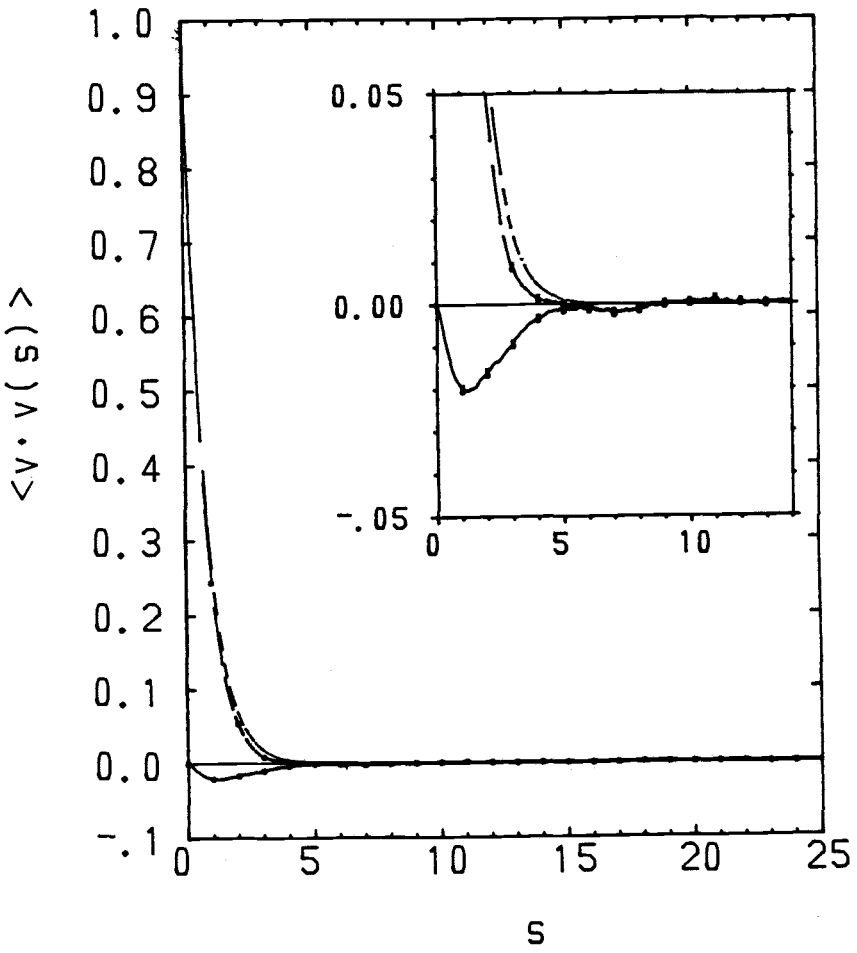

Figure 4.8 The same as figure 4.7, but the packing fraction is $\rho^* = 0.05$

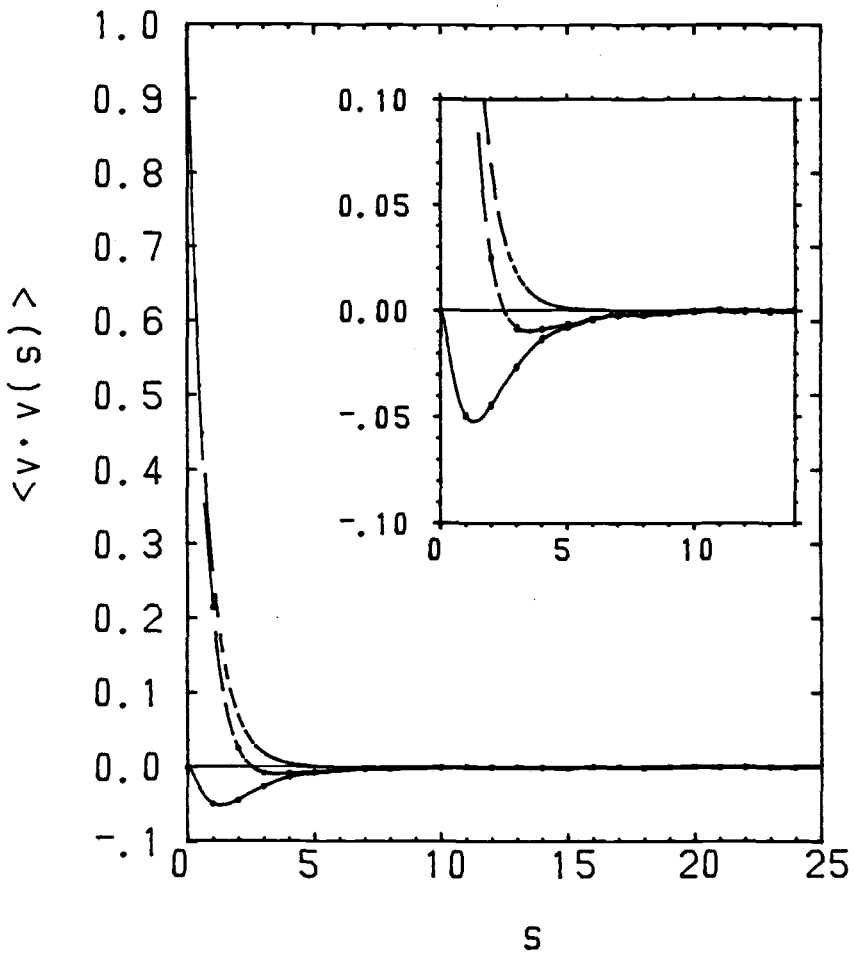

Figure 4.9 The same as figure 4.7, but the packing fraction is $\rho^* = 0.2$.

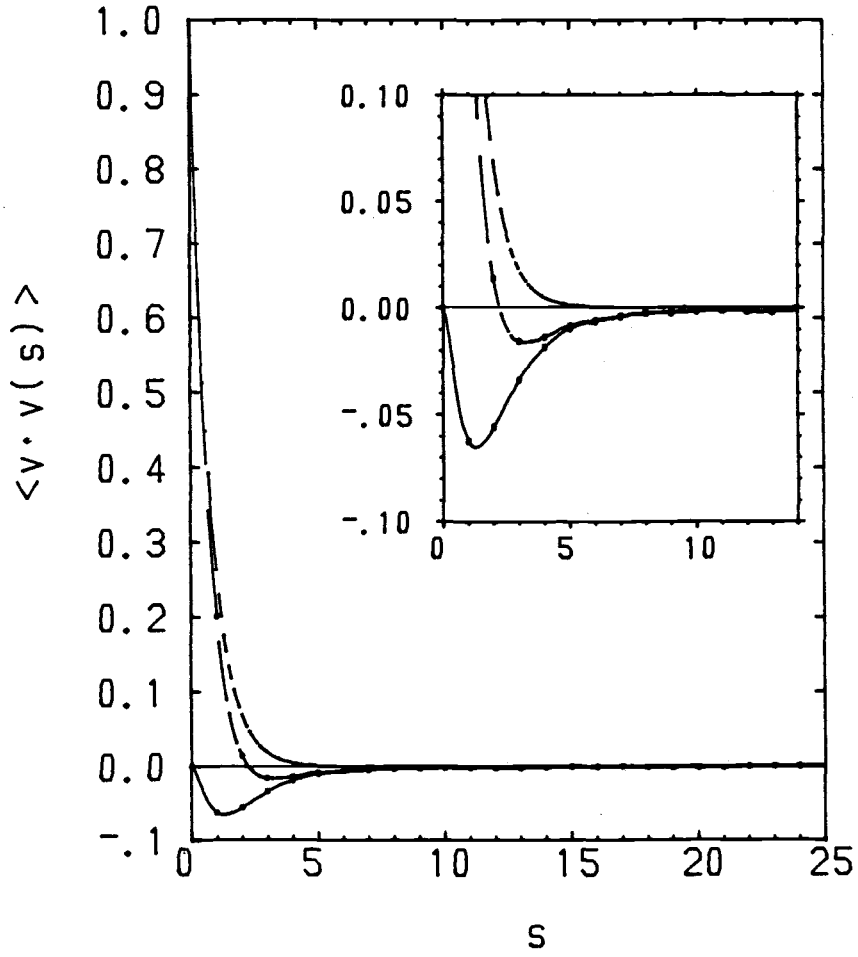

Figure 4.10 The same as figure 4.7, but the packing fraction is $\rho^* = 0.3$

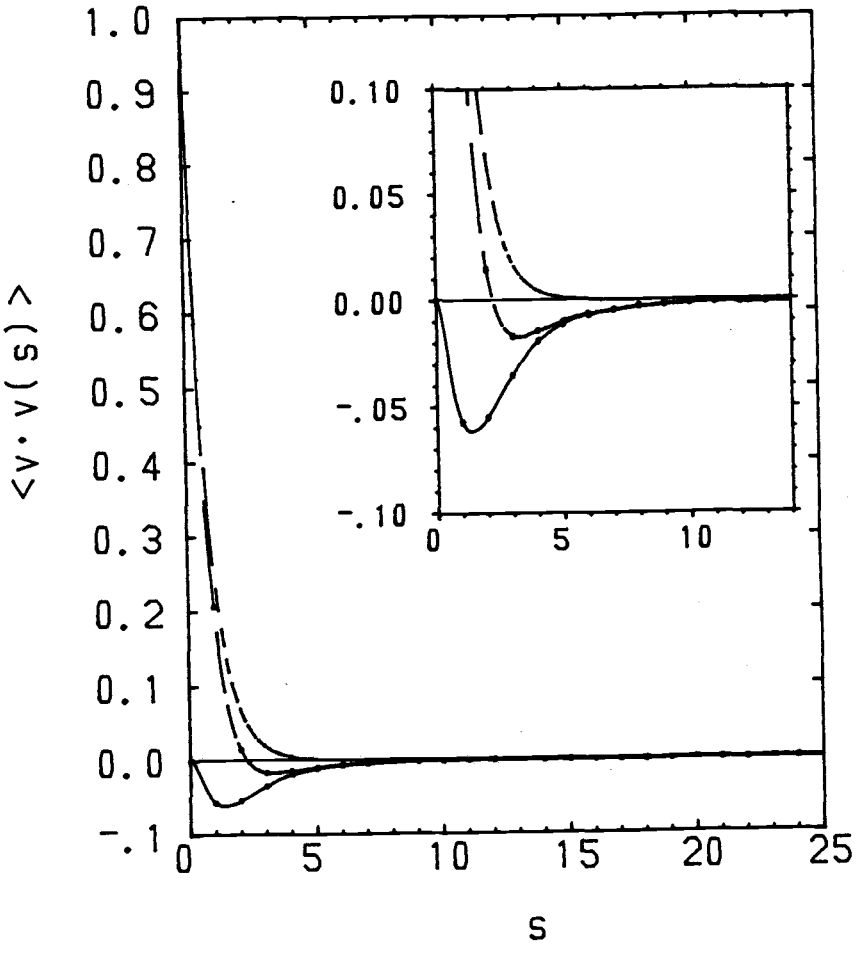

Figure 4.11 The same as figure 4.7, but the packing fraction is $\rho^* = 0.35$

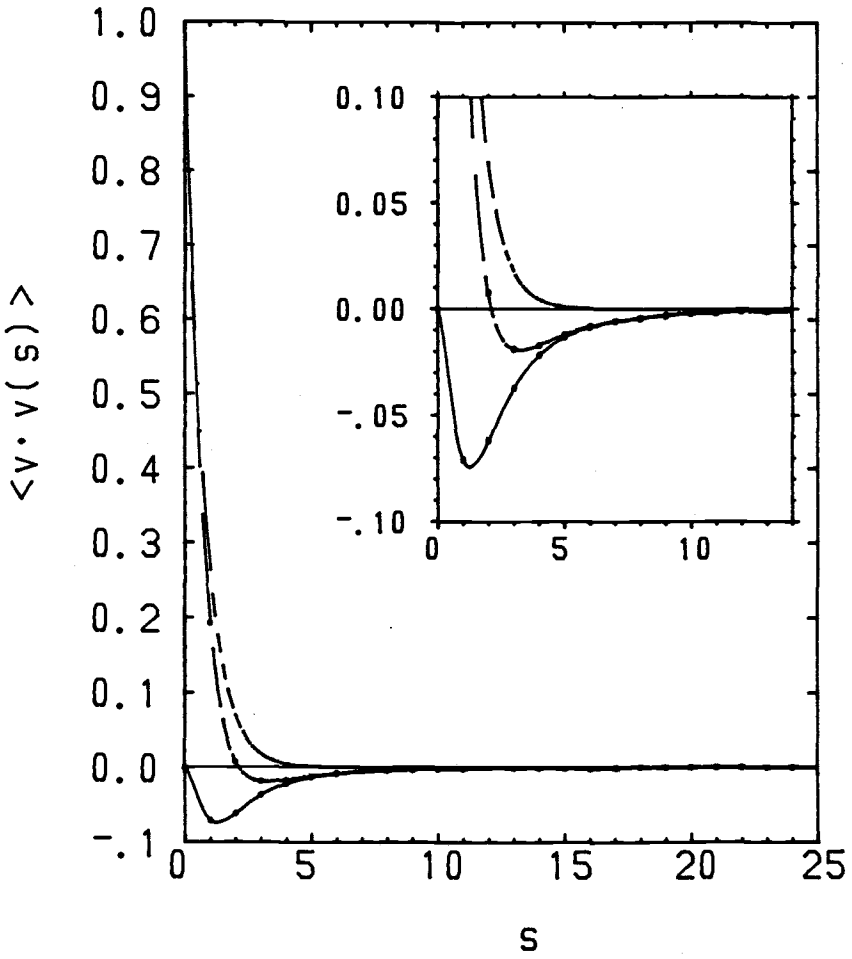

Figure 4.12 The same as figure 4.7, but the packing fraction is $\rho^* = 0.4$

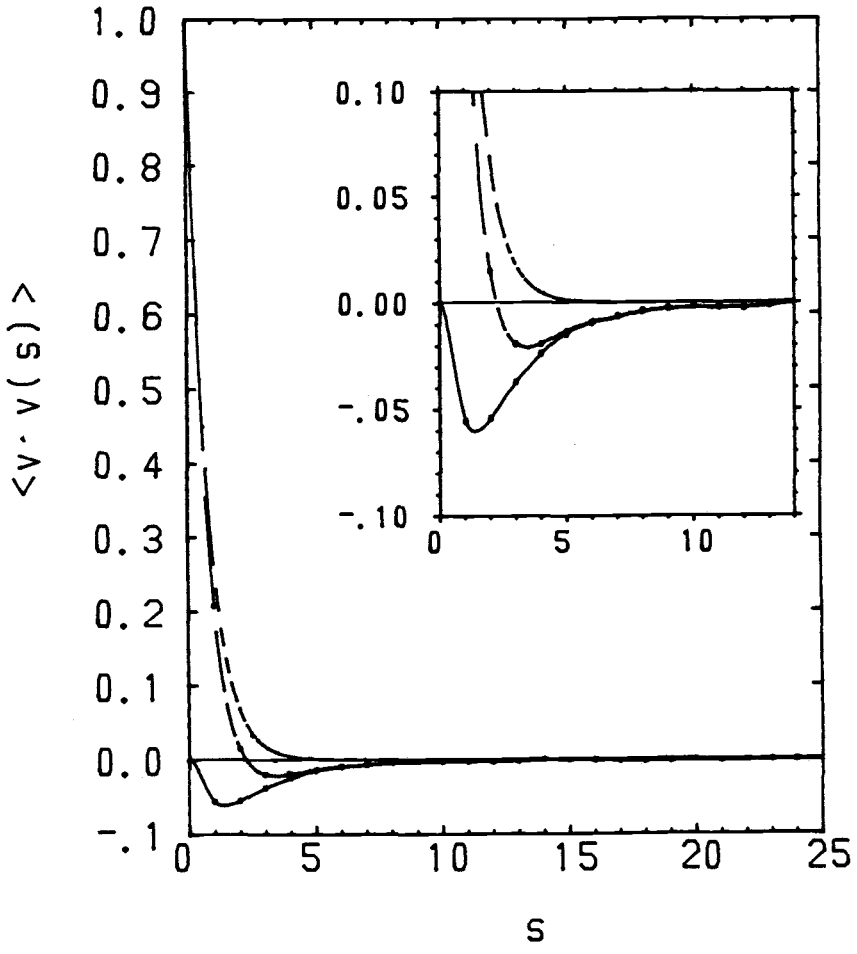

Figure 4.13 The same as figure 4.7, but the packing fraction is $\rho^* = 0.45$

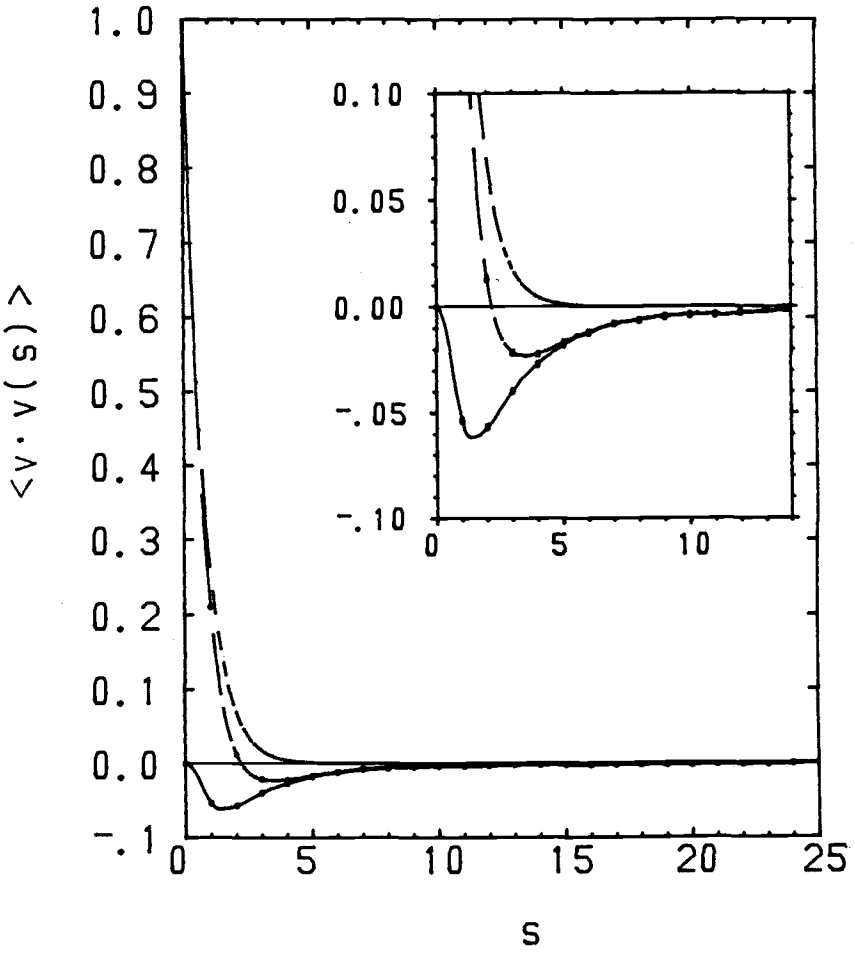

Figure 4.14 The same as figure 4.7, but the packing fraction is $\rho^* = 0.5$

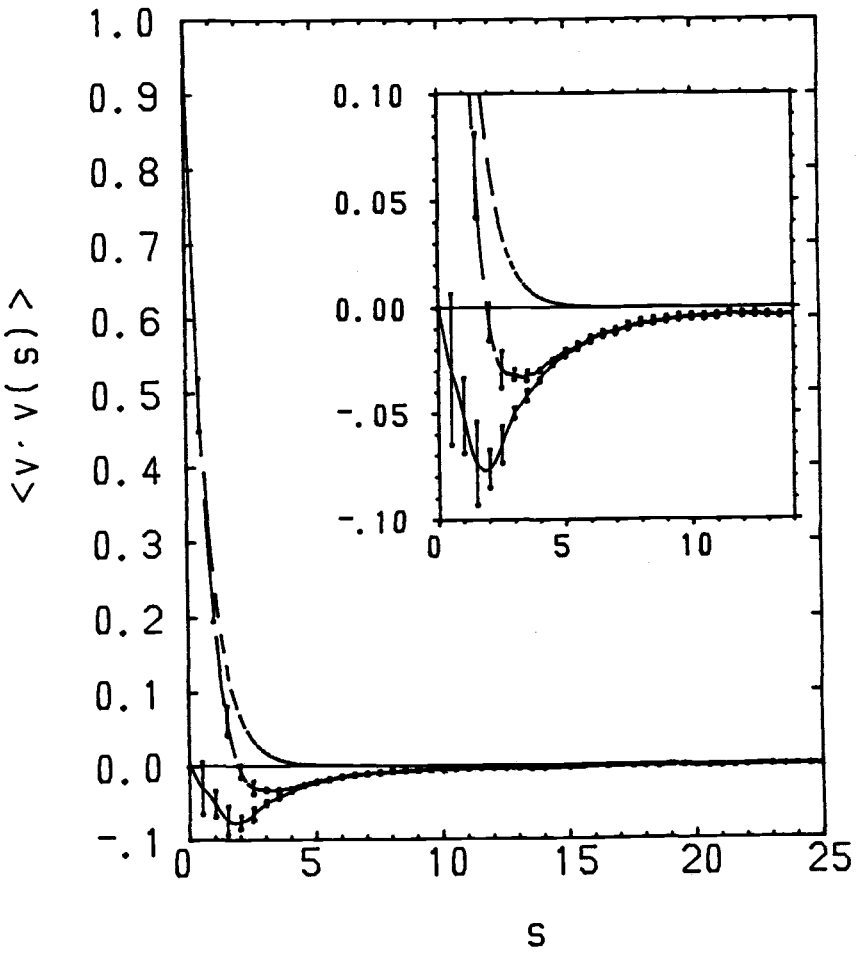

Figure 4.15 The same as figure 4.7, but the packing fraction is $\rho^* = 0.6$

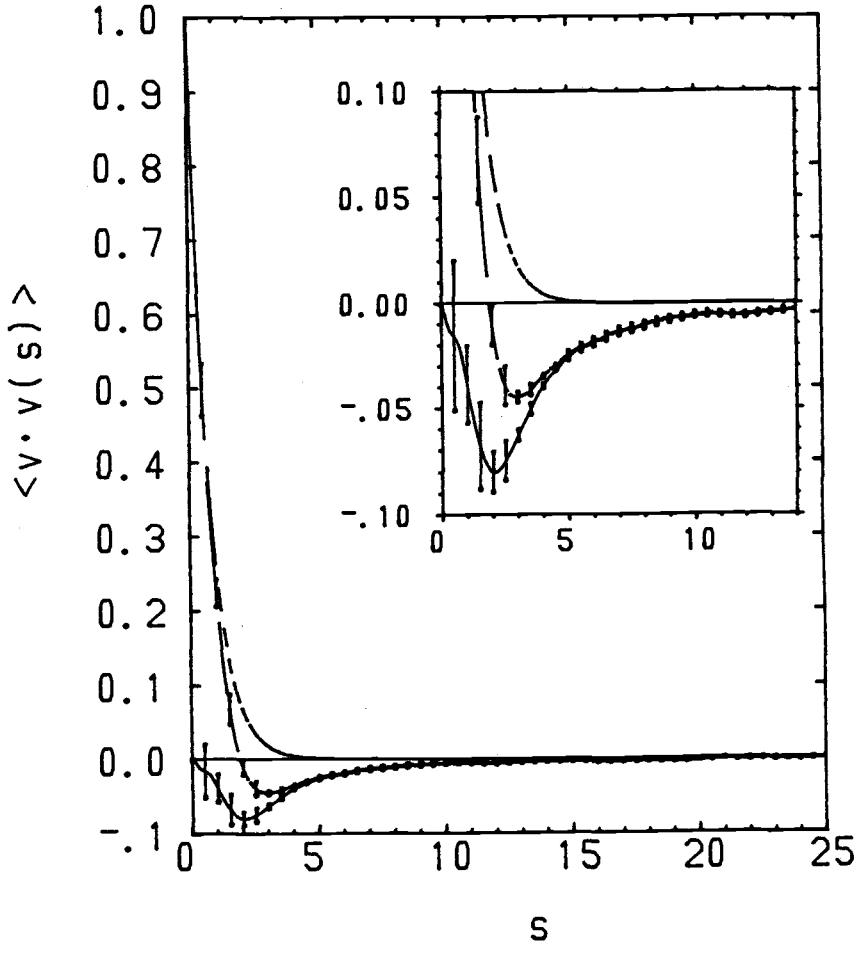

Figure 4.16 The same as figure 4.7, but the packing fraction is $\rho^* = 0.65$

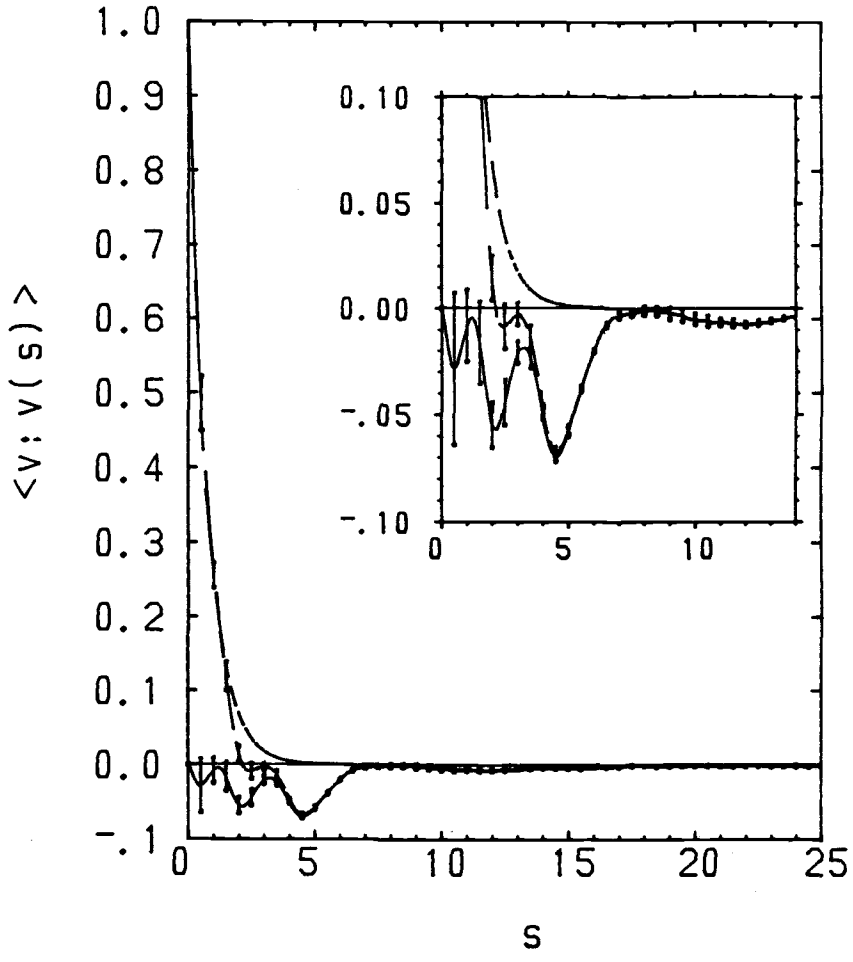

Figure 4.17 The same as figure 4.7, but the packing fraction is $\rho^* = 0.8$

and one standard deviation below the value. The error in the simulation values of the VAF is large compared to the magnitude of the negative portion of the VAF for the lowest densities and calculations based on the VAF tail for densities $\rho^* \leq 0.1$ are the least reliable of those reported here. At higher densities, the tail becomes more well-defined and results can be considered more reliable.

Figure 4.17 shows the VAF for the density $\rho^* = 0.8$. The VAF shows two, and perhaps three minima rather than the one seen at other densities. Because the packing fraction of 0.8 is above the density at which the phase transition takes place (31), it was expected that the VAF would be different then the lower density VAF's. The presence of multiple minima may be due to trapping of the moving particle. The error bars for the short-time VAF at this density and at $\rho^* = 0.6$ and .65 are much larger than those observed at other densities. Additionally, at $\rho^* = 0.6$ and 0.65, the VAF shows a different short time decay than other densities; a shoulder is apparent on the left side of the function $\langle \mathbf{v} \cdot \mathbf{v}(t) \rangle - \exp(-4s/3)$. It is unclear whether this is the result of inadequate sampling of phase space or of clustering in the system. For these densities, the traditional Monte Carlo procedure was used to generate configurations rather than the random placement method used at lower densities and it is possible that this results in repeated analysis of similar configurations. This inadequate sampling would, however, be expected to lead to smaller error bars than a true sample. During the testing of the random placement algorithm, there was a dramatic increase observed in the amount of time required to generate random placement configurations at

packing fractions greater than 0.5. All of this information suggests the gradual onset of a change in the normally homogeneous arrangement of scatterers at densities of $\rho^* > 0.5$, but more investigation would be required to prove that such a change is taking place.

The magnitude of the long-time tail of the VAF was determined by a least squares fit of the difference between the VAF and exp(-4s/3) for times ranging from 5s to 13s to the equations

$$\langle \mathbf{v}\cdot\mathbf{v}(t)\rangle = As^B \tag{65}$$

and

$$\langle \mathbf{v}\cdot\mathbf{v}(t)\rangle = as^{-2}. \tag{66}$$

The results of the fit to s^{-2} are given in table 4.2. The exponent B calculated from the free fit (eqn. (65)) ranged from -1.5 to -4 for all but the lowest density, although in most cases it was within ± 0.2 of -2; these results are given in table 4.3 along with details of the simulation itself. For the lowest density studied, $\rho^* = 0.01$, the exponent of the tail of the free fit for times of 5 to 13 Enskog collision times was positive, but the results of the fit of the same points with the exponent constrained to be -2 appear to give a resonable indication of the behavior of the correlation for times ranging for 3 to 20 Enskog collision times. This is shown in figure 4.18.

The magnitude of the tail from the simulation was obtained in units corresponding to an Enskog reduced time and the theoretical magnitude is usually given in units corresponding to the Boltzmann reduced time. The Enskog and Boltzmann reduced time units differ by a factor of $g(r_s)$. The magnitude obtained first is converted to units

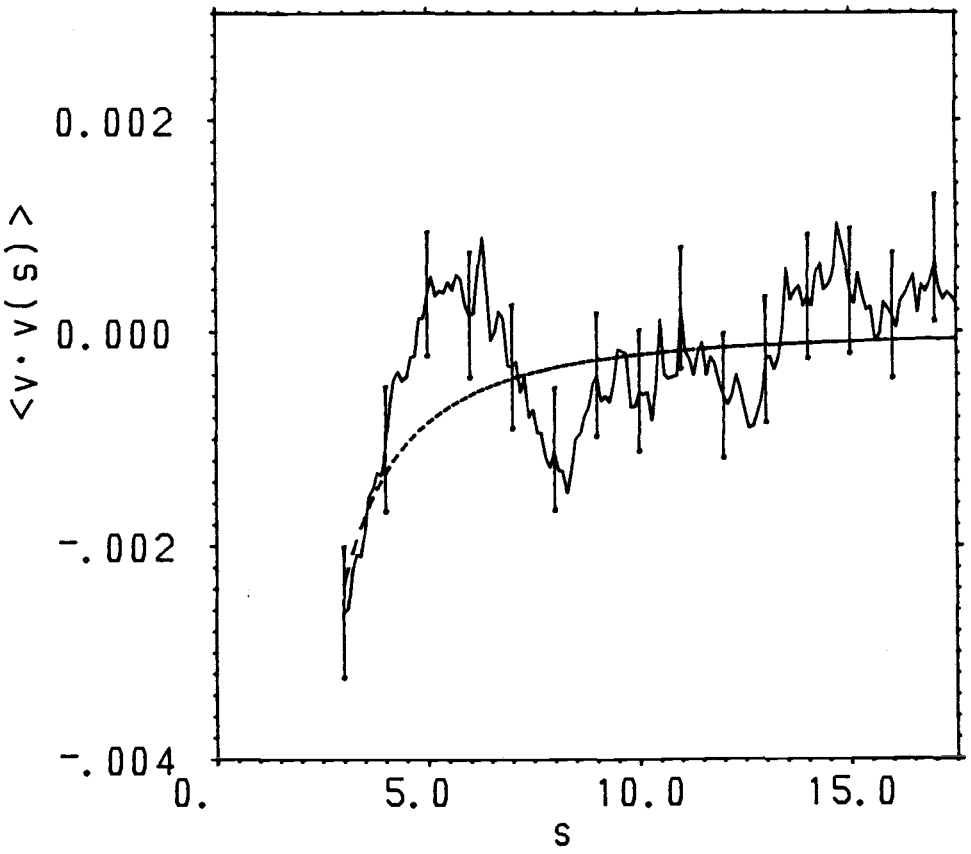

Figure 4.18 Curve-fitting of the VAF for the non-overlapping Lorentz gas with a packing fraction $\rho^* = 0.01$. The time, s, is given in units of $\pi\sigma/(\rho^* g(r_s))$. Error bars are one standard deviation above and one standard deviation below the simulation values. The dotted line is $\langle v\, v(t)\rangle = -0.02 s^{-2}$.

Table 4.2

Velocity autocorrelation function analysis for the non-overlapping LG

ρ^*	$-a^a$	$-\Lambda_b$	$-\alpha_c$
0.01	0.02(1)[d]	0.02(1)	$2(1)\times10^2$
0.05	0.04(2)	0.04(2)	8(4)
0.10	0.05(2)	0.04(2)	4(2)
0.20	0.08(3)	0.05(2)	2.5(9)
0.30	0.20(4)	0.10(2)	3.2(6)
0.35	0.21(4)	0.09(2)	2.5(5)
0.40	0.23(4)	0.08(2)	2.0(4)
0.45	0.29(5)	0.09(1)	1.9(3)
0.50	0.40(5)	0.10(1)	2.0(2)
0.60	0.51(4)	0.08(1)	1.3(1)
0.65	0.61(3)	0.08(1)	1.1(1)

[a] a is the coefficient in the fit of the VAF to $\langle \mathbf{v}\cdot\mathbf{v}(t)\rangle = as_B^{-2}$ where s_B is the Boltzmann collision time. [b] Λ is $ag(r_s)^{-2}$. [c] α is $\pi^2 a/[\rho^* g(r_s)^2]$. The number in parentheses is the estimated error in the last digit given. This number is the standard deviation of points from 5 to 13 s_E from the line $\ln\langle \mathbf{v}\cdot\mathbf{v}(t)\rangle = \ln(a) - 2\ln(s_E)$ for the first column. The deviation is multiplied by the appropriate factors to obtain the error for the other two columns.

corresponding to the Boltzmann reduced time by division by the radial distribution function $1/(1-\rho^*)$,

$$\langle \mathbf{v}\cdot\mathbf{v}(t)\rangle = as^{-2} = a[g(r_s)s_B]^{-2} = \Lambda s_B^{\,2} \tag{67}$$

where $s_B = 2\rho^*\langle v\rangle t/(\pi\sigma)$. The basic kinetic theory treatment of Ernst and Weijland (14) predicts that the VAF at long times will be

$$\langle \mathbf{v}\cdot\mathbf{v}(t)\rangle_{EW} = \rho^*(\pi s_B)^{-2}. \tag{68}$$

The coefficient, a, defined in eqn. (67) is further reduced to facilitate comparison with theory; the reduced magnitude α is defined by the relation

$$\langle \mathbf{v}\cdot\mathbf{v}(t)\rangle = \alpha\rho^*/(\pi s_B)^{-2}, \tag{69}$$

then

$$\alpha = \pi^2\Lambda/\rho^* = \pi^2 a/[\rho^* g(r_s)^2]. \tag{70}$$

Plotted in figure 4.19 are the values of the coefficient α. If the theory of Ernst and Weijland is correct, then the coefficient α will be independent of the density and the points should form a straight line of slope zero and intercept one. The predictions of more sophisticated theories (18-21), given by eqns. (52), (53), and (62), all dictate that the coefficient α should increase with density. Also plotted in the figure are the results of Masters and Keyes (19) and of MEvBD (18). It should be noted that only the work of MEvBD is directed explicitly at the non-overlapping LG; nevertheless it is clear that the simulation results are qualitatively different from the theoretical predictions. The simulation results indicate that α is a decreasing function of density. The large error bars on the low density points allow for the possibility that the actual behavior is independent of density, in accord with the theory of van Leeuwen and Weijland, but it

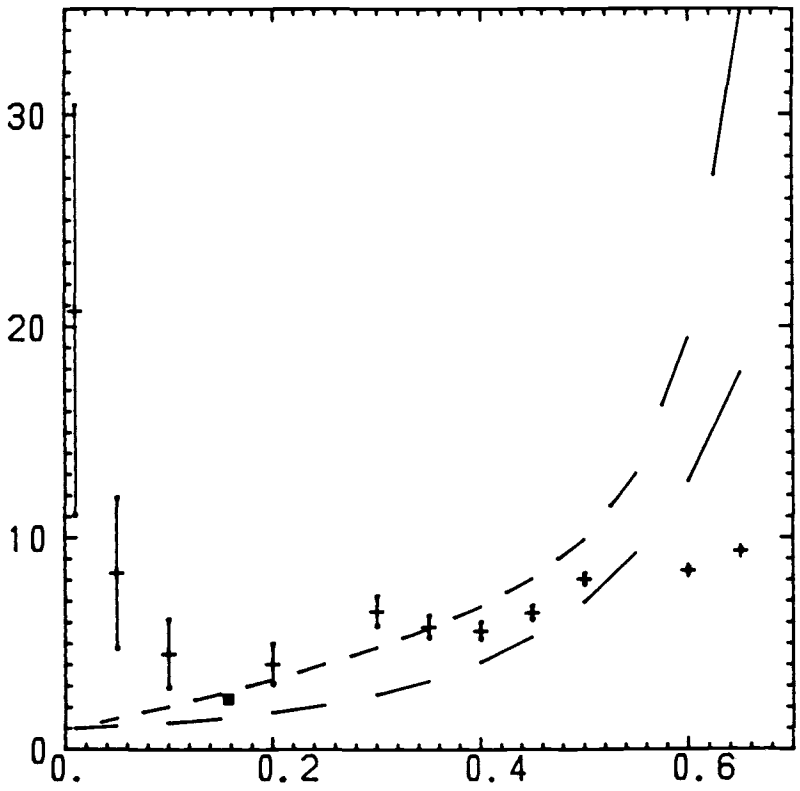

Figure 4.19 The magnitude of the long-time tail of the velocity autocorrelation function for the non-overlapping Lorentz gas as a function of the packing fraction. The points are the values α from the curve-fitting of $\langle \mathbf{v}\, \mathbf{v}(s)\rangle$,

$\langle \mathbf{v}\, \mathbf{v}(s)\rangle = \alpha[\rho^* g(r_s)^2/(\pi^2)]s_B^{-2}$. Error bars are one standard deviation above and one standard deviation below the simulation values. The single square is the value given by Lewis and Tjon (ref 12). The lower broken line is the prediction of Masters and Keyes (ref. 19), eqn. (52). The upper broken line is the result of Machta, Ernst, van Beijeren and Dorfman (ref. 18), eqn. (62).

Table 4.3

LG molecular dynamics simulation parameters

ρ^*	N[a]	N_t[b]	N_{MC}[c]	ζ_{max}[d]	τ_r[e]	-A[f]	B[g]	R_c[h]
0.01	2000	1000		50	40-50	-0.26	4×10^{-3}	-0.009
0.05	2000	1000		50	40-50	0.61	-2.25	-0.61
0.10	2000	1000		50	40-50	0.02	-1.51	-0.36
0.20	2000	1000		50	40-50	4.7	-3.88	-0.90
0.30	500	1000		50	40-50	0.21	-2.02	-0.93
0.35	500	2000		50	40-50	0.69	-2.58	-0.98
0.40	500	2000		50	40-50	1.6	-2.91	-0.99
0.45	500	1600		50	40-50	0.45	-2.19	-0.98
0.50	500	2000		50	40-50	0.54	-2.13	-0.99
0.60	500	600	200	25	20-25	0.66	-2.11	-0.99
0.65	500	600	200	25	20-25	0.48	-1.83	-0.98
0.80	500	600	200	25	20-25			

[a]N is the number of scatterers. [b]N_t is the number of trajectories (≡ configurations) included in the averages. [c]N_{MC} is the number of Monte Carlo cycles between successive trajectories. A cycle consists of an attempt to move each of the scatterers once. [d]ζ_{max} is the maximum time in units of Enskog collision times for which correlation functions were calculated. [e]τ_r gives the lower and upper limits of the times in units of Enskog collision times included in the calculation of the diffusion constant from $d\langle(\Delta r)^2\rangle/dt$. [f]A is the magnitude of the tail determined from a least squares fit of $\langle \mathbf{v}\cdot\mathbf{v}(t)\rangle = As_E^B$. [g]B is the exponent determined from a least squares fit of $\langle \mathbf{v}\cdot\mathbf{v}(t)\rangle = As_E^B$. [h]$R_c$ is the correlation coefficient for the line $\ln(\langle \mathbf{v}\cdot\mathbf{v}(t)\rangle) = \ln(A) - B\ln(s_E)$.

is unlikely that α is an increasing function of the density.

The results given here are in agreement with the single published low density result of Lewis and Tjon (12). An interesting point to note is that the values for the low density simulation results in units of Enskog collision times compare very favorably with the results of Alder and Alley for the low-density overlapping LG in units of Boltzmann collision times. This is illustrated in table 4.4.; the numerical values for similar densities are in agreement within experimental error. The density dependence of the low density results of Alder and Alley have been found to agree with kinetic theory results, although at high density the coefficient is underestimated by theory. The agreement of the results in table 4.4 with each other allows for the possiblity that the conversion of the theoretical predictions to a form which applies to the non-overlapping Lorentz gas

Table 4.4
Comparison of VAF results

This work[a]		Alder and Alley(9)[b]	
ρ^*	$-a$	ρ^*	$-\Lambda$
0.10	0.05(2)[c]	0.0942	0.026(5)
0.20	0.08(3)	0.157	0.060(5)
0.30	0.20(4)	0.314	0.20(5)

[a]These are the same results reported under a in table 4.3. [b]The coefficient of the fit $\langle \mathbf{v}\cdot\mathbf{v}(t)\rangle = \Lambda/s_B^2$ for the overlapping LG. Note that the units are different that those of a. [c]the number in parentheses is the uncertainty in the last digit.

involves $g(r_s)$,as was the case with the diffusion constant. However, the inclusion of factors of $g(r_s)$ or of $g(r_s)^2$ does not serve to bring the results and the theory into agreement.

Previous calculations of the magnitude of the long-time tail in the LG (9,10,12) have fit the value of the VAF to the t_{-2} decay at times greater than those considered here. The fit of Lewis and Tjon (12), for example, was from 8.5 to 19.0 collision times and Alder and Alley (9,10) did not consider points below ten collision times. It is possible that when the tail is fit over 5 to 13 collision times, the long-time tail itself is not being considered, but rather some intermediate decay.

The distributions of collision times for some representative systems are given in figures 4.20-4.22. For the lowest densities studied the distribution is nearly exponential. For higher densities, the distribution is still roughly exponential, but the maximum of the collision time distribution moves to greater collision times. At the highest density studied, a second maximum is observed at ~4.3 s_E. The average collision time and the position of the maximum are given in table 4.5. The average collision time, in all cases, is effectively the same as the Enskog collision time even though the distribution of collision times differs from the exponential predicted by Enskog kintic theory.

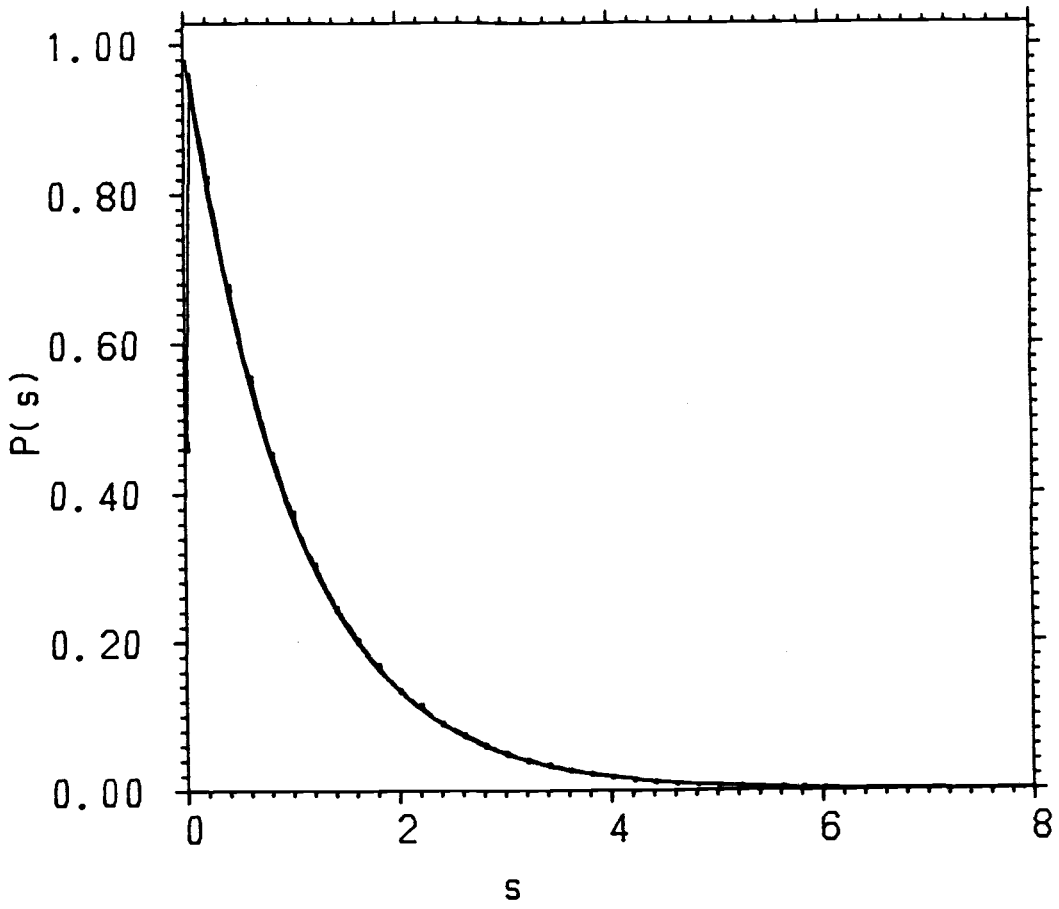

Figure 4.20 The distribution of collision times P(s) for the non-overlapping Lorentz Gas with a packing fraction $N\pi\sigma^2/V$ of 0.01. The time is given in units of $\pi\sigma/(2\rho^*\langle v\rangle g(r_s))$. Error bars are one standard deviation above and one standard deviation below the simulation values. Also plotted is the exponential $\tau\exp(-s/\tau)$ where τ is the actual mean time between collisions. At this density it is difficult to distinguish the actual distribution from the exponential.

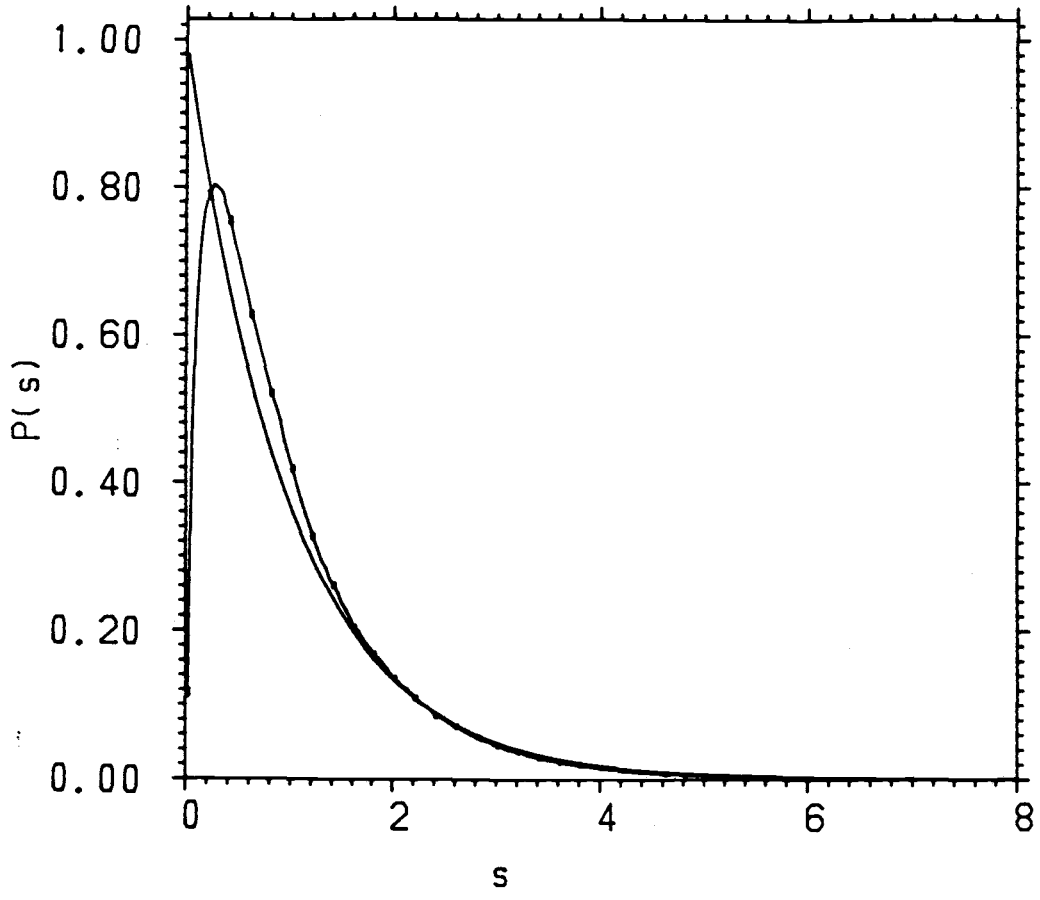

Figure 4.21 The same as figure 4.20, but the packing fraction is $\rho^* = 0.4$.

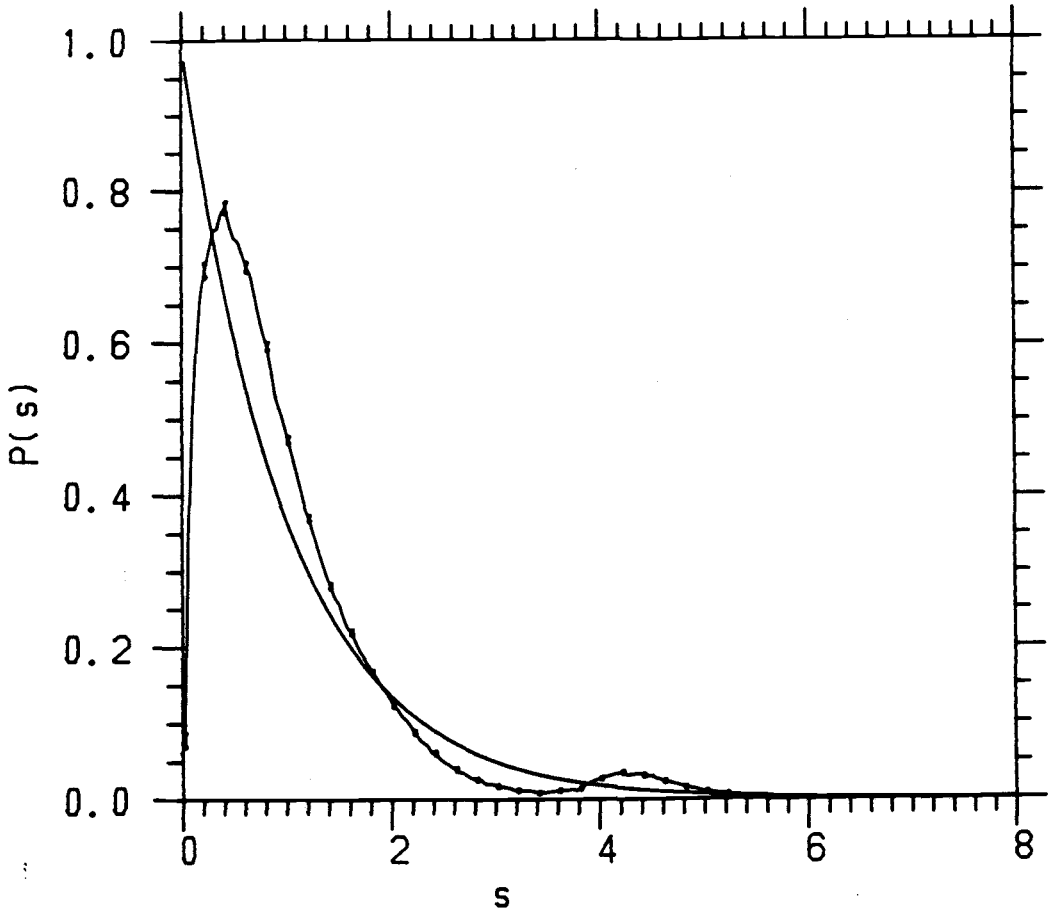

Figure 4.22 The same as figure 4.20, but the packing fraction is $\rho^* = 0.8$.

Table 4.4
Collision time distribution

ρ^*	actual collision time t/τ_E [a]	position of maximum	
		units of τ_E	units of σ [b]
0.01	1.00071	0.06(4) [c]	9.9
0.05	1.00036	0.06(4)	1.8
0.10	1.00141	0.10(4)	1.4
0.20	1.00206	0.14(4)	0.88
0.30	1.00013	0.22(4)	0.81
0.35	0.98660	0.26(4)	0.76
0.40	1.00096	0.26(4)	0.61
0.45	0.97953	0.26(4)	0.50
0.50	0.97867	0.22(4)	0.35
0.60	1.00190	0.34(4)	0.26
0.65	1.00419	0.30(4)	0.25
0.80	1.00437	0.42(4)	0.16

[a] τ_E is $\pi\sigma/(2\rho^* g(r_s))$. [b] This column gives the position of the maximum of the collision time distribution function in terms of the hard disk radius. [c] The number in parentheses is the estimated possible error in the last digit.

E. Conclusions

Computer simulation of the two-dimensional non-overlapping Lorentz gas has provided new information for comparison with existing analytic theory. Some of the puzzles which arise in liquid state theory are reproduced in the study of the LG; of interest in this work are the non-analytic dependence of the diffusion constant upon density and the production of a long-time negative tail for the VAF. Because the LG is much simpler than a liquid, it should be easier to determine the origin of these phenomena in the LG.

The diffusion constant was determined from the simulations for densities ranging from $\rho^* = 0.01$ to 0.80. The lowest density studied is comparable to a dilute gas and the highest density is above the fluid-solid phase transition which has been observed in simulations of hard disk fluids(32). It was found that the predictions of van Leeuwen and Weijland for the diffusion constant of the LG divided by the radial distribution function for the system were in remarkable agreement with the simulation values over this wide range of densities.

This result is significant for two reasons. The first of these is that a result which was derived with no provision for the structure of the non-overlapping arrangement of the scatterers could be brought into agreement with the simulation results by including the radial distribution function in the simplest manner possible. The radial distribution function was eliminated from the kinetic theory treatment of the diffusion coefficient by separating it into 1 and $g(r) - 1$. Terms including $g(r) - 1$ were taken to vanish using the rationale that

these terms would not contribute in the long time limit. The VAF's shown in figures 4-7-4.17 display the most significant differences from exponential behavior at short times and it is reasonable to assume that this difference will appear in the deviation of the diffusion constant from its low-density value. It is easy to see that a piece has been left out. Because the short time behavior will be dominated by the arrangement of scatterers very close to the moving particle and the terms involving g(r) were removed because they were finite in the long time limit, it is also reasonable to think that the left-out piece is related to the radial distribution function. Although the presence of the radial distribution function in the expression for D/D_0 has no rigorous basis, its inclusion is intuitively appealing and in accord with the corrections of Enskog to Boltzmann kinetic theory. van Leeuwen and Weijland obtained a first order density correction to the inverse diffusion constant which contains the rdf and also corresponds to the first order Enskog correction. This first order contribution suggests the inclusion of the full rdf in the denominator of the inverse diffusion constant. That the results using g(r) are in agreement with the simulation values supports the above reasoning.

The agreement between the kinetic theory result and the simulation values for the diffusion constant is also significant because of the wide range of densities to which the equation was found to apply. The density expansion of the diffusion constant obtained by van Leeuwen and Weijland included contributions from the free travel of the moving particle, the collision of the moving particle with one scatterer and the most frequently-occurring correlated collision sequences between

the moving particle and two of the stationary scatterers. Bruin (8) later calculated additional terms in the density expansion by considering less-frequent correlated collision sequences between the particle and the scatterers. The result is an equation which is nominally third order in density, yet represents the macroscopic behavior of the system even at high densities. It should be noted that the renormalization procedure which replaced each appearance of z^{-1} by $(z + 2\rho v\sigma)^{-1}$ obscured the physical relationship between the order in density of the coefficients of the expansion and the number of particles which are involved in the collison sequences. In a normal virial expansion of an intensive property, one particle effects appear as zeroth order in density, two particle effects as linear in density, three particle effects as quadratic, and so on. That relationship will no longer hold because the renormalization procedure introduces a factor of density into the denominator with each free propagation operator G_0. This means that although eqn. (42) is nominally a maximum of third order in density, it contains contributions from collision sequences involving a larger number of particles than is indicated by its order in density. The success of this equation, which is of fairly low order in density, in explaining the behavior of systems in which the scatterers are quite dense indicates that all of the correlated events which contribute significantly to the density dependence of the diffusion constant in the non-overlapping LG have been taken into account.

The analysis of the VAF of the non-overlapping LG did not provide results which are as clear-cut as the diffusion constant results. The

size of the deviation of the simulation VAF from the exponential predicted by Enskog kinetic theory was, as expected, found to increase with density. However, the increase was found to be less than that predicted by kinetic theory. In units of Enskog collision time, there is a significant increase in the magnitude of the s_E^{-2} tail, but in terms of the more common Boltzmann collision time, the coefficient increases with density only in the range $\rho^* = 0.01$ to 0.3 and appears to be linear at higher densities. This behavior is radically different from the theoretical predictions. The simplest of the theories, Ernst and Weijland's kinetic theory treatment, suggests that the coefficient in units of Boltzmann collision times should be linear in density, and the more complex theories that it should be of higher order in density. It is possible that the results reported here are in agreement with the results of Ernst and Weijland and that the simulation runs were not long enough to establish accurate averages of the VAF. It seems unlikely, however, that the errors are large enough to mask a density dependence corresponding to that predicted by Keyes and Mercer(20), Masters and Keyes(19), Götze, Leutheuser and Yip (21,22), or MEvBD(18).

It was hoped that a factor of the radial distribution could be introduced into the results to bring the theory and simulation values into agreement as was possible with the diffusion constant. This did not work for the VAF. The disagreement between the theoretical values for the magnitude of the long-time tail and the non-overlapping LG simulation results reported here is considerable, yet it is unclear whether this disagreement stems from a failure of the theory or from insufficient averaging or improper curve-fitting.

The distribution of collision times was observed to conform to those previously obtained by Lewis (11). The distributions were nearly exponential. The deviation of the simulation distributions from exponential was largest at short times and the deviations incraesed with increasing density. At all densities, the average time between collisions was very close to the Enskog collision time. These results are in agreement with the simulation results of Lewis(11) and his conclusion that the extension of low-density fluid theory to higher densities by simply including the non-exponential distribution of collision times is not correct.

The conclusions of this study, particularly those relating to the diffusion coefficient, can be used to guide the direction of similar studies of the more complex liquid state. The results of the VAF probably give rise to new questions, rather than answering the ones to which it was directed. Further study, involving longer computer simulations directed exclusively towards the VAF in the region of interest would probably be needed to answer these questions.

REFERENCES FOR CHAPTER 4

1. K. M. Case and P. F. Zweifel, 'Linear Transport Theory', Addison-Wesley, Reading, Mass. (1967).

2. R. Peierls in 'Lecture Notes in Physics, Volume 31, Transport Phenomena' edited by G. Kirczenow and J. Marro, Springer-Verlag, New York (1974) 2-33.

3. H. A. Lorentz, Proc. Amst. Acad. 7, 438, 585, 684 (1905).

4. E. H. Hauge in 'Lecture Notes in Physics, Volume 31, Transport Phenomena' edited by G. Kirczenow and J. Marro, Springer-Verlag, New York (1974) 338-378.

5. H. van Beijeren, Rev. Mod. Phys. 54, 195 (1982).

6. M. H. Ernst in 'Lecture Notes in Physics, Volume 253, 'Recent Developments in Nonequilibrium Thermodynamics: Fluids and Related Topics' edited by J. Casas-Vazques, D. Jou and J. M. Rubi, springer-Verlag, New York (1986) 175-216.

7. E. G. D. Cohen, Physics Today, January, (1984) 64-73.

8. C. Bruin, Physica 72, 287 (1979).

9. B. J. Alder and W. E. Alley in 'Perspectives in Statistical Physics, Volume IX of Studies in Statistical Mechanics' edited by H. J. Raveche, Elsevier-North-Holland, Inc, New York (1981) 5-21.

10. B. J. Alder and W. E. Alley, J. Stat. Phys. 19, 341 (1978).

11. J. C. Lewis, Chem. Phys. Lett. 76, 96 (1980).

12. J. C. Lewis and J. A. Tjon, Phys. Lett. 66A, 349 (1978).

13. J. M. J. van Leeuwen and A. Weijland, Physica 36, 457 (1976), A. Weijland and J. M. J. van Leeuwen, Physica 38, 35 (1968).

14. M. H. Ernst and A. Weijland, Phys. Lett. 34A,39 (1971).

15. J. Machta and S. M. Moore, Phys. Rev. 32A, 3164 (1985).

16. J. Machta and R. Zwanzig, Phys. Rev. Lett. 50, 1959 (1983); J. Machta and B. Reinhold, J. Stat. Phys. 42, 949 (1986); A. K. Harrison, J. Stat. Phys. 42, 935 (1986).

17. S. Fujita, Y. Okamura, E. Blaisten and S. V. Godoy, J. Chem. Phys. 73, 4569 (1980); J. Machta, J. Stat. Phys. 42, 941 (1986).

18. M. H. Ernst, J. Machta, J. R. Dorfman, and H. van Beijeren, J. Stat. Phys. 34, 477 (1984); J. Machta, M. H. Ernst, H. van Beijeren, and J. R. Dorfman, J. Stat. Phys. 35, 413 (1984).

19. A. J. Masters and T. Keyes, Phys. Rev. 25A, 1010 (1982);A. J. Masters and T. Keyes, Phys. Rev. 26A, 2129 (1982).

20. T. Keyes and J. Mercer, Physica 95A, 473 (1979).

21. W. Götze, E. Leutheusser and S. Yip, Phys. Rev. 25A, 533 (1982).

22. W. Götze, E. Leutheusser and S. Yip, Phys. Rev. 24A, 1008 (1981).

23. N. N. Bogoliubiv in 'Studies in Statistical Mechanics', edited by J. de Boer and G. E. Uhlenbeck, North-Holland, Amsterdam (1962) 5.

24. R. Zwanzig, Phys. Rev. 129, 486 (1963).

25. J. R. Dorfman and E. G. D. Cohen, J. Math. Phys. 8, 282 (1967).

26. T. Keyes and A. J. Masters, Adv. Chem. Phys., to be published.

27. B. J. Alder and T. E. Wainwright, Phys. Rev. 1A, 18 (1970); B. J. Alder, D. M. Gass and T. E. Wainwright, J. Chem. Phys. 53, 3813 (1970).

28. Y. Pomeau and O. Resibois, Phys. Rev. 19C, 63 (1975).

29. J. R. Dorfman and E. G. D. Cohen, Phys. Rev. 12A, 292 (1975).

30. N. Metropolis, A. W. Rosenbluth, M. N. Rosenbluth, A. H. Teller, and E. Teller, J. Chem. Phys. 21, 1087 (1953); Chapter 3 of this work.

31. J. A. Barker and D. Henderson, Rev. Mod. Phys. 48, 587 (1976).

32. J. L. Lebowitz, E. Helfand, and E. Praestgaard, J. Chem. Phys. 43, 774 (1965).

CHAPTER 5
RING CLOSURE DYNAMICS IN ALKANE CHAINS

A. Introduction

The relative motion of the chain ends of a series of polymethylene chains was investigated through analytic techniques and Brownian dynamics simulation and applied to the prediction of the rate of ring closure-like reactions for short hydrocarbon chains. The primary functions of interest in this work are the distance between chain ends and functionals of this end-to-end distance. The magnitude of the end-to-end distance for a single chain at a given time will depend on both the static and the dynamic properties of the molecule. That is, the end-to-end distance will be determined by the rate of conformational change for the molecule, as well as by the equilibrium distribution of chain conformations. The prediction of the rate of ring closure-like reactions requires knowledge of the contributions of the dynamic and static properties of the molecule; toward this end, the Wilemski-Fixman (WF) theory(1) for intramolecular diffusion-controlled reactions was reinvestigated. The equilibrium distribution of chain end separations was determined numerically using the rotational isomeric state model (RIS) of Flory(2) and dynamic properties were examined using Brownian dynamics simulation(3). Shimada and Szwarc(4) have determined rates of electron transfer between terminal alpha-napthyl groups separated by from 5 to 20 methylene units; these rates are compared to the theoretical predictions.

Shimada and Szwarc (4) determined that the rate of electron transfer k for the reaction

$$\alpha N\text{-}(CH_2)_n\text{-}\alpha N^{\cdot} \; = \; {}^{\cdot}\alpha N\text{-}(CH_2)_n\text{-}\alpha N \; ,$$

where αN- represents an alpha-napthyl substituent and n the number of methylene units in the chain, depended on n via

$$k \propto (n+1)^{-3/2} \qquad \text{for } n = 5 \text{ to } 20.$$

The rate of electron transfer is a reflection of the proximity of the chain ends to each other and computer simulation of chain molecules provides insight into whether static or dynamic processes control the chain end behavior and, in turn, the reaction rate.

B. Derivation of the Wilemski-Fixman expression for the reaction rate

The work of Wilemski and Fixman(1) and of Doi(5) provides the framework for the analytic approach to the study of the rates of intramolecular ring-closure type reactions. The reactions of interest are reversible diffusion-controlled reactions. The expression for the rate of the reversible reaction differs from that of the irreversible reaction by a factor of 2(6); attention will be focused on the equations describing the rate of irreversible reactions and the factor of 2 will be restored at the end of our analysis.

For a general intramolecular reaction, a diffusion equation for a space- and time-dependent distribution function $f(\mathbf{R},t)$ may be written which describes the irreversible removal of molecules from the pool of reactive molecules,

$$(\partial_t + \hat{L})f(\mathbf{R},t) = -\kappa S(R)f(\mathbf{R},t). \qquad (1)$$

In Eqn. (1) $\hat{L}$ is the Liouville operator, κ is the rate constant and S(R) is a sink function which describes the probability of reaction for

molecules in which the ends are separated by a distance R. Typically, S(R) decreases with increasing R reflecting the low probability of a closure-type reaction when molecule ends are far apart.

The diffusion equation can be used to determine the first order reaction rate k in the equation for the time evolution of the fraction of unreacted chains

$$\partial_t \phi(t) = -k\phi(t). \tag{2}$$

The route to k will follow Wilemski and Fixman(1) in a general sense. Equation (1) is integrated over **R** space and an equation is obtained for the fraction of unreacted molecules left at time t

$$\partial_t \phi(t) = -K\nu(t) \tag{3}$$

where $\phi(t)$ is defined by

$$\phi(t) = \int d\mathbf{R}\, f(\mathbf{R},t),$$

and $\nu(t)$ by

$$\nu(t) = \int d\mathbf{R}\, S(R) f(\mathbf{R},t).$$

The Laplace transforms of eqns. (2) and (3) can be used to define $\nu(t)$ and provide a route to k. The Laplace transform of eqn. (2)

$$z\phi(z) - 1 = k\phi(z)$$

can be solved for k to give

$$k = (1/\phi(z)) - z \tag{4}$$

where

$$\phi(z) = \int_0^\infty dt\, e^{-zt}\phi(t).$$

The Laplace transform of eqn. (3) is

$$z\phi(z) - 1 = - K\nu(z)$$

or

$$\phi(z) = (1/z) - (\kappa\nu(z)/z). \tag{5}$$

and

$$\nu(z) = \int_0^\infty dt\ e^{-zt}\nu(t).$$

The route to k, the experimental reaction rate, involves the determination of $\nu(z)$ using resolvent and projection operator techniques. The starting point is the Laplace transform of eqn. (1):

$$(z + i\hat{L})f(\mathbf{R},z) = f(\mathbf{R},t=0) - \kappa S(R)f(\mathbf{R},z). \tag{6}$$

If the system is assumed to be initially at equilibrium, $f(\mathbf{R},t=0) = f_{eq}$. The solution of eqn. (6) for $f(\mathbf{R},z)$ yields an equation

$$f(\mathbf{R},z) = (1/z)f_{eq} - \kappa\hat{G}(z)S(R)f(\mathbf{R},z) \tag{7}$$

where $\hat{G}(z)$ is the resolvent operator

$$\hat{G}(z) \equiv 1/(z + i\hat{L})$$

and eqn. (7) makes use of the identity $i\hat{L}f_{eq} = 0$. Equation (7) can be multiplied by S(R) to give the equation

$$S(R)f(\mathbf{R},z) = (1/z)S(R)f_{eq} - \kappa S(R)\hat{G}(z)S(R)f(\mathbf{R},z) \tag{8}$$

to which the projection operator $\hat{P}$,

$$\hat{P} = f_{eq}[S(R)/\langle S(R)\rangle] \int d\mathbf{R}... \tag{9}$$

can be applied. The notation $\langle...\rangle$ represents the equilibrium average of a variable as defined by $\int d\mathbf{R}\ f_{eq}\ ... = \langle...\rangle$. The projection operator given in eqn. (9) is a hybrid of the Mori(7) and Zwanzig(8) forms in that it introduces the sink function as a "vector" in a Mori-type projection operator and it also involves integration over phase space as in a Zwanzig-type projection operator. This particular projection operator was chosen because it generates the WF results with correction terms and thereby implements an exact closure of the set of equations. The operator $\hat{P}$ is applied to eqn. (8) followed by the

insertion of $\hat{P} + \hat{Q}$ where $\hat{Q} = 1 - \hat{P}$. The last step is equivalent to multiplication by 1. The resulting equation is

$$\hat{P}S(r)f(\mathbf{R},z) = (1/z)\hat{P}S(r)f_{eq} - \kappa\hat{P}S(r)\hat{G}(z)\hat{P}S(r)f(\mathbf{R},z) - \kappa\hat{P}S(r)\hat{G}(z)\hat{Q}S(r)f(\mathbf{R},z). \tag{10}$$

The process is repeated with the application of $\hat{Q}$ to eqn. (8) and insertion of $\hat{P} + \hat{Q}$ to give

$$\hat{Q}S(r)f(\mathbf{R},z) = -\kappa\hat{Q}S(r)\hat{G}(z)\hat{P}S(r)f(\mathbf{R},z) - \kappa\hat{Q}S(r)\hat{G}(z)\hat{Q}S(r)f(\mathbf{R},z). \tag{11}$$

Equation (11) is simpler than eqn. (10) because the initial condition term vanishes when it is acted upon by $\hat{Q}$. Equation (11) is solved for $\hat{Q}S(r)f(\mathbf{R},z)$ in terms of $\hat{P}S(r)f(\mathbf{R},z)$ and substituted back into eqn. (10) yielding

$$\{1 + \kappa\hat{P}S(r)\hat{G}(z)[1 + \kappa\hat{Q}S(r)\hat{G}(z)]^{-1}\}\hat{P}S(r)f(\mathbf{R},z) = (1/z)\hat{P}S(r)f_{eq} \tag{12}$$

Equation (12) may be written using $\nu(z)$ and the bra and ket notation for the equilibrium averages:

$$\{ 1 + \frac{\kappa\langle S(r)\hat{G}(z)[1 + \hat{B}]^{-1}S(r)\rangle}{\langle S(R)\rangle} \}\nu(z) = (1/z)\langle S(R)\rangle, \tag{13}$$

where $\hat{B} = \kappa\hat{Q}S(r)\hat{G}(z)$. The sink function S(R) can be written as the sum of its equilibrium average $\langle S(R)\rangle$ and the fluctuation $\delta S(R)$ about that average

$$S(R) = \langle S(R)\rangle + \delta S(R). \tag{14}$$

The substitution of eqn (13) into eqn. (14), the elimination of terms which vanish because of the action of the projection operator on equlibrium averages and some algebra lead to

$$\{1 + \frac{\kappa\langle\delta S(r)\hat{G}(z)[1 + \hat{B}]^{-1}\delta S(r)\rangle}{\langle S(R)\rangle} + \frac{\kappa\langle S(r)\rangle}{z} \}\nu(z) = (1/z)\langle S(R)\rangle. \tag{15}$$

Equation (15) is solved for $\nu(z)$ which is substituted into eqn. (5) for

$\phi(z)$ to give

$$\phi(z) = \frac{1 + \kappa\langle\delta S(r)\hat{G}(z)[1 + \hat{B}]^{-1}\delta S(r)\rangle/\langle S(R)\rangle}{z\left(1 + \frac{\kappa\langle\delta S(r)\hat{G}(z)[1 + \hat{B}]^{-1}\delta S(r)\rangle}{\langle S(R)\rangle} + \frac{\kappa\langle S(r)\rangle}{z}\right)}$$

which is in turn substituted into eqn (4) to give

$$k = \kappa\langle S(R)\rangle\{1 + \frac{\kappa\langle\delta S(r)\hat{G}(z)[1 + \hat{B}]^{-1}\delta S(r)\rangle}{\langle S(R)\rangle}\}^{-1}. \tag{16}$$

The WF result is reclaimed by setting $\hat{B}$ and z to zero,

$$k = \frac{\kappa\langle S(R)\rangle}{\{1 + (\kappa/\langle S(R)\rangle)\int_0^\infty dt\langle\delta S\delta S(t)\rangle\}}. \tag{17}$$

Equation (17) gives the rate for an irreversible reaction, for a reversible reaction, the above must be multiplied by two. The rate for a reversible reaction will be indicated by k_r,

$$k_r = 2k.$$

Following Doi(5), eqn. (17) can be written as the sum of two relaxation times

$$\tau_r = (1/k_r) = \tau_e + \tau_d \tag{18}$$

where

$$\tau_e = 1/(2\kappa\langle S(R)\rangle) \tag{19}$$

and

$$\tau_d = \tfrac{1}{2}\int_0^\infty dt\ \langle\delta S\delta S(t)\rangle/\langle S(R)\rangle^2. \tag{20}$$

Physically, τ_e measures the fraction of conformers in the reactive region and is an equilibrium property, whereas τ_d is the correlation time for the fluctuation of conformers and has dynamic as well as static contributions.

In the next section, the times in eqn. (18) will be evaluated utilizing the Rouse-Zimm model for flexible chains.

C. Rouse-Zimm dynamics

Low frequency motion in alkane chains of five carbon atoms or more has been successfully modelled by the Rouse-Zimm(9) normal polymeric modes(10). The use of the Rouse-Zimm modes is equivalent to the consideration of the alkane chain as a chain of beads with friction coefficient ζ joined by Hooke's Law springs. The Rouse-Zimm modes provide a convenient language for the interpretation of chain flexibility and because the Green's function $G(R,R_0,t)$ for the time evolution of end-to-end distance is known(5), the Rouse-Zimm chain will be employed for the evaluation of the time correlation function in eqn. (20) and the equilibrium average in eqn. (19).

The time correlation function given in eqn. (20) is written in terms of a Green's function as

$$\langle \delta S \delta S(t) \rangle = \int_0^\infty dR dR_0 \, f_{eq} \delta S(R_0) G(R,R_0,t) \delta S(R). \tag{21}$$

Doi(5) has determined the Green's function for the Rouse-Zimm chain to be

$$G(R,R_0,t) = \frac{8rr_0}{\pi E(t)(1-E(t)^2)^{1/2}} \exp\left[- \frac{E(t)^2(r^2 + r_0^2)}{(1-E(t)^2)} \right] \sinh\left[\frac{2rr_0E(t)}{(1-E(t)^2)} \right]$$

where

$$r^2 = 3R^2/2\Lambda^2 \quad \text{with} \quad \Lambda^2 = \langle R^2 \rangle$$

and

$$E(t) = \langle r \cdot r(t) \rangle / \langle r^2 \rangle = \langle R \cdot R(t) \rangle / \langle R^2 \rangle. \tag{22}$$

The correlation function for the end-to-end vector for a Rouse chain with N segments is given by (11)

$$E(t) = (2/M\Lambda^2) \sum_{j=1}^{N} \mathrm{ctn}^2(j\pi/2M) \langle \rho_j^2 \rangle \exp(-t/\tau_j) \tag{23}$$

where

$$M = N + 1$$

$$\rho_j = \Sigma_i \ (2/M)^{1/2} \sin(ij\pi/M) b_i$$

and b_i is a bond vector connecting adjacent atoms. The relaxation times in eqn. (23) are given by

$$\tau_j = (\zeta b^2/k_B T)(1-\chi)/[12\sin^2(j\pi/2M)(1+\chi)]$$

in which ζ is the friction constant ($6\pi\eta b/2$ for a backbone atom of radius b/2), $k_B T$ is Boltzmann's constant times the absolute temperature, and χ is the cosine of the bond angle supplement for the chain (in this case, $\chi = \cos(70°)$). Equation (23) is strictly valid only for the long wavelenth orientational modes of polymers, however, Brownian dynamics calculations have demonstrated(10) that the relaxation time for the slowest mode, τ_1, is calculated accurately for chains with constant bond lengths and constant bond angles and as few as five or six bonds. The higher modes, j=2 and above, are not well-represented by the Rouse-Zimm analysis(10) because higher-frequency modes are sensitive to the torsional potential which is absent in eqn. (23).

The Green's function $G(R,R_0,t)$ may be written in terms of a sum over the associated Laguerre polynomials,

$$G(R,R_0,t) = \frac{8r^2 r_0^2}{\pi^{1/2}} \exp(-r^2-r_0^2) \sum_{n=0}^{\infty} L_n^{1/2}(r^2) L_n^{1/2}(r_0^2) \frac{n! E(t)^{2n}}{(n+1/2)!}, \qquad (24)$$

where $L_n^{1/2}(r^2)$ is the n^{th} rank Laguerre polynomial of order one-half defined by

$$L_n^{1/2}(x) = \frac{e^x}{n!\sqrt{x}} \frac{d^n}{dx^n} (x^{n+1/2} e^{-x}).$$

The Laguerre (or Sonnine) polynomials are eigenfunctions of the

diffusion operator for a Rouse-Zimm chain and dynamical variables such as the sink function may be expanded in terms of these orthogonal polynomials. An arbitrary sink function S(R) would be expressed as

$$S(R) = \sum_{n=0}^{\infty} a_n L_n^{1/2}(r^2),$$

and $\langle S(R)\rangle = a_0$ leaving

$$\delta S(R) = \sum_{n=1}^{\infty} a_n L_n^{1/2}(r^2).$$

The correlation function for the fluctuation of the sink function then reduces to

$$\langle \delta S \delta S(t)\rangle = \frac{2}{\sqrt{\pi}} \sum_{n=0}^{\infty} a_n^2 \frac{(n+1/2)!}{n!} E(t)^{2n}, \tag{25}$$

This is a general result valid for any form of the sink function. For the particular case of a Gaussian sink function, defined by

$$S(R) = \exp(-3\xi R^2/2\Lambda^2) = \exp(-\xi r^2), \tag{26}$$

with

$$\xi = (2/3)(\Lambda/R_x b)^2$$

and R_x is a distance in units of bond length at which reaction may be expected to take place, the expansion coefficients are

$$a_n = (1 + \xi)^{-3/2}(\xi/(1 + \xi))^n. \tag{27}$$

The insertion of eqn. (27) into eqn. (25) followed by the execution of the sum yields

$$\langle \delta S \delta S(t)\rangle = \frac{1}{(1 + \xi)^3} \left[\frac{1}{(1 - \lambda E(t)^2)^{3/2}} - 1 \right] \tag{28}$$

where $\lambda = (\xi/(1 + \xi))^2$. The equilibrium average of a Gaussian sink function is given by

$$\langle S(R)\rangle = 1/(1 + \xi)^{3/2}. \qquad (29)$$

Equations (28) and (29) are in agreement with the analysis of Doi(5) and provide analytic expressions for the times τ_d and τ_e in eqn. (18).

D. Numerical calculations

Computer simulations of flexible chains were carried out to provide values for the correlation functions and the averages used in eqn. (18) for the reaction rate and to compare to the Rouse-Zimm mode predictions of the previous section. Equilibrium averages were calculated using the rotational isomeric state (RIS) model (2). Brownian dynamics simulation was used to determine the correlation functions for the end-to-end distance and the sink functions. The equilibrium calculations will be described first and the results compared to the Rouse-Zimm mode predictions. The Brownian dynamics simulations and results will then be considered and predicted reaction reaction rates compared with the experimental values.

1. Equilibrium properties

Equilibrium averages were determined for molecules with fixed bond lengths, bond angles and a three-fold symmetric potential energy function for the torsional potential; in accord with the RIS model, all allowed configurations were generated and weighed equally in determining the averages. The properties calculated were $\langle S(R)\rangle$ and $\langle(\delta S(R))^2\rangle/\langle S(R)\rangle^2$ for chains ranging in length from three to ten bonds with a series of Gaussian sink functions of the form

$$S(R) = \exp(-3R^2/2b^2R_x^{\,2}).$$

The series included values of 1, 1.5, 2, 3, and 5 bond lengths for the reduced reactive distance R_x. The average $\langle S(R) \rangle$ can be interpreted as the fraction of conformers for which the chain ends are within the reactive distance R_x of each other. The fluctuation average can be considered an equilibrium constant $K_{eq} = \langle (\delta S(R))^2 \rangle / \langle S(R) \rangle^2$ for the number of open rings versus closed rings. The Rouse-Zimm analysis predictions, obtained from eqns. (28) and (29), can be further simplified for long Gaussian chains and short reactive distances. In that limit, Λ^2 is given by Flory(2) as

$$\Lambda^2 = Nb^2(1 + \chi)/(1 - \chi)$$

which is of the order of Nb^2, thus

$$\xi = (\Lambda/R_x b)^2 \simeq N/R_x^2$$

and consequently,

$$\langle S(R) \rangle = O(N^{-3/2})$$

and

$$K_{eq} = (1-\lambda)^{-3/2} \simeq (\xi/2)^{-3/2} = [N(1 + \chi)]^{3/2}/[27R_x^{2(1 - \chi)}]^{3/2}. \quad (30)$$

It can be seen that, for long chains, the chain length dependence of both τ_e, which is defined by eqn (19) as $\tau_e = (2\kappa\langle S(R) \rangle)^{-1}$, and K_{eq} is $N^{3/2}$.

The results of the RIS calculations for these variables are shown in figures 5.1 and 5.2. Figure 5.1 shows that in the limit of long chains and short reactive distances, that is, for chains of six through ten bonds and reactive distances of one bond, the values of $\langle S(R) \rangle$ diminish as $N^{3/2}$. For shorter chains and for sink functions with the larger values for the reactive distance, the N dependence of $\langle S(R) \rangle$ is weaker than expected. In figure 5.2, the plot of K_{eq} versus log N

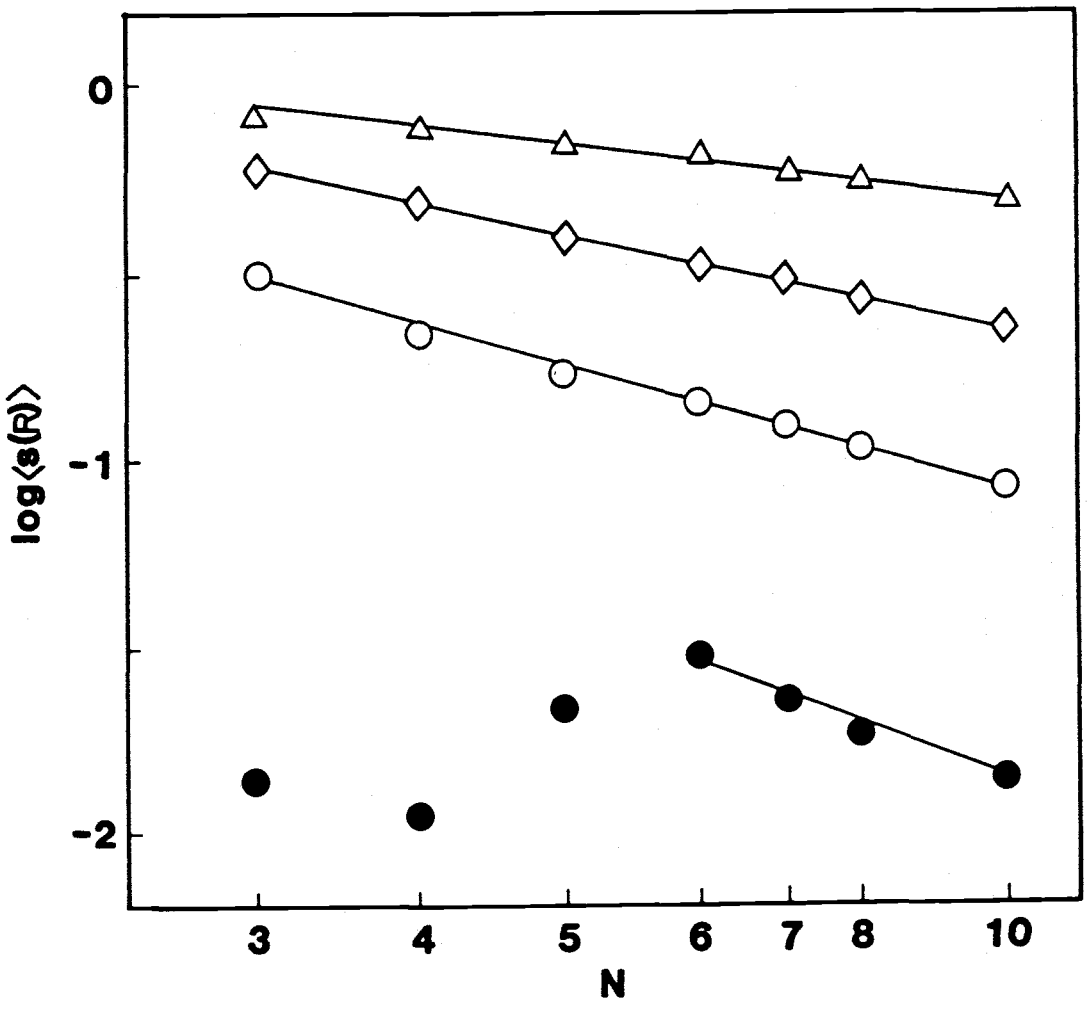

Figure 5.1 The equilibrium value of the reactive sink function S(R) as a function of the number of bonds. The closed cirles indicate a reactive distance, R_x, of one bond, open circles an R_x of two bonds, diamonds an R_x of three bonds and triangles an R_x of five bonds.

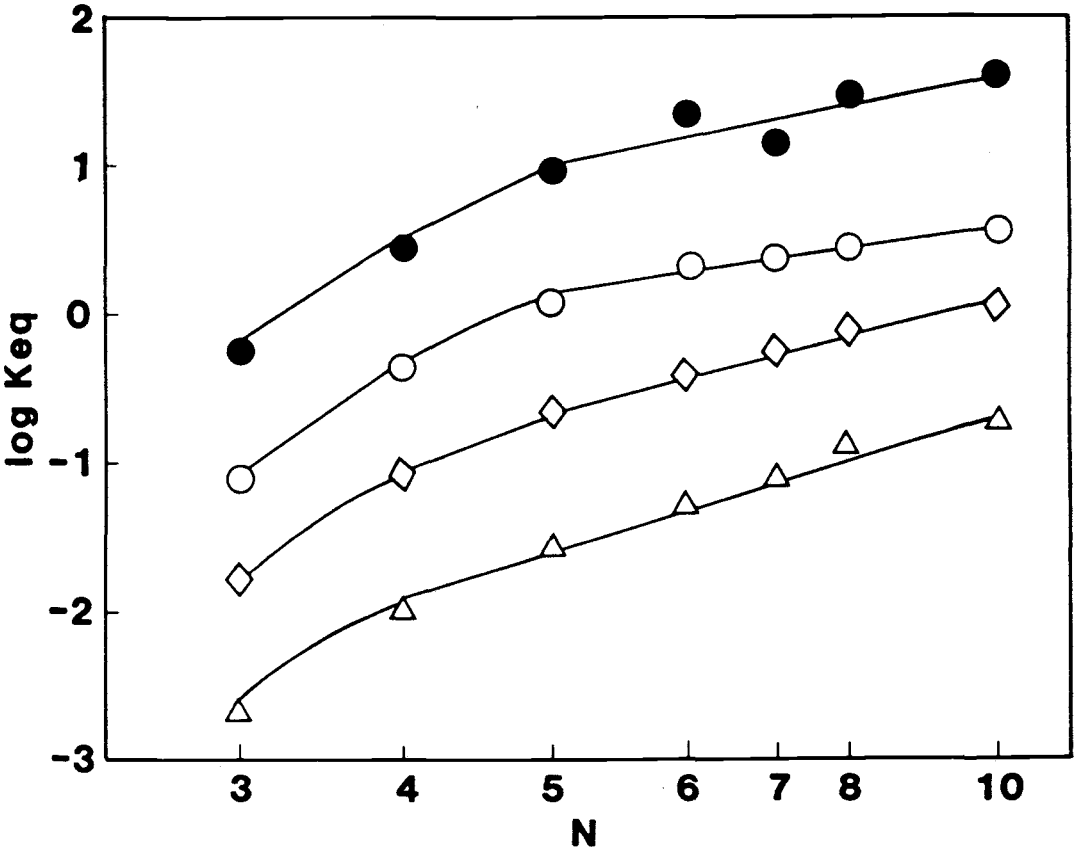

Figure 5.2 The equilibrium constant $K_{eq} = \langle(\delta S(R))^2\rangle / \langle S(R)\rangle^2$ as a function of the number of bonds. The symbols are the same as in figure 5.1

indicates an N dependence of K_{eq} that ranges from $N^{3/2}$ to $N^{5/2}$ with some scatter. As with <S(R)>, the Rouse-Zimm/Gaussian chain prediction of a 3/2 power law dependence on N is borne out for short reactive distance sink functions and the longest of the simulated chains.

2. Dynamical properties

The Brownian dynamics simulations which are reported here were undertaken using a program developed by Marshall Fixman(3), modified to provide the information of interest. In Fixman's algorithm a single chain molecule is modelled as a bead and stick structure subject to torsional forces and bond angle and bond length constraints. The solvent is included as a series of random forces acting on this bead and stick molecule. This is equivalent to utilizing the Langevin equation to follow the time evolution of the molecule. Because the interest is on the behavior of an isolated chain in solution, the Brownian dynamics model is well-suited for this study. The simulations are used to determine the time dependence of the end-to-end vector, the end-to-end distance and functionals of the end-to-end distance for hydrocarbon chains containing 5 to 15 carbon atoms.

For this work, the simulated chains were considered to have rigidly fixed bond lengths and nearest-neighbor bond angles; the torsional potential was

$$U(\Theta) = \tfrac{1}{2}\Xi(1-\cos(3\Theta)).$$

The barrier height Ξ was taken to be $5k_BT$ or 3 kcal/mole at room temperature, a value representative of the trans-gauche energy barrier

for normal alkanes(12). Chains of four, seven, eight, ten and fifteen bonds were included in the simulation study.

Self-correlation functions were determined for the variables R, δR^2, and the series of Gaussian sink functions of the form used in the equilibrium calculations. The correlation functions were normalized and fit piecewise to a power law for short times and an exponential for long times,

$$C(t) = \begin{cases} 1 - \alpha t^{\beta} & \text{short } t \\ a\, e^{-bt} & \text{long } t. \end{cases} \tag{31}$$

Correlations times were then calculated analytically by integration of the functions arising from the piecewise fit. The trajectories used were typically twice as long as those employed for previous orientational relaxation problems(13). One hundred equally weighted trajectories were used to calculate the reported averages; each trajectory consisted of 1000 to 3000 time steps of 0.0025 reduced time units. One time unit is defined as $\zeta b^2/k_B T$ where b is the bond length (1.54Å for polymethylene chains) and ζ is the friction constant for a backbone atom. For a polymethylene chain at 25°C in a solvent with a shear viscosity of 1 cp, each time unit corresponds to 8.4 ps.

The easiest correlation functions to understand should be $\langle \mathbf{R}\cdot\mathbf{R}(t)\rangle$ and $\langle \delta R^2\, \delta R(t)^2\rangle$. Because R is a vector, it should relax as a result of overall rotation of the molecule as well as internal conformation changes. Equation (23) for E(t) can be intergrated over time to give an expression for the correlation time of $\langle \mathbf{R}\cdot\mathbf{R}(t)\rangle$,

$$\tau_E = \int_0^\infty E(t)$$

$$= (2/M\Lambda^2) \sum_{j=1}^{N} \tau_j \, \mathrm{ctn}^2(j\pi/2M) \langle \rho_j^2 \rangle \tau_j \qquad (32)$$

The average value of ρ_j^2 is given by

$$\langle \rho_j^2 \rangle = \Sigma_i \, (2/M)^{1/2} \sin(ij\pi/M) \, \Sigma_n \, (2/M)^{1/2} \sin(nj\pi/M) \, \langle \mathbf{b}_i \cdot \mathbf{b}_n \rangle \qquad (33)$$

where the sums are taken over the N chain segments. The average correlation between bond vectors $\langle \mathbf{b}_i \cdot \mathbf{b}_n \rangle$ will be approximated by the expression for the correlations in a freely-rotating chain(11) as $\chi^{|i-n|}$, where χ is the cosine of the bond angle supplement. In the limit of long chains, $\langle \rho_j^2 \rangle$ is given by

$$\langle \rho_j^2 \rangle = (1 - \chi^2)(1 - 2\chi\cos(j\pi/M) + \chi^2)^{-1}.$$

For short chains, the sum can be written as a complicated analytic expresion of χ and $j\pi/M$; the expression will not be reproduced here, but will be evaluated explicitly for each of the chains studied as the need arises. If the long chain limit of $\langle \rho_j^2 \rangle$ is substituted into eqn. (32) and the result evaluated in the limit of large N, the correlation time τ_E is predicted to be proprtional to N^2. Figure 5.3 indicates that for the short chains studied in this work, τ_E scales linearly with N rather than quadratically. The results of the explicit evaluation of eqn. (32) for short chains are given in Table 5.1 along with the Brownian dynamics results. The analytic predictions consistently underestimate the Brownian dynamics correlation times by a factor of ~6; however, the N dependence of the Rouse-Zimm model correlation times is in good agreement with the simulation results. Figure 5.3 is a plot of the Brownian dynamics and Rouse-Zimm correlation times; the Rouse-Zimm predictions have been scaled so that the two models are in exact agreement for the 15-bond chain. It is

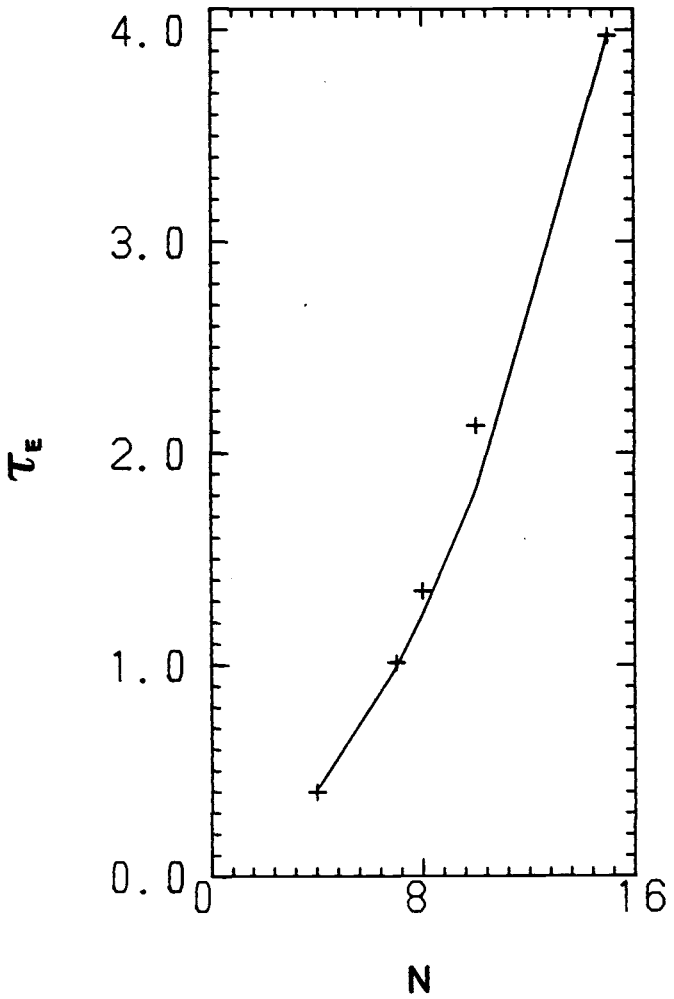

Figure 5.3 The correlation time for the relaxation of the end-to-end vector. The line is τ_E as calculated for the Rouse-Zimm model using eqn. (32) and Λ^2 from the RIS model calculations for all but the 15-bond chain. For the 15-bond chain Λ^2 is from the BD simulation. The time units for the Rouse-Zimm numbers are $\zeta b^2/k_B T$. The squares represent τ_E as calculated using the BD simulation; the time units are scaled such that the BD and Rouse-Zimm results are in exact agreement for the 15-bond chain.

evident that the N dependence is quite similar.

Table 5.1

τ_E from Brownian dynamics and Rouse-Zimm calculations

# of bonds	τ_E Brownian dynamics	τ_E Rouse-Zimm model
4	2.409	0.407
7	6.016	0.987
8	8.142	1.236
10	12.835	1.819
15	23.943	3.974

Correlation times are reported in units of $\zeta b^2/k_B$.

The relaxation of δR^2, unlike that of R which can relax with overall chain rotation as well as internal isomerization, will be governed only by internal chain motions. In small molecules, internal and overall rotations are fast and take place on a comparable time scale; hence the relaxation of R and δR^2 should occur at a similar rate. For longer chains, overall rotation becomes very much slower than internal isomerization and R should therefore relax more slowly than the scalar δR^2. The Rouse-Zimm model Greens's function given by eqn (24) can be used to estimate the difference in the rates of relaxation. The relaxation of R is described by E(t) defined in eqn. (22). It can be shown that δR^2 is identical to the first order Laguerre polynomial $L_1^{1/2}(r^2)$; the correlation function can then be written as

$$\frac{\langle \delta R^2 \, \delta R(t)^2 \rangle}{\langle (\delta R^2)^2 \rangle} = \frac{\langle L_1^{1/2}(r^2) L_1^{1/2}(r(t)^2) \rangle}{\langle (L_1^{1/2}(r^2))^2 \rangle} = [E(t)]^2. \qquad (34)$$

Equation (34) indicates that if the vector relaxation E(t) is dominated

by a single exponential, δR^2 will decay at twice the rate of R. Figure 5.4 is a plot of the correlation times calculated from Brownian dynamics values of $\langle \mathbf{R}\cdot\mathbf{R}(t)\rangle$ and $\langle \delta R^2 \delta R(t)^2\rangle$; it can be seen that the difference between the correlation times is small for the shortest chains and remains small for all but the longest molecule, the fifteen bond chain. The difference between the correlation times for the fifteen bond chain, the largest chain studied and the one which would be expected to conform most closely to a Rouse-Zimm model is a factor of 2.3, rather than the predicted value of 2. For shorter chains, the relaxation of $\langle \delta R^2 \delta R(t)^2\rangle$ is not well-described by the Rouse-Zimm analysis. This is somewhat surprising in light of the good qualitative agreement between the analytic and simulation results for $\langle \mathbf{R}\cdot\mathbf{R}(t)\rangle$ relaxation.

The determination of the reaction rate requires information about dynamic properties of the chosen sink function as well as the equilibrium properties determined in the RIS simulations. Specifically, eqn. (20) calls for the correlation time for the fluctuation of the sink function, that is, the time integral of the normalized self-correlation function $\langle \delta S \delta S(t)\rangle / \langle (\delta S)^2\rangle$. This correlation time will be defined as τ_s;

$$\tau_s = \int_0^\infty dt \, \langle \delta S \delta S(t)\rangle / \langle (\delta S)^2\rangle \qquad (35)$$

Shown in figure 5.5 are representative Brownian dynamics time correlation functions for the seven bond chain for several values of the reactive distance R_x for a Gaussian sink function. Some of the time correlation functions display a plateau region like that of the lowermost curve of figure 5.5 and occasionally, there appear to be

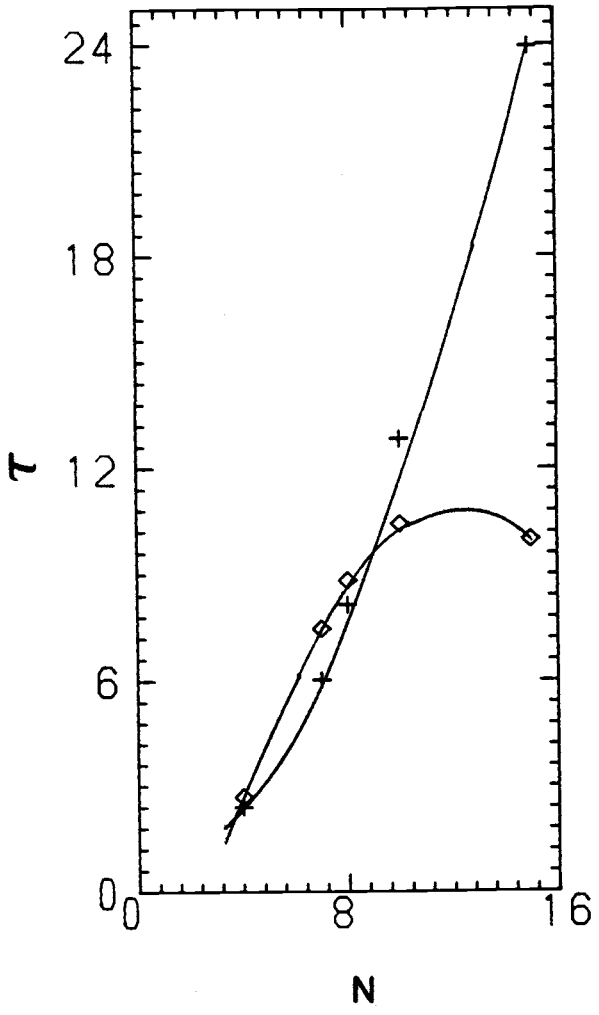

Figure 5.4 The correlation times for the relaxation times of the end-to-end vector, $\langle \mathbf{R}\cdot\mathbf{R}(t)\rangle$ (crosses), and the end-to-end distance, $\langle \delta R^2\, \delta R^2(t)\rangle$ (diamonds), as calculated from the BD simulation. The times are given in units of $\zeta b^2/k_B T$.

oscillations in the functions. Increasing the length of time of each run did not affect these features indicating that they are not the result of insufficient sampling. The unusual features are most prominent and most obviously oscillatory for the longest chains and the shortest reactive distances. As the chains become shorter or the reactive distance longer, the oscillations appear to be damped to plateau-like regions and for the shortest molecule, the four bond chain, it is unclear whether the correlation function exhibits a plateau region or decays exponentially. (See plots of the correlation functions in Appendix A.) The time of onset of the oscillations or plateaus in the correlation functions appears to be consistent for a given length of chain and to increase with chain length; for the seven bond chain, the feature is a plateau at ~1.2 reduced units of time, for the 15 bond chain, an oscillation is observed with a maximum at ~4 reduced units of time. The curves were fit using the power law and exponential functions given in eqn. (31). For the correlation functions displaying plateaus and oscillations, the use of such a fit introduces error into the calculation of the correlation times. The calculation of the end-to-end distance functionals proved to be more costly and to yield much larger error bars than previous calculations of orientational correlation functions(13).

It is easy to speculate that the anomalous features are the result of a collective mode oscillation; the simplest of the collective isomerizations in alkanes gives rise to the Kramer's rate. The Kramer's rate $1/\tau_K$ is the rate of isomerization for three bond hydrocarbon segments from the trans- conformation to either of the

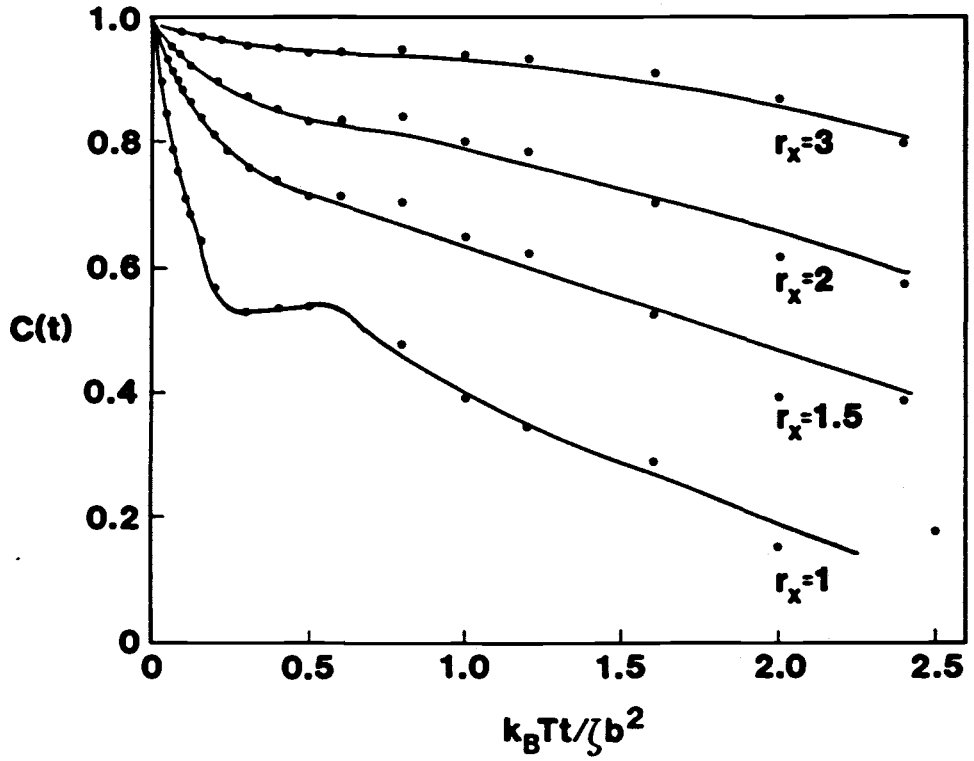

Figure 5.5 Time correlation functions C(t) for the seven-bond chain for several reactive distances. The time is given in reduced units.

gauche- conformations and depends weakly on chain length (14,15). For a butane chain with tetrahedral bond angles, τ_K is (16)

$$\tau_K \simeq 0.106\zeta b^2 \exp(\Xi/k_B T)/\Xi, \tag{36}$$

where Ξ is the barrier height for isomerization from the trans- to the gauche- conformers. For butane with the same torsional potential as was used in the simulation, the Kramer's correlation time is 3.15 reduced units of time. It appears that the oscillations in the sink function correlation functions are occurring on approximately the same time scale as the isomerizations which control the Kramer's rate. Further investigation of the sink function correlation functions, including simulations aimed at elucidating the unusual features observed in this work, will have to be undertaken before their shape is understood.

Figure 5.6 is a plot of the correlation times for various reactive distances as a function of chain length. The data has been smoothed by drawing curves through the irregular array. Despite the scatter, for the sink functions with the longest reactive distances, a decrease in the correlation times with increasing chain length is evident. It is reasonable to expect this trend since a reactive distance of three or four bonds spans a sizable portion of the allowed relative separation of the chain ends. The δS correlation function measures the time dependence of the fluctuation of the number of conformers for which the end separation is within the appropriate volume; the larger the appropriate volume is relative to the total volume available, the slower the fluctuation in time of the number of 'closed' conformers. For the shortest reactive distance sink functions, a clear trend is difficult to ascertain, but it appears that the correlation times are

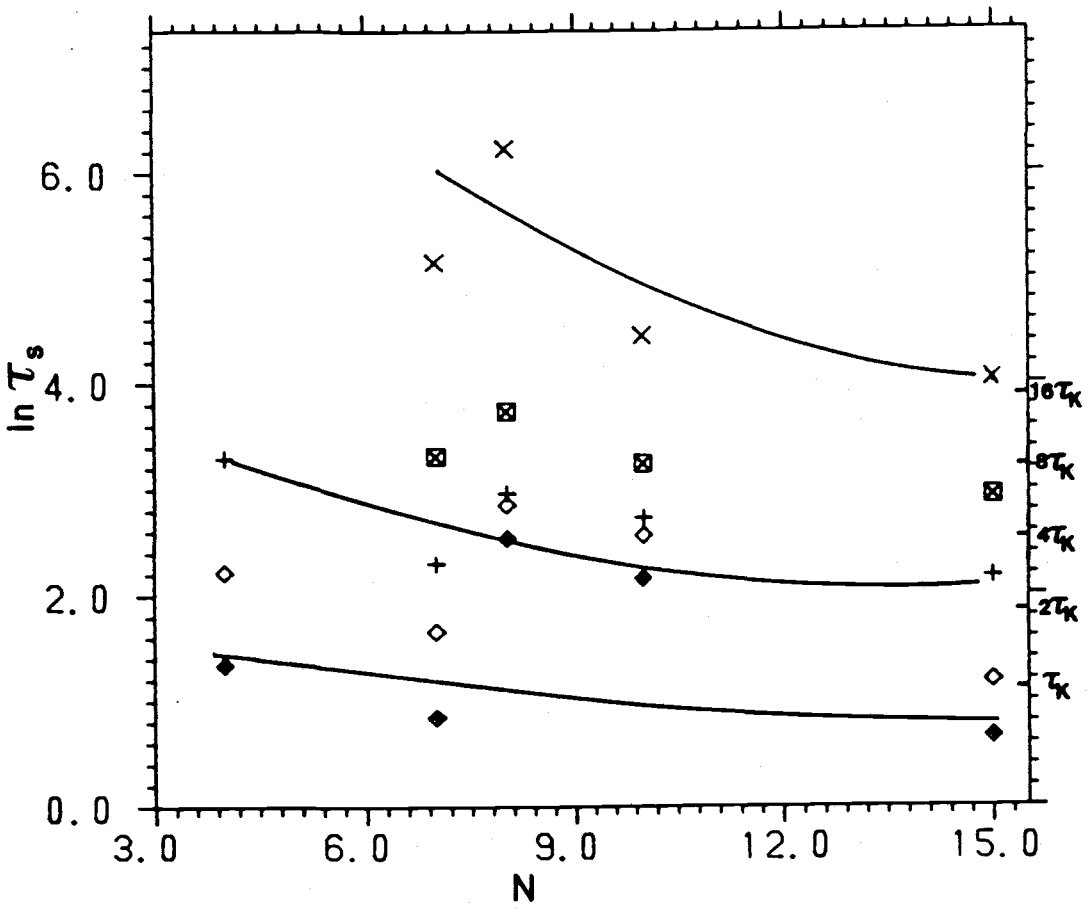

Figure 5.6 The correlation times, τ_s, for the sink functions plotted against the number of bonds, N. The correlation times for the Kramer's rate for butane as given by eqn. (36) are indicated on the right. The sink function with the reactive distance, R_x, of 1.0 bond lengths is indicated by ◆, 1.5 by ◇ ,2.0 by +, 3.0 by ⊠, and 5.0 by ×.

independent of chain length. Plotted on the right hand side of figure 5.6 are multiples of the inverse of the Kramer's rate $1/\tau_K$ for butane. The correlation times τ_s of the shortest reactive distance sink functions studied approach the Kramer's correlation time and can be approximated by

$$\tau_s = R_x \tau_K . \tag{37}$$

The application of the Rouse-Zimm analysis to the correlation time τ_s requires the integration of the correlation function $\langle \delta S \delta S(t) \rangle$. This is most easily accomplished using the expression for the correlation function given by eqn. (25). The assumption is made that the decay of E(t), the correlation function for the vector between the chain ends, is exponential,

$$E(t)^{2n} \simeq \exp(-2nt/\tau_E) \tag{38}$$

where $\tau_E = \int_0^\infty E(t)$. From eqns. (25), (35), and (36), the correlation time is

$$\tau_s = \frac{2}{\langle (\delta S)^2 \rangle \sqrt{\pi}} \sum_{n=1}^{\infty} a_n^2 \frac{(n + \tfrac{1}{2})!}{n!} \int_0^\infty \exp(-2nt/\tau_E). \tag{39}$$

The integration can be performed and eqn. (27) for the expansion coefficients used to give

$$\tau_s = \frac{2}{\langle (\delta S)^2 \rangle \sqrt{\pi}} \sum_{n=1}^{\infty} \frac{1}{(1 + \xi)^3} \left(\frac{\xi}{1 + \xi} \right)^{2n} \frac{\tau_E}{2n} \frac{(n + \tfrac{1}{2})!}{n!}.$$

$$= \frac{\tau_E}{\langle (\delta S)^2 \rangle \sqrt{\pi} (1 + \xi)^3} \sum_{n=1}^{\infty} \left(\frac{\xi}{1 + \xi} \right)^{2n} \frac{(n + \tfrac{1}{2})!}{n(n!)}$$

$$= \frac{\tau_E}{\langle (\delta S)^2 \rangle \sqrt{\pi} (1 + \xi)^3} \sum_{n=1}^{\infty} \frac{\lambda^n (n + \tfrac{1}{2})!}{n(n!)}. \tag{40}$$

where $\lambda = (\xi/(1+\xi))^2$. Equation (40) has been evaluated numerically for the 4, 7, 8, 10 and 15 bond chains using the τ_E given by eqn. (32) and eqn. (28) with t = 0 for $\langle(\delta S)^2\rangle$. The results are given in Table 5.2 , along with other explicit calculations of the Rouse-Zimm mode predictions. There is a consistent increase in τ_s with increasing chain length and increasing reactive distance. This trend is not in agreement with the Brownian dyanmics results shown in figure 5.6. If eqn. (40) is evaluated in the limit of long Gaussian chains, τ_s is predicted to increase with increasing chain length as N. As with the relaxation of R^2, the Rouse-Zimm mode explicit predictions of the sink function correlation times are not in agreement with the Brownian dynamics.

The dynamical variable of interest in this work is τ_d defined in eqn. (20); τ_d will figure directly in calculations of the reaction rate. Figure 5.7 is a plot of the Brownian dynamics results for τ_d; no simple dependence on N can be determined from this plot. If τ_s is multiplied by $\frac{1}{2}K_{eq} = \frac{1}{2}\langle(\delta S)^2\rangle/\langle S\rangle^2$, the result is τ_d as given by eqn. (20). For the long chain limit of the Rouse-Zimm modes, K_{eq} has been shown to vary with chain length as $N^{3/2}$ and τ_s as N; this leads to a dependence of τ_d on $N^{5/2}$. Explicit evaluation of the Rouse-Zimm equations for short chains reveals a similar $N^{5/2}$ dependence for τ_d (table 5.2). Because of the lack of agreement between the Rouse-Zimm and Brownian dynamics trends for τ_s, the discrepancy between the results for τ_d is expected.

In the next section, the numerical results reported above will be utilized in a calculation of the reaction rate and the application of

Table 5.2

Explicit Evaluation of Chain-End Variables Using the Rouse-Zimm Modes

# of bonds	R_x	$\langle S(R) \rangle$	$\langle (\delta S)^2 \rangle / \langle S \rangle^2$	τ_s	τ_d
4	1.0	0.0753	4.4203	0.0922	0.2028
4	1.5	0.1880	1.4605	0.1363	0.0996
4	2.0	0.3168	0.6593	0.1635	0.5043
7	1.0	0.0317	11.0559	0.1451	0.8014
7	1.5	0.0897	3.6167	0.2433	0.4370
7	2.0	0.1711	1.6557	0.3186	0.2638
7	3.0	0.3541	0.5380	0.4101	0.1103
7	5.0	0.6311	0.1147	0.4716	0.0270
8	1.0	0.0258	13.6635	0.1629	1.1108
8	1.5	0.0746	4.4473	0.2788	0.6199
8	2.0	0.1457	2.0345	0.3742	0.3807
8	3.0	0.3148	0.6667	0.4955	0.1652
8	5.0	0.5923	0.1460	0.8379	0.0426
10	1.0	0.0184	19.2137	0.1987	1.9368
10	1.5	0.0547	6.2264	0.3532	1.1014
10	2.0	0.1105	2.8435	0.4899	0.6968
10	3.0	0.2551	0.9411	0.6803	0.3200
10	5.0	0.5259	0.2143	0.8379	0.0898
15	1.0	0.0107	33.3828	0.3197	5.3052
15	1.5	0.0332	10.5150	0.5980	3.1534
15	2.0	0.0700	4.7694	0.8694	2.0741
15	3.0	0.1770	1.5832	1.2996	1.0243
15	5.0	0.4203	0.3874	1.7325	0.2278

Correlation times are reported in units of $\zeta b^2/k_B$.

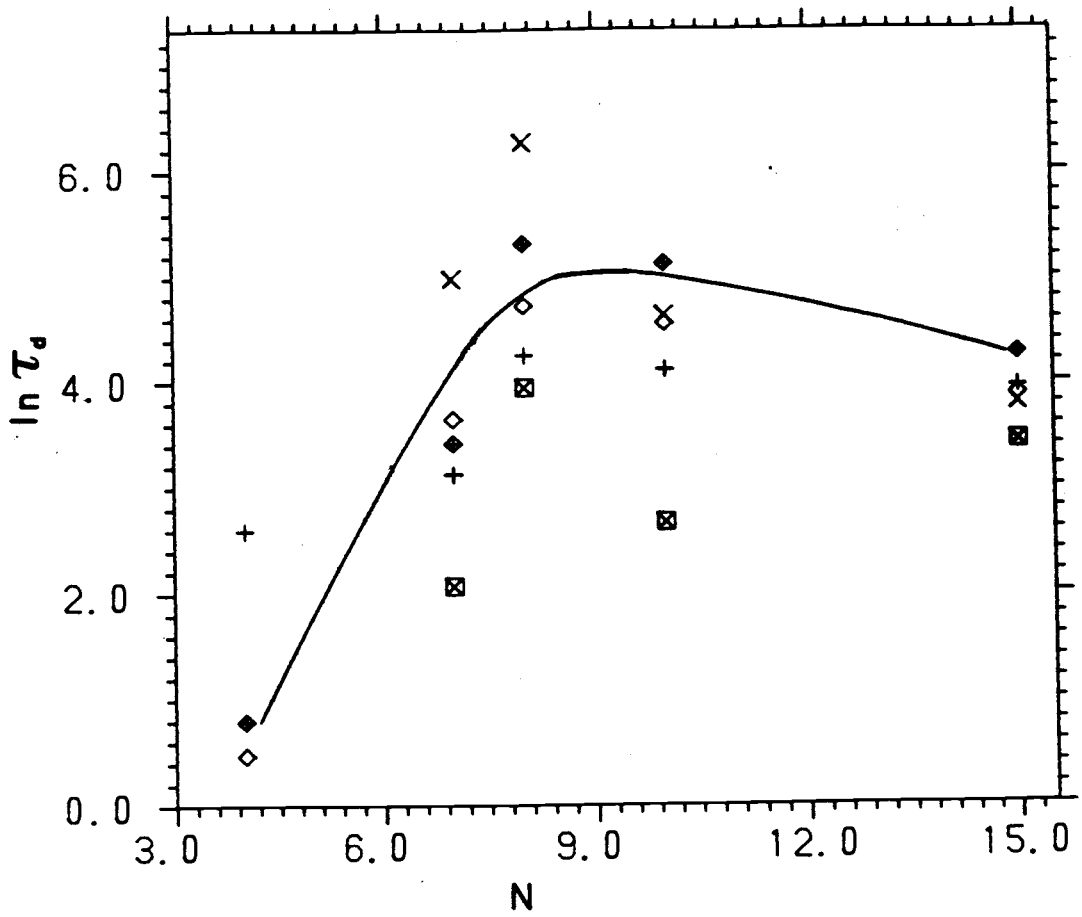

Figure 5.7 The relaxation time, τ_d, for the sink functions plotted against the number of bonds, N. The legend is the same as for figure 5.6.

this work to the study of alkane chain dynamics will be discussed.

E. Discussion

The correlation times τ_s and the average values of the sink functions <S> can be used to determine a reaction rate for ring closure-type reactions using eqn. (18). The calculation of the reaction rate for electron transfer requires the nearest neighbor reaction rate, that is, the rate of electron transfer for groups within the reactive region. The rate chosen was 1×10^{12} seconds. This corresponds to rates obtained from Arrhenius plots of experimental data for intermolecular transfer of electrons between α-napthyl groups on linear alkanes(4). The results of the reaction rate calculation, scaled to conform to the experimental conditions of Shimada and Szwarc(4) (HMPA at 0° C, η = 6.23 cp) are given in figures 5.8 and 5.9. Figure 5.8 was obtained from the Brownian dynamics data for both the dynamic and equilibrium contributions; figure 5.9 gives reaction rates derived using the Brownian dynamics data for the correlation time τ_s and the RIS data for the equilibrium properties $\langle(\delta S)^2\rangle$ and <S>. Because RIS simulations were not undertaken on the 15 bond chain, the rates given for that molecule are the same on both plots and involve the Brownian dynamics data for the correlation time and the equilibrium properties. It can be seen that the experimental trend is not well-modelled by the simulation results although the actual values of the reaction rates are in fair agreement. Since the simulation model did not include the bulky napthyl moieties or possible orientational dependence of the reaction, it is surprising that the

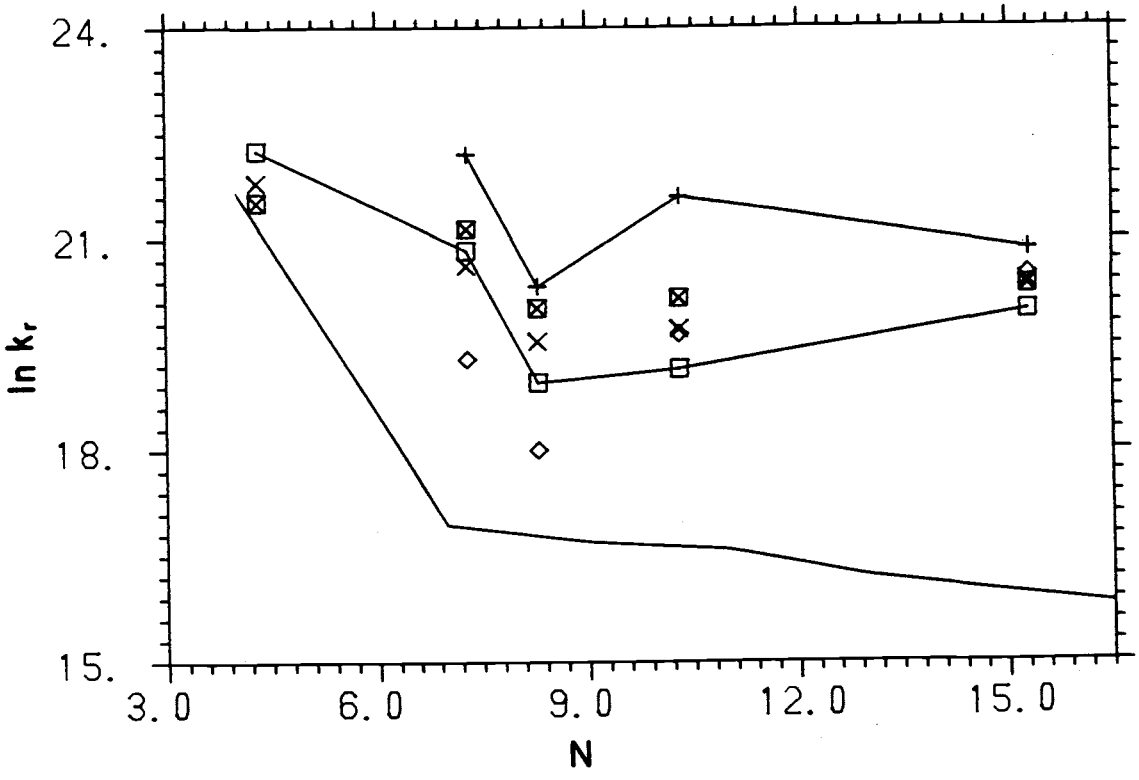

Figure 5.8 The reaction rate for electron transfer as a function of chain length. The solid line indicates the experimental results of Shimada and Szwarc (ref 4). The points indicate the rate as calculated using eqn. (18) and the results of the BD simulation. The reactive distance R_x was taken to be 1.0 (□), 1.5 (×), 2.0 (⊠), 3.0 (+) and 5.0 (◇) bond lengths.

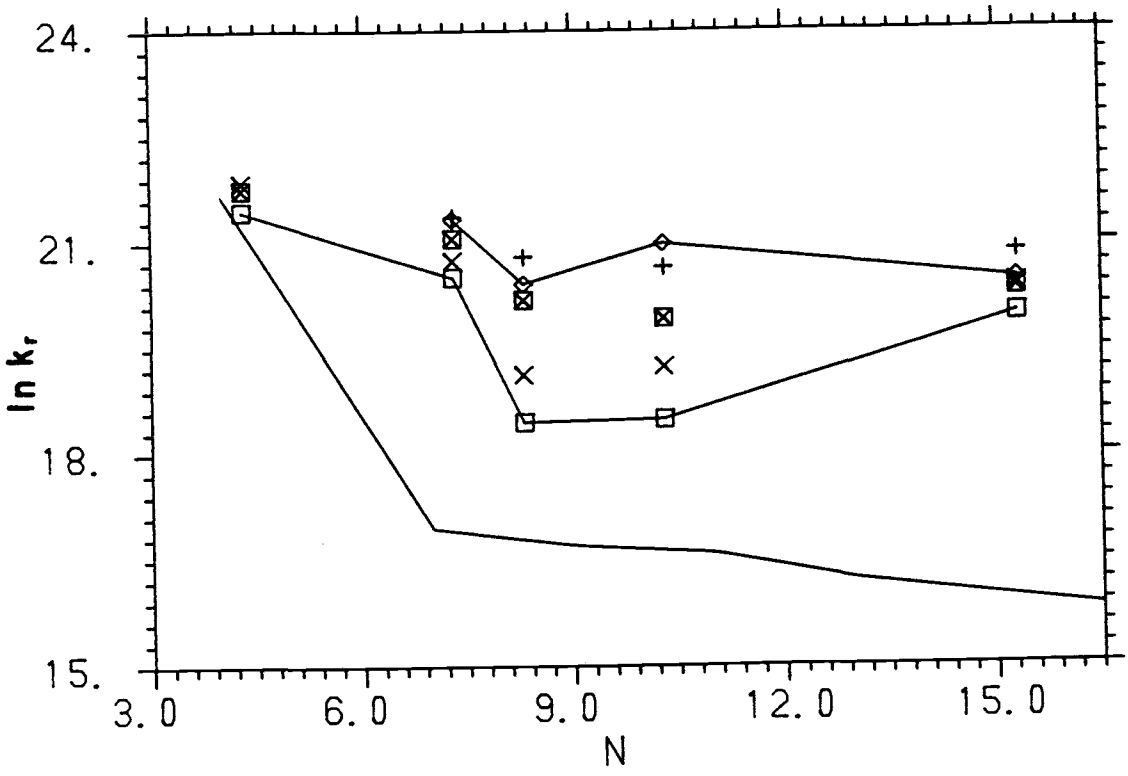

Figure 5.9 The reaction rate for electron transfer as a function of chain length. The BD results are used for the correlation times and the RIS model results for equilibrium contributions in eqn. (18). The legend is the same as figure 5.8.

experimental and simulation rates are at all close. The simulation correlation times for the longest chains involve the largest uncertainty because of the unorthodox decay observed in the sink correlations functions, and it is the longest chains which show the greatest divergence from the experimental values; further investigation of the sink correlation functions could result in calculated reaction rates more in agreement with the experimental values.

The Rouse-Zimm mode predictions of the reaction rate can be determined from eqn. (18) which gives the reaction rate as comprised of an equilibrium part and a dynamic part. In the calculations of the reaction rates from the simulation results, the dynamic part τ_d was observed to dominate the rate because of its magnitude relative to τ_e. The substitution of the long chain limit of the Rouse-Zimm mode results for $\langle S \rangle$ and τ_d into eqn (18) gives

$$k_r \simeq (N^{3/2}/\kappa + N^{5/2})^{-1}.$$

Whether the equilibrium contribution which goes as $N^{3/2}$ or the dynamic contribution proportional to $N^{5/2}$ will control the reaction rate predicted by the Rouse-Zimm model will depend upon the size of the nearest neighbor reaction rate. For a slow reaction, when κ is small, the rate will be dominated by the equilibrium term and show a chain length dependence of $N^{-3/2}$. When κ is large, as it is for electron transfer, or N is larger than κ^{-1}, the rate will be dominated by the dynamic contribution and vary with chain length as $N^{-5/2}$. Explicit calculations using the Rouse-Zimm predictions for $\langle S \rangle$, $\langle (\delta S)^2 \rangle$ and τ_s are plotted in figure 5.10. The actual values of the reaction rates are larger than the experimental numbers by 2-4 orders of

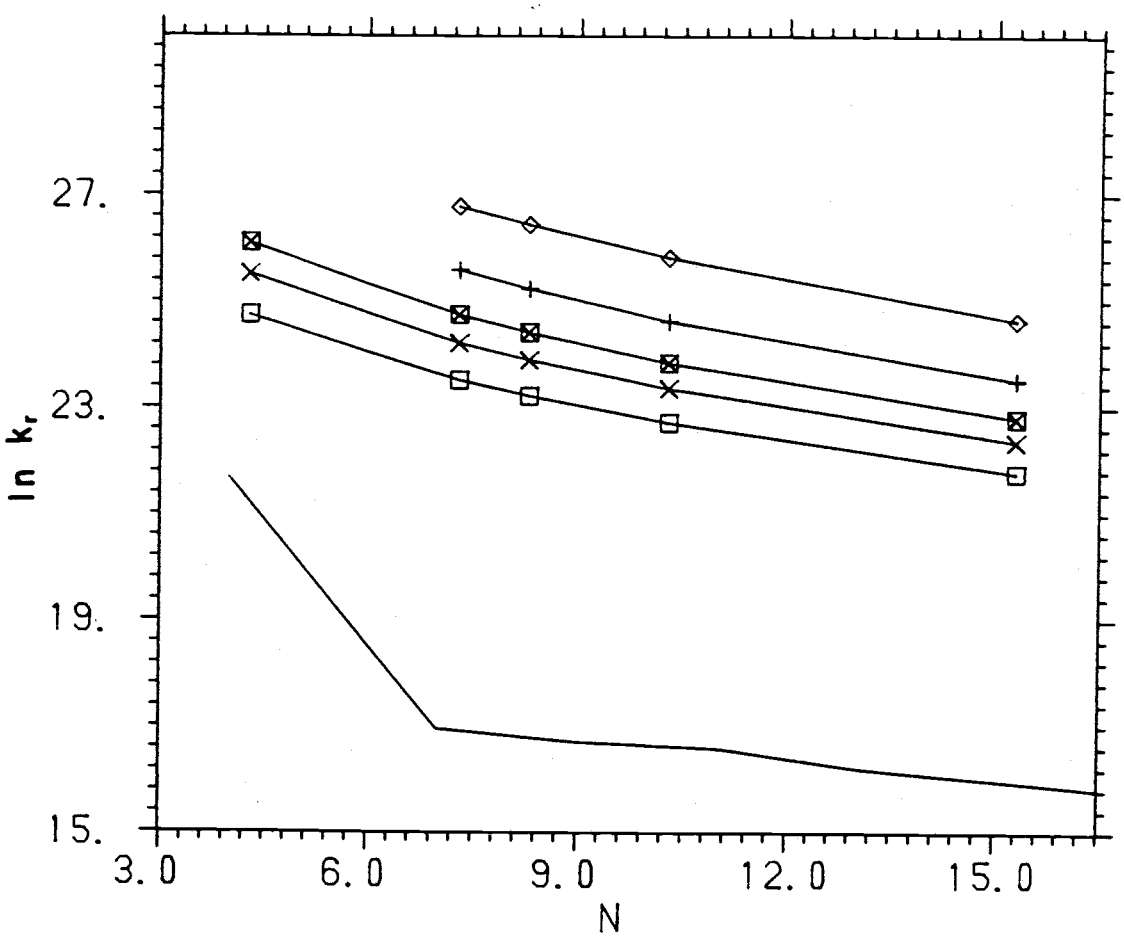

Figure 5.10 The reaction rate for electron transfer as a function of chain length. The Rouse-Zimm predictions are used for $\langle S \rangle$, $\langle (\delta S)^2 \rangle$ and τ_s in eqn. (18). The legend is the same as figure 5.8.

magnitude and the chain length dependence is observed to be $N^{-5/2}$, indicating that the major contribution to the calculated reaction rate is from the dynamic behavior of the chain. The $N^{-5/2}$ dependence of the reaction rate agrees with the analysis of Doi(5).

There have been several calculations of the frequency of chain end contact in terminally substituted alkane chains. Sisido and Shimada(6) have computer-simulated the intramolecular electron transfer reaction of $\alpha N\text{-}(CH)_n\text{-}\alpha N^{\cdot}$ using a rotational isomeric model in which the electron transfer probability was expressed as a step function. The critical reactive distance determined in the simulation was between 5.2 and 6.5 C-C bond lengths (8-10 Å). Calculation of the rate was effected using a static model and a dynamic model. The static model provided the equivalent of <S>, but for a Heaviside step function form of S(R) rather than the Gaussian probability function employed in this work. To obtain the results of the dynamic model, the results of the static model were multiplied by a factor related to the mean lifetime of reactive conformations. Because the dynamic factor was assumed to be chain-length independent, the authors found that the static and dynamic terms displayed the same chain-length dependence, $N^{-3/2}$.

Nairn and Braun(17) have undertaken a similar investigation using a rotational isomeric model in conjunction with a series of bond jumps to determine the rate of intramolecular end-to-end contact in alkanes. The rates were determined as first passage time, i.e., an intial Monte Carlo-generated conformation was allowed to undergo a series of bond motions until the ends came within contact distance. The process was repeated with other Monte Carlo-generated initial conformations to

obtain a first order rate constant for the disapearance of chains. There are several approximations made in this type of simulation and these are discussed by Nairn and Braun. This method calculates a true first-order rate constant and their findings are in accord with the $N^{-3/2}$ power law observed experimentally.

The results of the Brownian dynamics simulations are not as clearcut as the results of the work of Sisido and Shimada(6) and of Nairn and Braun(17). The agreement between the calculated rates reported here and the experimental rates is fair. If the large error bars associated with the sink function correlation times are taken into account, and it is assumed that τ_s is independent of chain length, then eqns. (36), (37) and eqn. (30) evaluated for a tetrahedral chain,

$$K_{eq} \simeq 8.24N^{3/2}/R_x^3,$$

can be combined to give the rate of the reversible diffusion-controlled reaction as

$$k_r = (2k_BT/3\pi\eta b^3)N^{-3/2}R_x^2(\Xi/k_BT)\exp(-\Xi/k_BT) \qquad (41)$$

Although eqn. (41) is approximate, it should represent the functional dependence of the reaction rate on the torsional barrier, Ξ, the number of bonds in the chain, N, the solvent shear viscosity, η and the reactive distance R_x measured in units of C-C bonds. Calculations of the reaction rate for the chains examined in the experimental work of Shimada and Szwarc(4) indicate that if the reactive distance is taken to be one carbon-carbon bond, the results of eqn. (41) are within a factor of three of the experimental rates.

F. Summary and Conclusions

The focus of this work was an understanding of the origin of the chain length dependence of the rate of reaction for ring-closure type reactions of substituted alkane chains. For electron transfer between terminal α-napthyl groups, this rate has been found to be proportional to the $(n+1)^{-3/2}$ where n is the number of methylene units in the alkane chain(4).

The Wilemski-Fixman expression for the diffusion-controlled reaction rate was derived using projection operator techniques. The expression for the rate constant is comprised of a contribution from the equilibrium behavior and a contribution from the dynamic behavior. For a rapid reaction such as electron transfer the dynamic contribution is expected to dominate the reaction rate.

The Rouse-Zimm normal modes were used to obtain explicit expressions for the quantities appearing in the WF rate and compared to the results of Brownian dynamics and RIS simulation of short alkane chains. The overall success of the Rouse-Zimm model in mimicking the chain end behavior studied in this work is limited. Equilibrium properties are described adequately by the Rouse-Zimm predictions in the Gaussian limit because the equilibrium properties of the chain are approximately Gaussian rather than because of properties of the Rouse-Zimm model itself. The Rouse-Zimm analysis did provide results in agreement with the simulation results for E(t), the relaxation of the end-to-end vector. The Rouse-Zimm description of the time dependence of scalar quantities such as functionals of the end-to-end distance, R^2 and S(R) was not in agreement with the simulation

results nor were Rouse-Zimm reactions rates in aggreement with the simulation or experimental results. The Rouse-Zimm modes have proven successful in describing some orientational correlations in short alkane chains such as the vector relaxation E(t) and those described in reference 10, however, it appears that they do not provide an accurate assessment of the time evolution of chain properties which depend only on internal chain isomerization and not on alterations of the overall molecular orientation.

The Brownian dynamics simulations were used to obtain information about the time evolution of the end-to-end vector **R**, the fluctuation in the end-to-end distance squared δR^2 and the Gaussian sink functions S(R). Rotational isomeric model simulations were used to provide equilibrium properties of the chains. The results of the dynamics simulations indicate that the sink correlation functions do not decay exponentially, but rather exhibit unexpected plateaus or oscillations. It is reasonable to assume this behavior is the result of a collective mode oscillation, but its exact nature is unclear; further simulation focussed on these unusual features is indicated.

The Rouse-Zimm analysis and the simulation results were combined to form eqn. (41), an approximate relation for the rate constant for ring-closure type reactions. Although this expression contains the 'dynamic' contribution to the WF reaction rate, the chain length dependence arises from the equilibrium factor K_{eq} rather than the purely dynamic correlation time τ_s. This implies that it is in fact the static properties which control the reaction rate.

REFERENCES FOR CHAPTER 5

1. G. Wilemski and M. Fixman, J. Chem. Phys. 60, 866 (1974).

2. P. J. Flory, 'Statistical Mechanics of Chain Molecules' Interscience, New York (1969).

3. M. Fixman, J. Chem. Phys. 69, 1527, 1538 (1978).

4. K. Shimada and M. Szwarc, J. Am. Chem. Soc. 97, 3313 (1975).

5. M. Doi, Chem. Phys. 9, 455 (1975).

6. M. Sisido and K. Shimada, J. Am. Chem. Soc. 99, 7785 (1977).

7. H. Mori, Prog. Theor. Phys. 33, 423 (1965).

8. R. Zwanzig, in 'Proceedings of the 1973 Les Houches Summer School in Theoretical Physics', Gordon and Breach, New York (1974).

9. P. E. Rouse, J. Chem. Phys. 21, 1272 (1953); B. H. Zimm, ibid 24, 269 (1956).

10. G. T. Evans, J. Chem. Phys. 74, 4621 (1981).

11. M. Fixman and G. T. Evans, J. Chem. Phys. 68, 195 (1978).

12. H. Yamakawa, 'Modern Theory of Polymer Solutions', Harper & Row, New York, (1971).

13. G. T. Evans and D. C. Knauss, J. Chem. Phys. 72, 1504 (1980).

14. J. Skolnick and E. Helfand, J. Chem. Phys. 72, 5489 (1980).

15. J. A. Montgomery, S. L. Holmgren, and D. Chandler, J. Chem. Phys. 73, 3688 (1980).

16. D. C. Knauss and G. T. Evans, J. Chem. Phys. 73, 3423 (1980).

17. J. A. Nairn and C. L. Braun, J. Chem. Phys. 74, 2241 (1981).

BIBLIOGRAPHY

B. J. Alder and W. E. Alley, J. Stat. Phys. 19, 341 (1978).

B. J. Alder and W. E. Alley in 'Perspectives in Statistical Physics, Volume IX of Studies in Statistical Mechanics' edited by H. J. Raveche, Elsevier-North-Holland, Inc, New York (1981) 5-21.

B. J. Alder, D. M. Gass and T. E. Wainwright, J. Chem. Phys. 53, 3813 (1970).

B. J. Alder and T. E. Wainwright, Phys. Rev. 1A, 18 (1970).

J. A. Barker and D. Henderson, Rev. Mod. Phys. 48, 587 (1976).

A. Blair, N. Metropolis, J. von Neumann, A. Taub and M. Tsingou, 'A Study of The Numerical Solution to Two-dimensional Hydrodymanical Problem', Contract W-7405-Eng-36, Los Alamos Scientific Lab., NM (1957).

N. N. Bogoliubiv in 'Studies in Statistical Mechanics', edited by J. de Boer and G. E. Uhlenbeck, North-Holland, Amsterdam (1962) 5.

T. Boublik, Mol. Phys. 27, 1415 (1974).

T. Boublik, Mol. Phys. 29, 412 (1975).

T. Boublik, Mol. Phys. 51, 1429 (1984).

T. Boublik, I. Nezbeda, and O. Trinka, Czech. J. Phys. B26, 1081 (1976).

C. Bruin, Physica 72, 287 (1979).

K. M. Case and P. F. Zweifel, 'Linear Transport Theory',Addison-Wesley, Reading, Mass. (1967).

D. G. Chae, F. H. Ree and T. Ree, J. Chem. Phys. 50, 1581 (1969).

E. G. D. Cohen, Physics Today, January, (1984) 64-73.

M. A. Cotter and D. E. Martire, J. Chem. Phys. 52, 1902,1909 (1970).

M. Doi, Chem. Phys. 9, 455 (1975).

J. R. Dorfman and E. G. D. Cohen, J. Math. Phys. 8, 282 (1967).

J. R. Dorfman and E. G. D. Cohen, Phys. Rev. 12A, 292 (1975).

J. R. Dorfman and H. van Beijeren in 'Statistcal Mechanics, Part B: Time-Dependent Prcoesses', edited by B. J. Berne, Plenum Press, New York (1977).

M. H. Ernst in 'Lecture Notes in Physics, Volume 253, 'Recent Developments in Nonequilibrium Thermodynamics: Fluids and Related Topics' edited by J. Casas-Vazques, D. Jou and J. M. Rubi, springer-Verlag, New York (1986) 175-216.

M. H. Ernst, J. Machta, J. R. Dorfman, and H. van Beijeren, J. Stat. Phys. 34, 477 (1984).

M. H. Ernst and A. Weijland, Phys. Lett. 34A,39 (1971).

G. T. Evans, J. Chem. Phys. 74, 4621 (1981).

G. T. Evans and D. C. Knauss, J. Chem. Phys. 72, 1504 (1980).

G. A. Few and M. Rigby, Chem. Phys. Lett. 20, 433 (1973).

M. Fixman, J. Chem. Phys. 69, 1527 (1978).

M. Fixman and G. T. Evans, J. Chem. Phys. 68, 195 (1978).

P. J. Flory, 'Statistcal Mechanics of Chain Molecules', Interscience, New York (1969).

S. Fujita, Y. Okamura, E. Blaisten and S. V. Godoy, J. Chem. Phys. 73, 4569 (1980).

R. M. Gibbons, Mol. Phys. 17, 81 (1969).

W. Götze, E. Leutheusser and S. Yip, Phys. Rev. 24A, 1008 (1981).

W. Götze, E. Leutheusser and S. Yip, Phys. Rev. 25A, 533 (1982).

C. G. Gray and K. E. Gubbins, 'Theory of Molecular Fluids, Volume 1. Fundamentals', Oxford University Press, New York (1984).

A. Hall, Messeng Math 2, 113 (1873).

A. K. Harrison, J. Stat. Phys. 42, 935 (1986).

E. H. Hauge in 'Lecture Notes in Physics, Volume 31, Transport Phenomena' edited by G. Kirczenow and J. Marro, Springer-Verlag, New York (1974) 338-378.

E. Helfand, H. L. Frisch and J. L. Lebowitz, J. Chem. Phys. 34, 1036 (1961).

D. K. Hoffman and C. F. Curtiss, Phys. Fluids 7, 1887 (1964).

V. N. Kabadi and W. A. Steele, Ber. Bunsenges. Phys. Chem. 89, 9 (1985).

V. N. Kabadi, Ber. Bunsenges. Phys. Chem. 90, 332 (1986).

Lord Kelvin, Phil Mag 2, 1 (1901).

T. Keyes and A. J. Masters, Adv. Chem. Phys., to be published.

T. Keyes and J. Mercer, Physica 95A, 473 (1979).

T. Kihara, Adv. Chem. Phys. 5, 147 (1963).

D. C. Knauss and G. T. Evans, J. Chem. Phys. 73, 3423 (1980).

D. Knuth, 'The Art of Computer Programming, Volume 2, Seminumerical Algorithms', Wesley (1961).

G. Lasher, Sci. Res. 4, 22 (1969).

A. M. Law and W. D. Kelton, 'Simulation Modeling and Analysis', McGraw-Hill, New York (1982).

J. L. Lebowitz, E. Helfand, and E. Praestgaard, J. Chem. Phys. 43, 774 (1965).

J. C. Lewis, Chem. Phys. Lett. 76, 96 (1980).

J. C. Lewis and J. A. Tjon, Phys. Lett. 66A, 349 (1978).

H. A. Lorentz, Proc. Amst. Acad. 7, 438, 585 (1905).

J. Machta, J. Stat. Phys. 42, 941 (1986).

J. Machta, M. H. Ernst, H. van Beijeren, and J. R. Dorfman, J. Stat. Phys. 35, 413 (1984).

J. Machta and S. M. Moore, Phys. Rev. 32A, 3164 (1985).

J. Machta and B. Reinhold, J. Stat. Phys. 42, 949 (1986).

J. Machta and R. Zwanzig, Phys. Rev. Lett. 50, 1959 (1983).

A. J. Masters and T. Keyes, Phys. Rev. 25A, 1010 (1982).

A. J. Masters and T. Keyes, Phys. Rev. 26A, 2129 (1982).

E. Meeron and A. J. F. Siegert, J. Chem. Phys. 48, 3139 (1968).

N. Metropolis, A. W. Rosenbluth, M. N. Rosenbluth, A. H. Teller, and E. Teller, J. Chem. Phys. 21, 1087 (1953).

J. A. Montgomery, S. L. Holmgren, and D. Chandler, J. Chem. Phys. 73, 3688 (1980).

P. A. Monson and M. Rigby, Chem. Phys. Lett. 58, 122 (1978).

P. A. Monson and M. Rigby, Molecular Physics 39, 977 (1980).

H. Mori, Prog. Theor. Phys. 33, 423 (1965).

D. A. McQuarrie, 'Statistical Mechanics', Harper and Row, New York (1976).

J. A. Nairn and C. L. Braun, J. Chem. Phys. 74, 2241 (1981).

I. Nezbeda, Czech. J. Phys. B30, 601 (1980).

I. Nezbeda and T. Boublik, Czech. J. Phys. B28, 353 (1978).

L. Onsager, Phys. Rev. 37, 405 (1931).

L. Onsager, Phys. Rev. 38, 2265 (1931).

J. Pavlicek, I. Nezbeda and T. Boublik, Czech. J. Phys. 29B, 1061 (1979).

R. Peierls in 'Lecture Notes in Physics, Volume 31, Transport Phenomena' edited by G. Kirczenow and J. Marro, Springer-Verlag, New York (1974) 2-33.

J. K. Percus in 'Equilibrium Theory of Classical Fluids', edited by H. L. Frisch and J. L. Lebowitz, Benjamin, New York, II-33 (1964).

J. K. Percus and G. J. Yevick, Phys. Rev. 110, 1 (1958).

Y. Pomeau and O. Resibois, Phys. Rev. 19C, 63 (1975).

H. Reiss, H. L. Frisch and J. L. Lebowitz, J. Chem. Phys. 31, 369 (1969).

A. B. Ritchie, Jr., J. Chem. Phys. 46, 608 (1967).

P. E. Rouse, J. Chem. Phys. 21, 1272 (1953)

R. Y. Rubenstein, 'Simulation and the Monte Carlo Method', Wiley, New York (1981).

R. S. C. She and G. T. Evans, J. Chem. Phys. 85, 1513 (1986).

R. S. C. She, C. James, and G. T. Evans, J. Chem. Phys. 85, 1513 (1986).

K. Shimada and M. Szwarc, J. Am. Chem. Soc. 97, 3313 (1975).

M. Sisido and K. Shimada, J. Am. Chem. Soc. 99, 7785 (1977).

J. Skolnick and E. Helfand, J. Chem. Phys. 72, 5489 (1980).

H. van Beijeren, Rev. Mod. Phys. 54, 195 (1982).

J. M. J. van Leeuwen and A. Weijland, Physica 36, 457 (1976).

J. Viellard-Baron, J. Chem. Phys. 56, 4729 (1972).

J. Viellard-Baron, Molecular Physics 28, 809 (1974).

L. Verlet and J. J. Weiss, Phys. Rev. 5, 939 (1972).

A. Weijland and J. M. J. van Leeuwen, Physica 38, 35 (1968).

G. Wilemski and M. Fixman, J. Chem. Phys. 60, 866 (1974).

H. Yamakawa, 'Modern Theory of Polymer Solutions', Harper & Row, New York, (1971).

B. H. Zimm, J. Chem. Phys. 24, 269 (1956).

R. Zwanzig, Phys. Rev. 129, 486 (1963).

R. Zwanzig, in 'Proceedings of the 1973 Les Houches Summer School in Theoretical Physics', Gordon and Breach, New York (1974).

APPENDIX

APPENDIX

This appendix contains plots of the correlation functions of functionals of the the end-to-end distance of short alkane chains. The correlation functions were calculated using Brownian dynamics simulation and are discussed in Chapter 5.

The figure captions are self-explanatory. All times, T, listed in this appendix are in units of $\zeta b^2/(k_B T)$, where ζ is friction constant for a single bead and b is one C-C bond length. The quantity $k_B T$ is Boltzmann's constant multiplied by the absolute temperature. For a polymethylene chain at 25° C in a solvent with a shear viscosity of 1 cp, each time unit corresponds to about 8.4 ps.

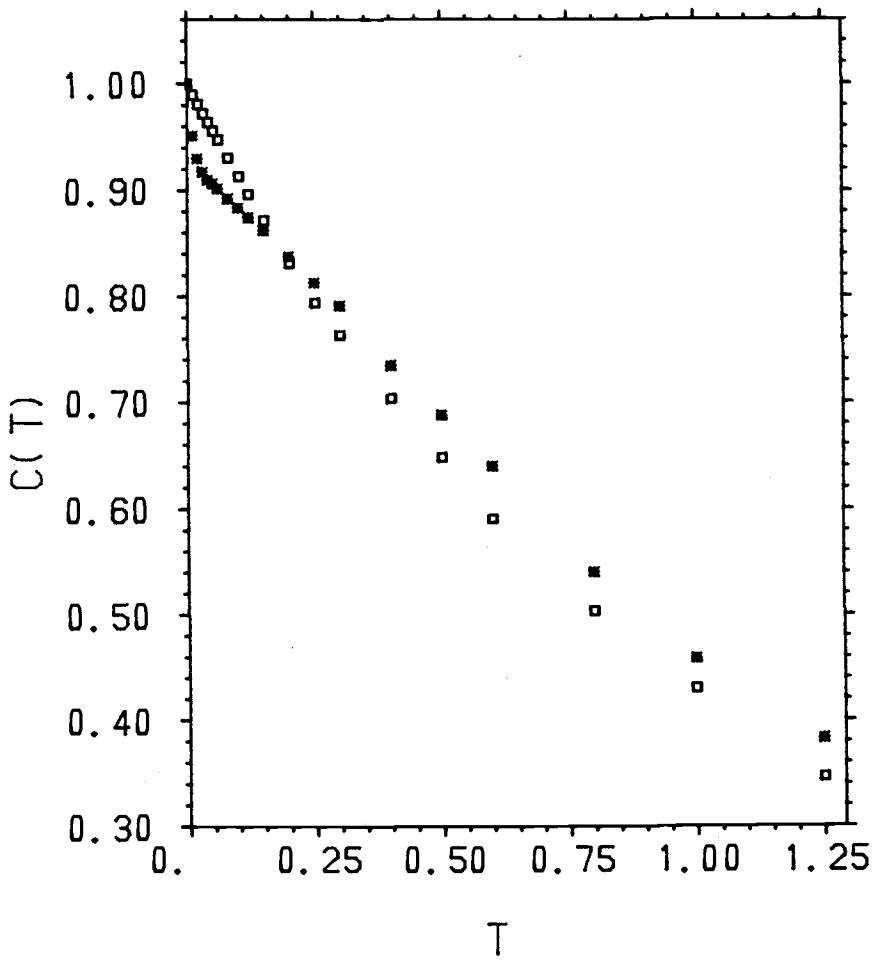

Figure A.1 The correlation functions $\langle \mathbf{R}\,\mathbf{R}(T)\rangle$ (open squares) and $\langle \delta R^2\,\delta R^2(T)\rangle$ (closed squares) for an alkane chain with four C-C bonds. All times, T, are given in units of $\zeta b^2/(k_B T)$.

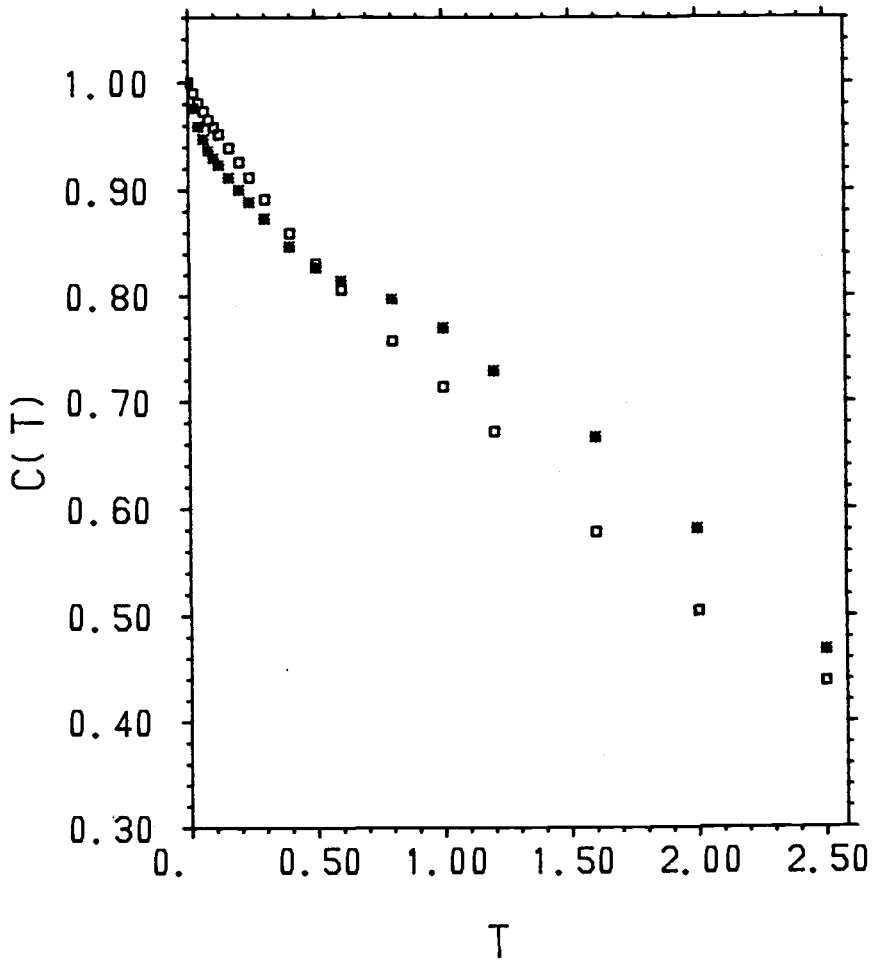

Figure A.2 The same as figure A.1, but the alkane chain has seven C-C bonds.

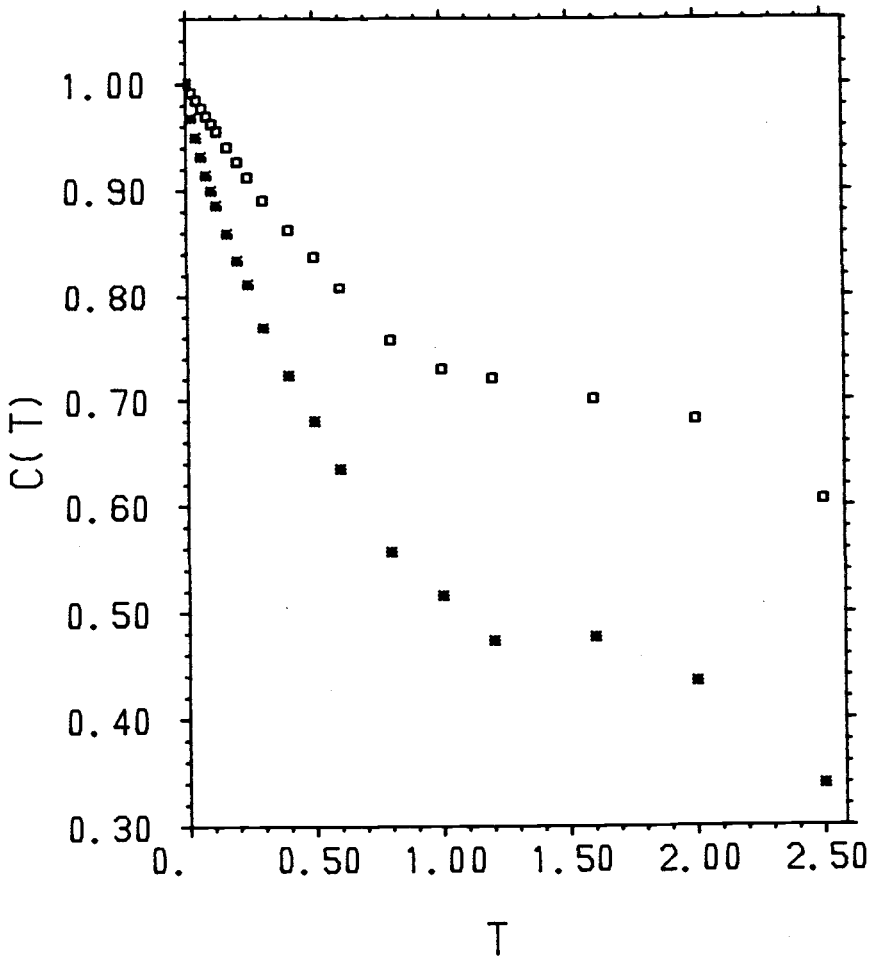

Figure A.3 The same as figure A.1, but the alkane chain has eight C-C bonds.

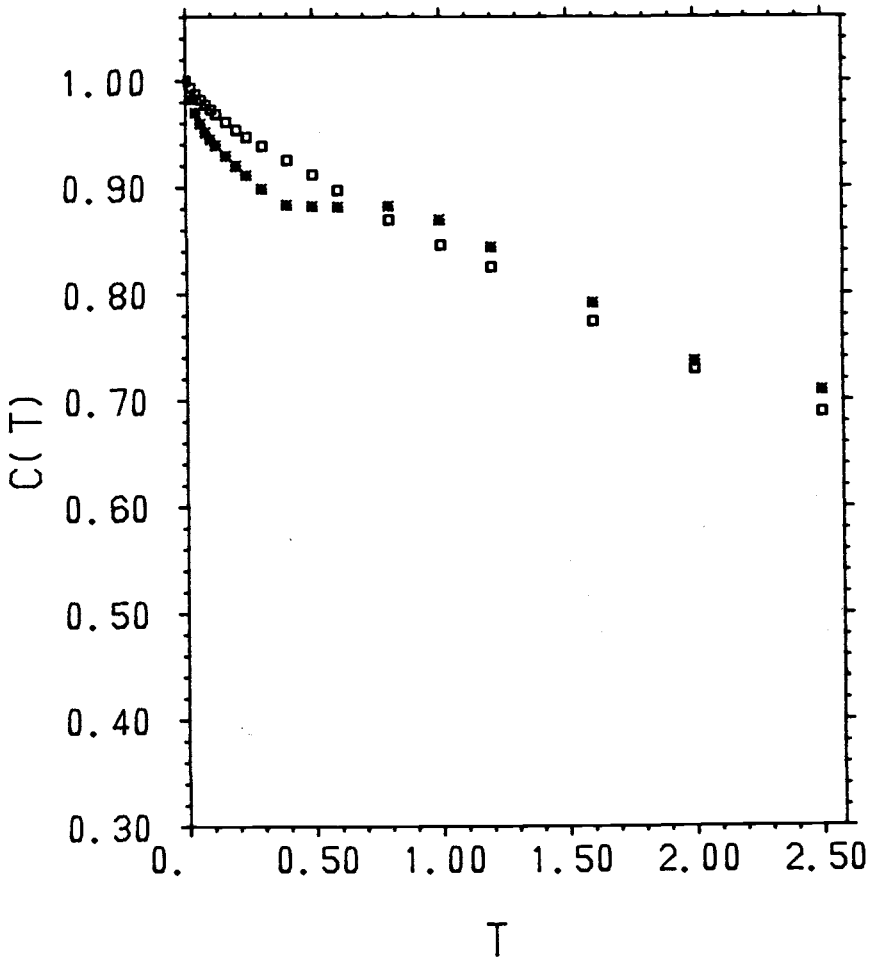

Figure A.4 The same as figure A.1, but the alkane chain has ten C-C bonds.

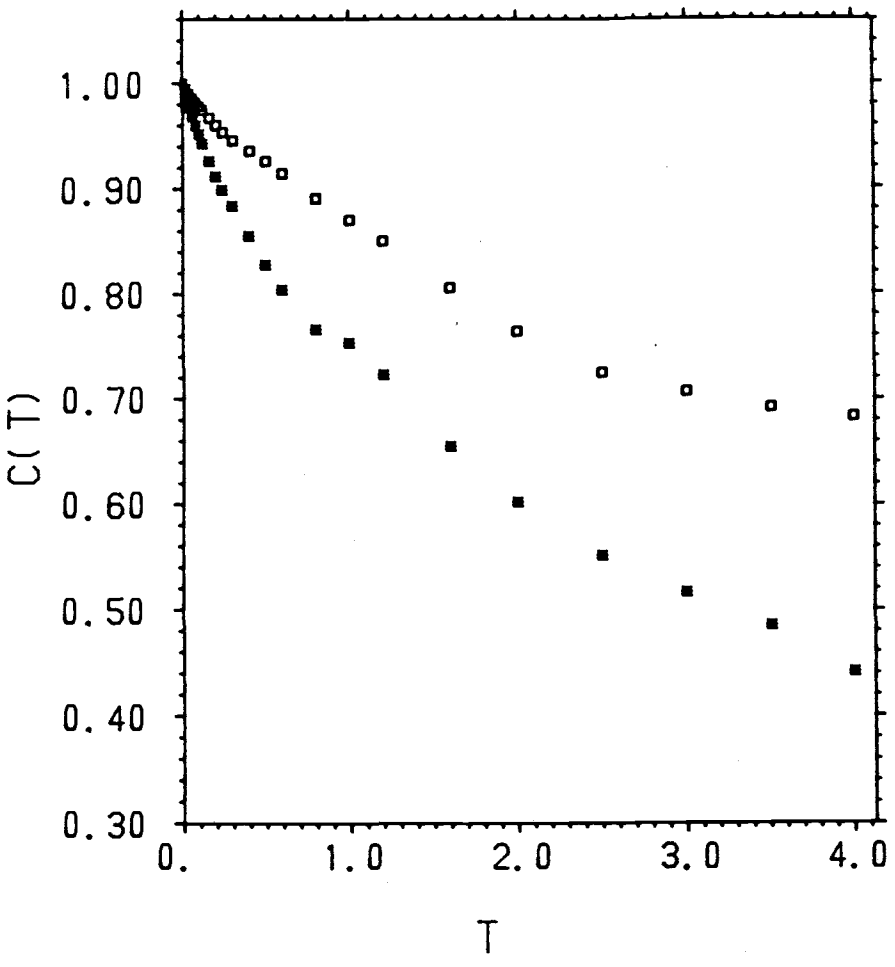

Figure A.5 The same as figure A.1, but the alkane chain has 15 C-C bonds.

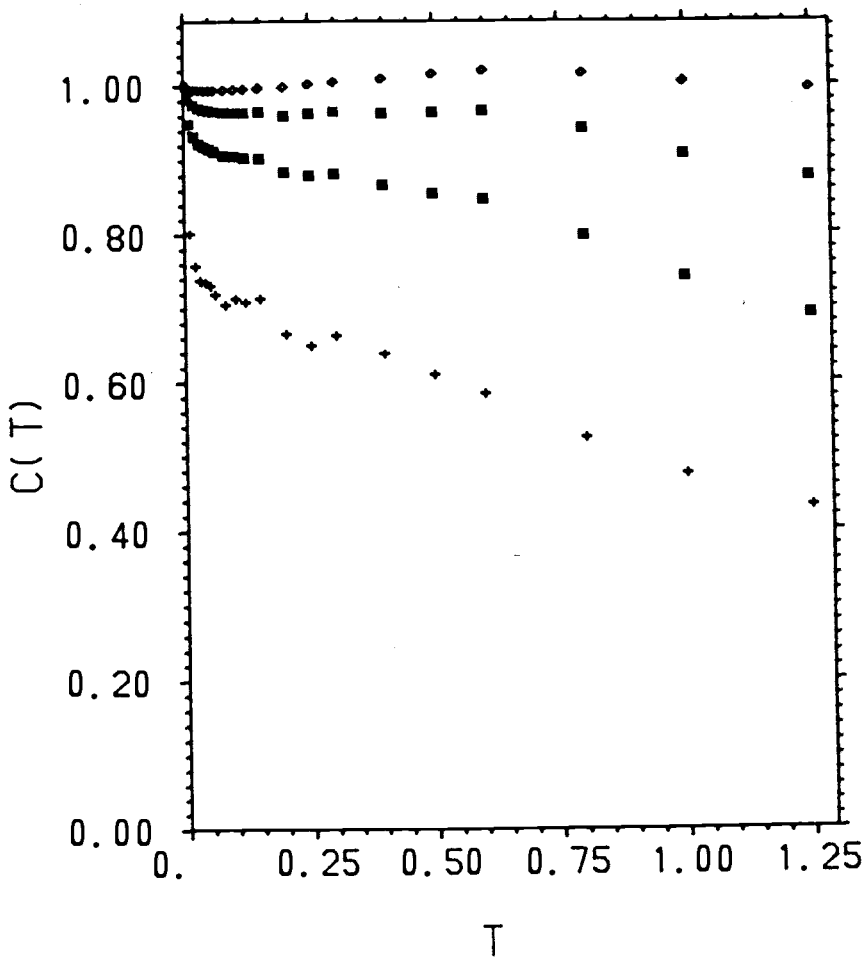

Figure A.6 The correlation functions for the sink functions $\langle \delta S \delta S(t) \rangle / \langle (\delta S)^2 \rangle$, where $S(r) = \exp(-3R^2/2b^2R_x^2)$, for a methylene chain with four C-C bonds. The reactive distances R_x are 1.0 bond lengths (plusses), 1.5 bond lengths (squares), 2.0 bond lengths (asterisks), 3.0 bond lengths (diamonds). All times, T, are given in units of $\zeta b^2/(k_B T)$.

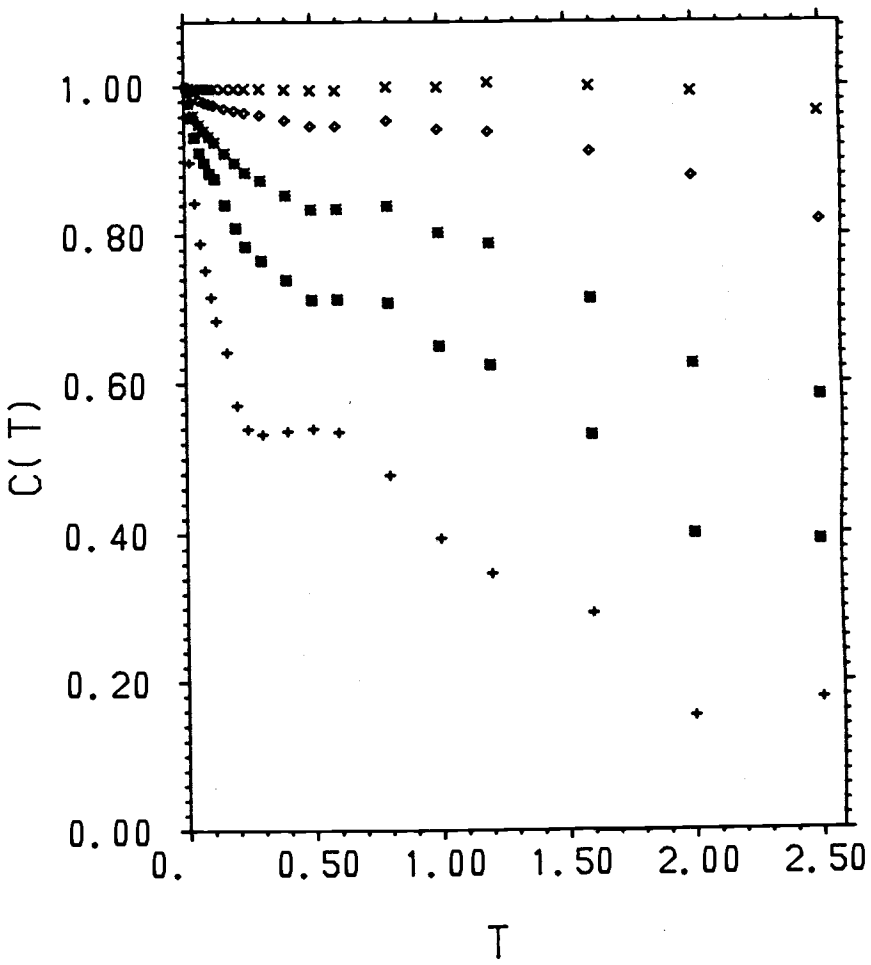

Figure A.7 The same as figure A.6, but for a chain of seven C-C bonds. Additional points for R_x = 5.0 bond lengths are included (crosses).

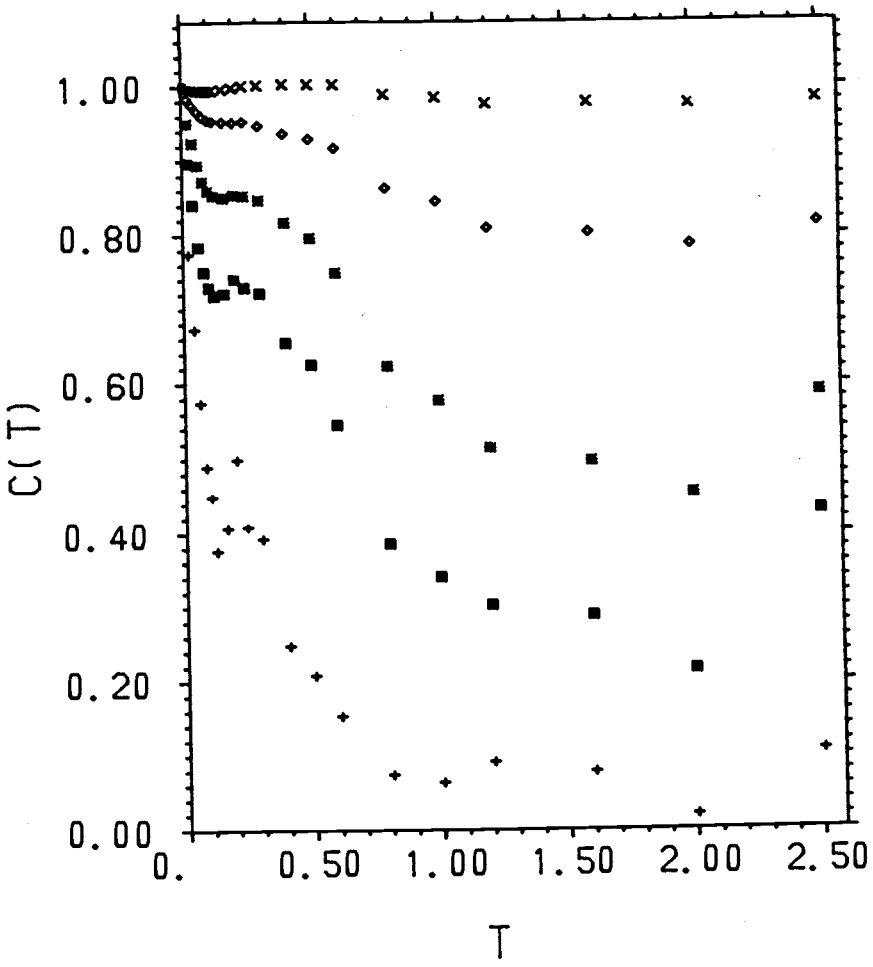

Figure A.8 The same as figure A.7, but for a chain of eight C-C bonds.

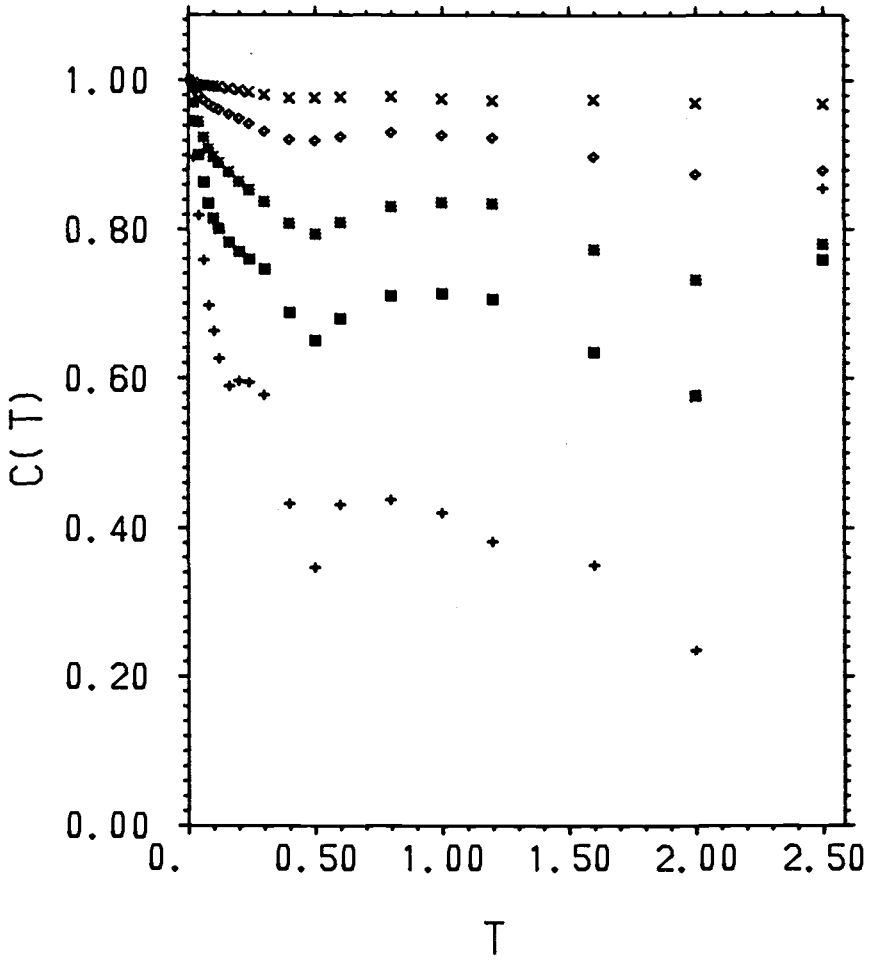

Figure A.9 The same as figure A.7, but for a chain of ten C-C bonds.

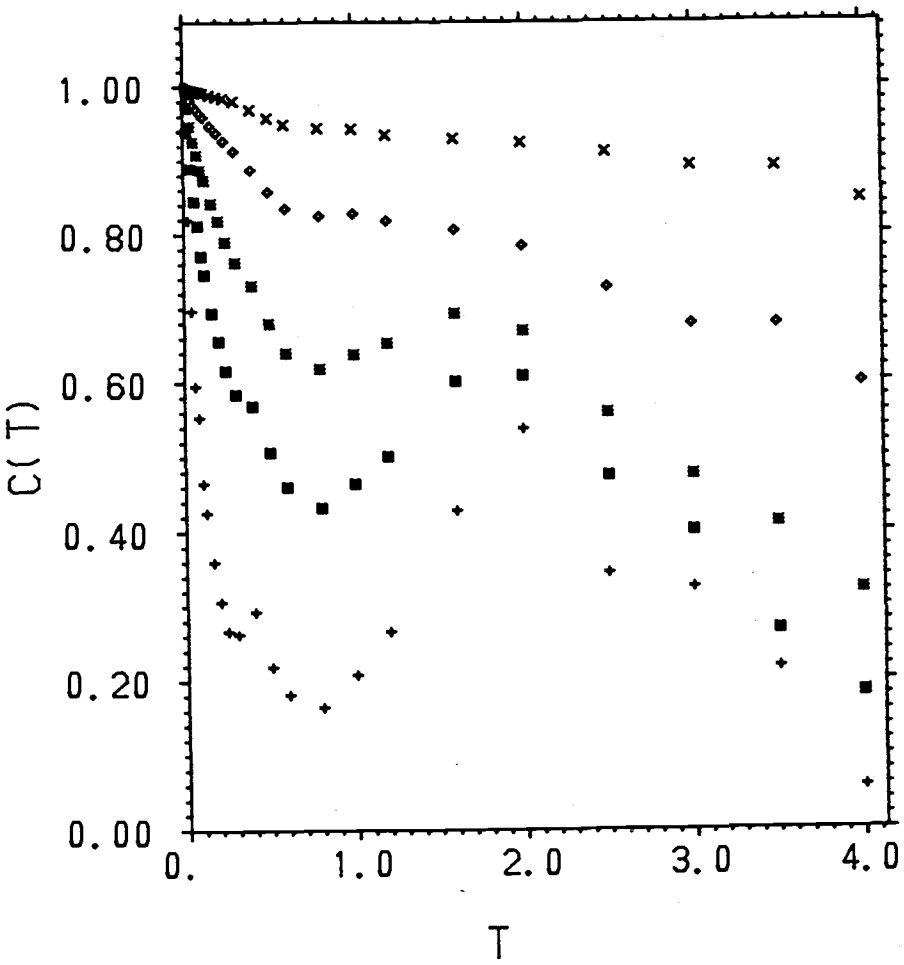

Figure A.10 The same as figure A.7, but for a chain of 15 C-C bonds.